ESD-TR-87-277

Technical Report
802

Transition-Metal Oxide Superconductivity

G.F. Dionne

20 April 1988

Lincoln Laboratory

MASSACHUSETTS INSTITUTE OF TECHNOLOGY

LEXINGTON, MASSACHUSETTS

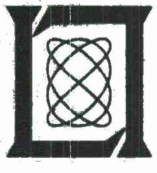

**Prepared for the Department of the Air Force
under Electronic Systems Division Contract F19628-85-C-0002.**

The work reported in this document was performed at Lincoln Laboratory, a center for research operated by Massachusetts Institute of Technology, with the support of the Department of the Air Force under Contract F19628-85-C-0002.

The ESD Public Affairs Office has reviewed this report, and it is releasable to the National Technical Information Service, where it will be available to the general public, including foreign nationals.

This technical report has been reviewed and is approved for publication.

FOR THE COMMANDER

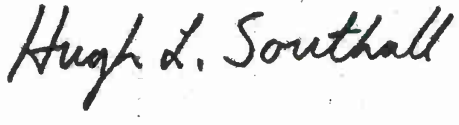

Hugh L. Southall, Lt. Col., USAF
Chief, ESD Lincoln Laboratory Project Office

Non-Lincoln Recipients

PLEASE DO NOT RETURN

Permission is given to destroy this document when it is no longer needed.

MASSACHUSETTS INSTITUTE OF TECHNOLOGY
LINCOLN LABORATORY

TRANSITION-METAL OXIDE SUPERCONDUCTIVITY

G.F. DIONNE
Group 96

TECHNICAL REPORT 802

20 APRIL 1988

LEXINGTON MASSACHUSETTS

ABSTRACT

The phenomenon of superconductivity in transition-metal oxides is discussed from the standpoints of electron transfer mechanisms and the transition from superconduction to normal conduction. As general background, covalent bonding, magnetic exchange, and spin-orbit and Jahn-Teller stabilizations of the $3d^n$ transition-metal ion series are reviewed, and candidate ion pairs for possible orbital electron transfer arising from delocalization exchange between mixed-valence cations of the same element are identified. As explanations for the reported superconducting effects, it is suggested that polarons associated with ion pairs of the $d^9 \rightarrow d^8$ ion combination in 180-degree bond geometries and $d^1 \rightarrow d^0$ combination in 90-degree geometries become itinerant within cell boundaries through energy-free electron transfers made possible by strong orbital exchange coupling. Each mobile polaron is tethered to its stationary source (here the cause of the mixed valence), and its range of motion is determined by local charge neutrality requirements, with boundaries established where the orbital exchange energy becomes balanced by the electrostatic attractive energy between the mobile charge and its source. For the 180-degree case of $Cu^{2+(3+)}$ (i.e., $Cu^{2+} \leftrightarrow Cu^{3+} + e^-$) in perovskites, several possible single-electron transfer situations are described, with a $d^9 \rightarrow d^8$ (low-spin) transfer judged the most likely situation. The $d^1 \rightarrow d^0$ case is represented by $Ti^{3+(4+)}$, but may also include members of the more covalent $4d^n$ and $5d^n$ series, $Nb^{4+(5+)}$ or $Ta^{4+(5+)}$, preferably in a 90-degree spinel-type geometry.

The proposed superconduction model is based on continuous linkages between polaron cells that result in moving chains of uniformly spaced charge carriers. Calculated estimates indicate that radii of polaron cell boundaries on the order of 30 to 40 A may be anticipated in the perovskite system, in general agreement with estimates based on experiment. The transition to the normal conduction state is determined by the electron-hopping activation energy ($E_{hop} \leq 10$ meV for Cu oxides) that arises from magnetic, ligand-field, and lattice ionic and elastic stabilizations. Widespread superconduction can exist below a critical temperature, where the fraction of electrons with thermal energies below the activation energy is sufficient to sustain continuous supercurrent paths. A phenomenological theory of normal resistivity and superconduction transition temperature as functions of composition for the $La_{2-x}Sr_xCuO_4$ and $YBa_2Cu_3O_y$ perovskite families provides excellent agreement with experiment. Reported superconduction and structural data for the related $Bi_2(Sr,Ca)_3Cu_2O_{8+y}$ system are also included in the discussion. Based on the above concepts, general criteria for superconductivity in oxides are summarized.

Among the important conclusions from these analyses are (i) that superconductivity can exist in systems where the spin-independent orbital exchange energy of a polaron exceeds its stabilization energy, provided that antiferromagnetic coupling does not impose a spin-flip excitation energy requirement, (ii) that in tetragonal perovskites superconduction should occur principally in the x-y plane (perpendicular to the tetragonal c axis) and specifically in the Cu(2) pyramidally coordinated complexes of the O^{2-}-deficient compounds, and (iii) that ordering of the sources that produce the mixed-valence $Cu^{2+(3+)}$ ions in this plane is essential for achieving high transition temperatures, current densities, and critical magnetic fields. With optimized mixed-valence cation ordering in systems where strong covalent d-electron coupling is present with weak magnetic exchange effects, critical temperatures above 300 K could be possible. For long-term stability of electrical and magnetic properties, however, both chemical and thermodynamic equilibria under specified operating conditions are imperative.

TABLE OF CONTENTS

LIST OF ILLUSTRATIONS

LIST OF TABLES

TRANSITION-METAL OXIDE SUPERCONDUCTIVITY

1. INTRODUCTION

Normal electrical conduction is the continuous transfer of charge under the influence of an electric field. For a fixed field, the current is limited by resistance that results from fields among the charges themselves, collisional excitations in a gas, and interactions with phonons (lattice vibrations) in a solid. Superconduction in a solid occurs where the electron transport mechanism is effectively without resistance and an electric field is not required to sustain the current. Until recently, it has been a phenomenon found principally in select classes of metallic compounds and limited to temperatures below 25 K.

To explain the source of superconductivity at higher temperatures (in some cases greater than 90 K), recently discovered[1-5] in the mixed-valence $Cu^{2+(3+)}$ ceramic perovskites (typically tetragonal A_2BO_4 in Fig. 1, where Cu occupies octahedral B sites and the bracketed valence indicates the minority or impurity ion), Bednorz et al.[2] mentioned the possibility of an electron transfer mechanism involving two valence states of the copper ions. In contrast to this new phenomenon, normal (conventional) conduction in metal oxides is inefficient at low temperatures, but is also attributed to an effect peculiar to the mixed-valence condition. The Verwey electron "hopping" mechanism [6] most commonly encountered in ferrimagnetic oxides (i.e., the $Fe^{2+} \leftrightarrow Fe^{3+} + e^-$ reaction between sites on the same sublattice) is responsible for the substantial room-temperature conductivity of spinel magnetite $Fe[Fe^{2+}Fe^{3+}]O_4$. For a similar conduction phenomenon observed with Mn perovskites[7] that involved $Mn^{3+(4+)}$ pairs, Zener[8] proposed that the electron transfer process takes place through superexchange with the oxygen anion linking the two metal cations, limited by an activation energy that controls the electron mobility. Perhaps the most significant earlier work relevant to these questions was offered by Goodenough as an explanation for the metallic properties of pure La_2CuO_4 through hole conduction in d-orbital bands.[9]

The Cu perovskite superconducting electron transfer mechanism, however, must represent resistanceless transport and differs from the Fe spinel and the Mn perovskite cases in the fulfillment of specific requirements to permit delocalization superexchange of the type first described by Anderson.[10] Above the superconducting transition temperature, Cu perovskite

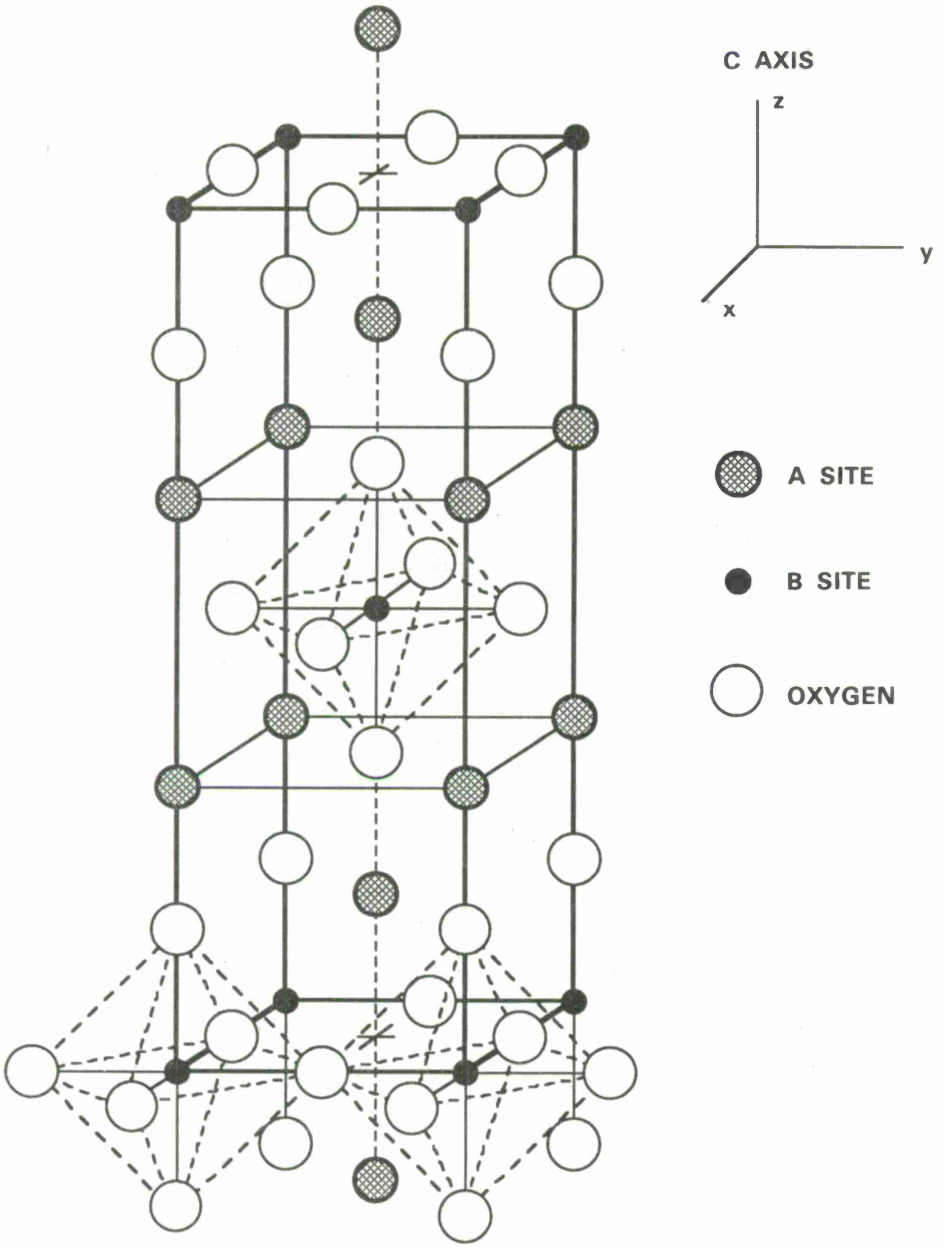

Figure 1. Tetragonal perovskite A_2BO_4 unit cell (commonly referred to as the K_2NiF_4 structure) showing square x-y plane locations of octahedral-site B cations at the cell end faces.

features a normal conductivity which decreases with temperature similar to a metal; Fe spinel and Mn perovskite, however, have the opposite temperature dependence—more typical of a band-model semiconductor. Unlike metals, where the normal electrons are unbound but not unimpeded, and semiconductors which require excitation to generate electron-hole pairs or charge carriers from ionized impurities, superconduction by orbital transfer must occur between mixed-valence ions of the same element on adjacent and equivalent cation sites, without activated electron hopping from bound orbital states.

It is proposed here that high-temperature superconductivity represents a fourth conduction situation that arises from widespread transferring of electrons among the partially filled e_g orbitals of the $Cu^{2+(3+)}$ pairs, i.e., through $Cu^{2+} \leftrightarrow Cu^{3+} + e^-$ exchanges, provided (in the ideal) that the individual transfer sites are energetically equivalent. For $Fe^{2+(3+)}$ pairs, different bonding situations are involved and this orbital transfer mechanism is not available; conduction can therefore occur only by thermally generated electron hopping with an activation energy E_{hop} of magnetic and elastic origins. In contrast to the Bardeen-Cooper-Schriefer (BCS) theory[11] that has been successful in explaining the superconducting properties of metals and other low temperature superconductors, this concept does not require the existence of phonon-mediated electron "pairs." Since it is the extra electrons (or holes) that are involved in the delocalization superexchange, only these carriers would be involved in the case of oxides, with transport made possible by the d-electron orbital exchange (or covalent) interaction.

In Sections 2 and 3 of this report, the properties of d^n ions as they relate to the various magnetic exchange interactions that can permit orbital electron transfer between equivalent sites are reviewed, some possible electron transfer situations are described, and the origins of the polaron stabilization (activation) energy are discussed. In Section 4, the formation of the superconducting state by linkages of mobile polaron cells, the origin of the transition temperature to the normal state, and the critical magnetic field and current densities are analyzed. Finally, general conditions necessary for superconduction are listed in Section 5, followed by a discussion of superconducting oxide systems in the context of the above models, together with some recommendations for future research.

2. ORBITAL ELECTRON TRANSFER

A. Conducting Electrons and Polarons

The physics of electrical conduction in metal oxides is a complex subject involving the entire spectrum of solid-state theory. As discussed in Goodenough's comprehensive review,[12] the electron states in cations with unfilled d shells (transition-metal ions) can range from pure d orbitals determined by the local crystal fields, as in the case of isolated ions in a paramagnetic system, to Hartree-Fock wave functions of a collective-electron band model. In the former case, the d electrons are considered to be localized in their orbitals and represent a generally insulating situation of entirely ionic bonding, particularly if only one ionic species of a given element is present in low concentrations. Where covalent bonding to anions (e.g., O^{2-}) is present, the d-electrons can become collective in a more dense concentration of closely interacting ions, with the ligand-field energy levels broadening into bands. Conventional band theory may then be invoked as the electron states become governed by Fermi statistics.

In the general case of interacting cations of the same valence (i.e., equal numbers of d electrons), an excitation energy U representing the mutual electrostatic repulsion of orbiting electrons is required to effect an electron transfer by raising the valence of one ion and lowering the valence of the other, in much the same manner as the creation of a hole-electron pair in a conventional band model semiconductor. As employed by Goodenough, a phenomenological band-broadening parameter b, representing the spin-independent (i.e., orbital) part of the one-electron transfer energy between d electrons of nearest neighbor ions (orbital transfer integral), may be employed to explain the growth of oxide metallic behavior from localized to collective conditions (see Fig. 2). Increasing b values produce a gradual merging of the filled and unfilled bands into a single collective electron half-filled band that could permit the occurrence of superconductivity when a threshold is reached.[13] Large b values can result from direct cation-cation interactions via small site separations or through strong cation-anion-cation covalent mixing of cation d and anion p orbital wave functions.

This interaction parameter also applies to the case where cations of the same element (a transition metal) occur in different valence states[13] as a result of an electrostatic charge balance requirement (minimization of Madlung energy) imposed by the presence of either a mixture of stationary fixed-valence cations in a different sublattice or conditions arising from non-

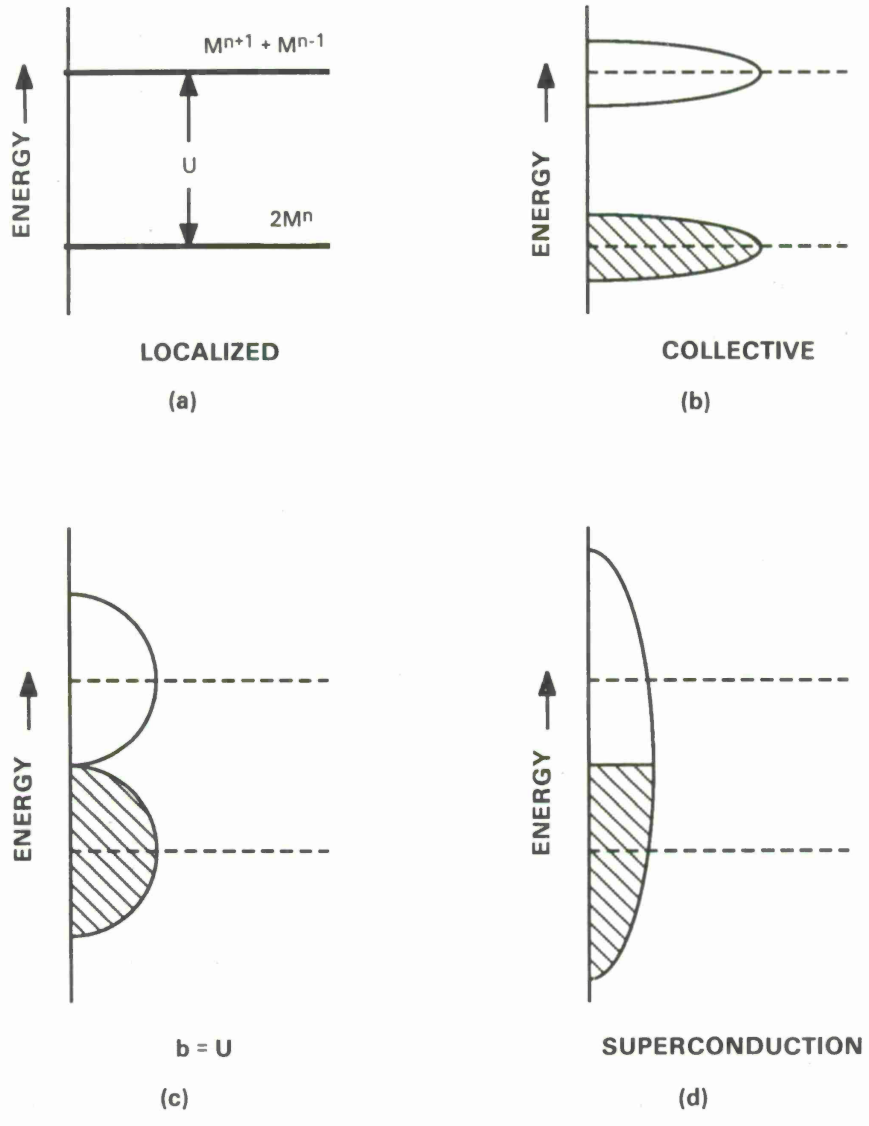

94292-2

Figure 2. Growth of the proposed collective-electron superconducting state for the transfer event $2M^n \rightarrow M^{n+1} + M^{n-1}$ - U: (a) localized-electron crystal field state, $b < b_c$ (the collective electron energy threshold); (b)collective- electron state due to band broadening, $b \sim b_c$; (c) semiconductor to semimetal transition, $b \sim b_g$; and (d) collective- electron superconduction, $b \sim b_{cs}$. (Based on Reference 12, Fig. 12)

stoichiometry. In this situation, there is an odd number of electrons involved and the transfer would represent a simple translational shift, with the two ions exchanging valence states. Provided that the two sites are electrostatically and magnetically equivalent, there would be no net first-order energy change, i.e., $U \sim 0$.

As an alternative description of superconductivity, the orbital overlap b parameter as the fundamental criterion will be employed here in a slightly different manner. Instead of the superconducting state considered as arising from a growth (in a figurative sense) of band overlapping in a collective system already densely populated with charge carriers, the system will be treated spatially as the coalescing of isolated regions or cells of local superconduction that exist initially because of the strong covalent interaction (large b), in this case between d orbitals overlapping through the medium of an oxygen 2p orbital in the perovskite lattice. When the volume density of these regions reaches a percolation threshold, the superconducting state is established as the isolated cells form linkages.

From the definition of the localized electron as applied to this case of mixed-valence cations emerges the concept of the "small" polaron, a charge carrier on an "impurity" ion trapped by self-induced elastic deformations of its local environment and magnetic coupling (a magnetic polaron). In succeeding sections, electron delocalization that permits the formation of large polarons (brought into existence by large b values) will be examined as a source of resistanceless transfer acting in competition with the conventional hopping semiconduction mechanism.

B. Covalency and Superexchange

For energy-free electron transfer via covalent bonding, the electron must retain the energy of its bonding orbital in the transfer. Energy barriers created by interactions associated with the particular cation sites can prevent orbital transport. In addition to the usual lattice elastic and electrostatic energy stabilizations of ionic crystals, a d-electron is coupled to its site environment through magnetic superexchange effects that result from orbital overlapping of covalent bonding electrons, crystal fields that interact with orbital angular momenta (including energy stabilizations by Jahn-Teller (JT) distortions), and spin-orbit (SO) coupling that also produces stabilization effects by lattice distortions (of opposite sense to the JT effects) in the presence of magnetic order below a Curie or Neel temperature.[14] The critical conditions for orbital electron transfer, however, are more likely determined by the subtleties of the covalent bonds that result from the d and p

orbital wave function overlapping.

Covalent bonding is not only a medium by which d electrons may be transferred between different cation sites,[15] but is also the source of magnetic exchange interactions that determine ferro- and antiferromagnetism. For this reason, these phenomena must be treated together. In these discussions, certain simplifications and estimates are adopted in applying the complex theory of magnetic exchange, and only the more dominant situations as they pertain to electron transfer and magnetic exchange coupling will be examined. In the discussion that follows, much of the content has been summarized from published work by Anderson,[10,16] Goodenough,[14,17] Kanamori,[18] Goodenough and Loeb,[19] and Goodenough and Longo.[20]

There are two basic kinds of exchange to consider in a magnetic oxide: direct exchange (cation-cation) and superexchange (cation-anion-cation). Associated with superexchange are four covalent bonding configurations between metal d electrons and oxygen 2p electrons, as shown in Fig. 3;* the σ and π configurations can also apply to the direct overlapping of d-electron orbitals on adjacent metal cations, without the oxygen intermediary. Since σ bonds feature direct overlapping of wave functions, they not only give rise to stronger bonds and greater magnetic coupling, but also more pronounced electron transfer effects.

From these basic definitions of covalent bonds, there emerge three important types of exchange couplings, which can be either σ or π: (I) half-filled$\leftrightarrow$half-filled d orbitals, which produce strong antiferromagnetism that results from a correlation effect with localized electrons that accounts for the simultaneous partial bond formation on each side of the oxygen anion via its two $2p\sigma$ electrons of opposite spin, (II) half-filled$\leftrightarrow$empty d orbital, capable of spin-independent electron transfer, and (III) filled$\leftrightarrow$half-filled d orbital, requiring a ferromagnetic (or dynamic antiferromagnetic) alignment of the two ions for orbital tranfer to occur. With an odd number of d electrons, types II and III can involve delocalization or the actual transfer of electrons between cations,[9] where the extra electrons drift between cations with the magnitude of the transfer (exchange) integral b depending on the extent of overlap between d and p orbitals (particularly effective with e_g-$p\sigma$-e_g bonds and also direct t_{2g}-$t_{2g}\sigma$ overlaps). It is important to note that where antiferromagnetism is dominant between the two ions, only type II can produce electron transfer

* These wave functions represent individual cation orbitals prior to formation of molecular orbital functions, which are linear combinations of cation-anion orbitals that eventually build into energy bands. The magnitudes of the linear coefficients are proportional to the amount of covalence. Although covalent effects determine the magnitude of the b interaction parameter, for the present discussion it is sufficient to work with the directional characteristics of these basic functions.

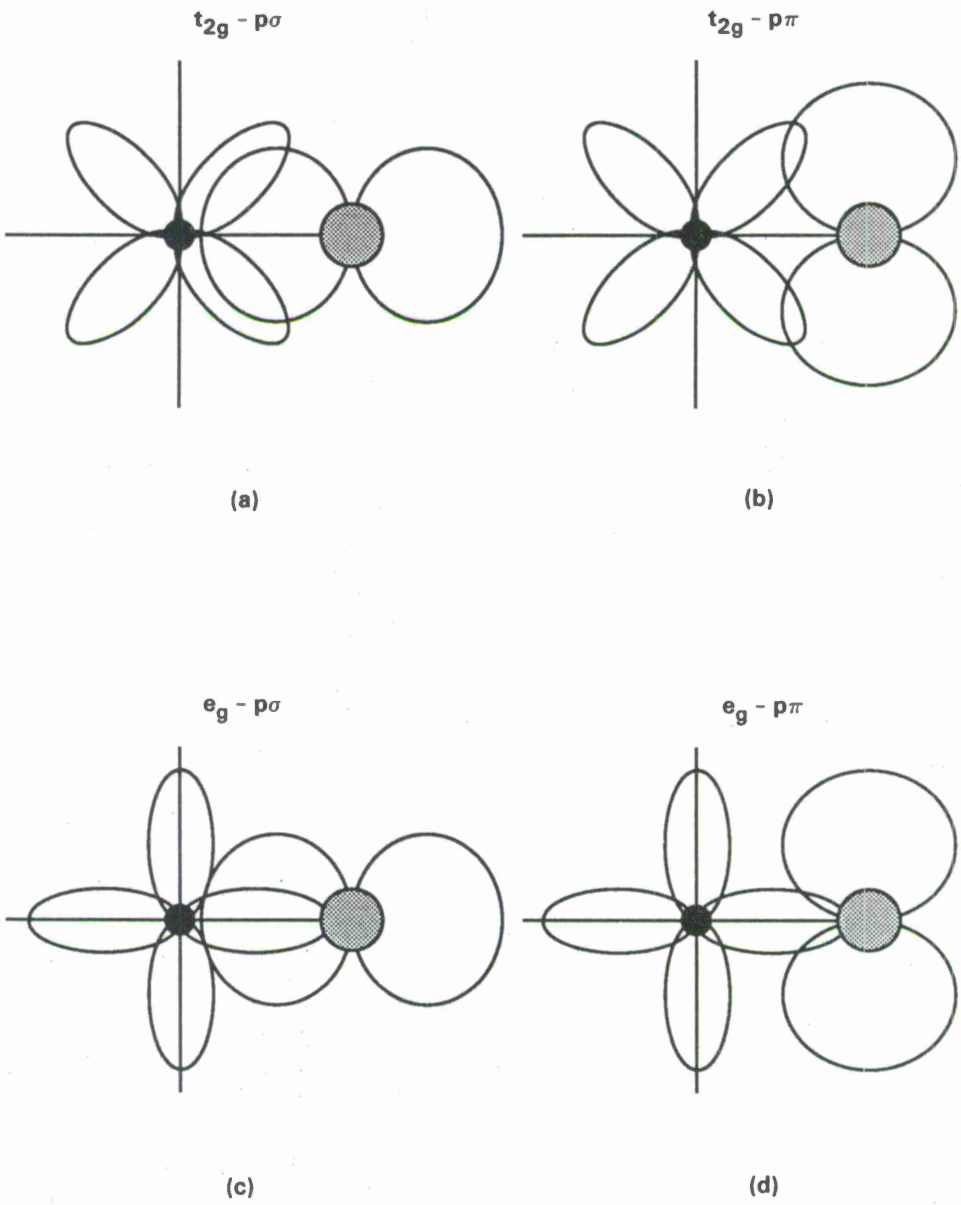

Figure 3. Basic covalent bonding configurations: (a) t_{2g}-pσ, (b) t_{2g}-pπ, (c) e_g-pσ, and (d) e_g-pπ. Wave function overlap is greatest for pσ bonds, particularly e_g-pσ.

without an energy expense associated with a spin reversal of the transfer electron required to maintain spin pairing in the filled orbit.

Since the $Cu^{2+(3+)}$ and $Fe^{2+(3+)}$ systems are both potential candidates for the proposed orbital electron transfer as an alternative or perhaps competing mechanism to "normal" conduction, the conditions for its onset might be considered here. If the transfer occurs with no change in energy involved, i.e., the before and after states are indistinguishable except for a shift in location (translation), then the magnetic states of the two ions are critical, along with the lattice site environments. As depicted in Fig. 4, the covalency of the $Cu^{2+(3+)}$ superexchange coupling would create an equal probability of the electron occupying either cation, suggesting that a single energy state might exist for the particular B-O-B group with a wave function that would encompass all three ions. The delocalization exchange transfer mechanism may best describe this phenomenon, which is most effective in cation-anion-cation bonding.[14,20] In this manner, the overlapping of metal d and oxygen 2p orbitals may permit electron movement between the two B ions with no energy involved. In a classical sense, it could be argued that the electron oscillates continously between the two cation sites.

C. Orbital Interaction and Bonding Geometry

The orbital interaction energy is derived from the transfer or exchange integral b, which can be estimated from the ligand-field energy splitting parameter Dq that represents the difference in wave function overlap between the lower energy t_{2g} orbitals, with lobes that point away from the oxygen ligands in an octahedral coordination (see Fig. 5), and the e_g functions, with lobes directed at the oxygen for 180-degree $p\sigma$ bonds.[21] For the $3d^n$ transition series, a review of octahedral-site orbital occupancies is given in Fig. 6, with a more detailed summary of spin values and estimates of b for simple oxides listed in Table I. Since orbital transfer would be expected only via the e_g orbitals in this 180-degree geometry, superconduction would be confined to the ions with transfer electrons occupying these levels. For cases where the transfer electron is not in this upper manifold, an excitation to these levels is first required, thus eliminating any possibility of an energy-free transfer.

An important difference between the Cu perovskite and Fe spinel systems, therefore, lies in the nature of orbital overlapping and the chemical bond angles in these two structures. If it is assumed that the "extra" d electron can make a resistanceless transfer to a neighboring ion of the

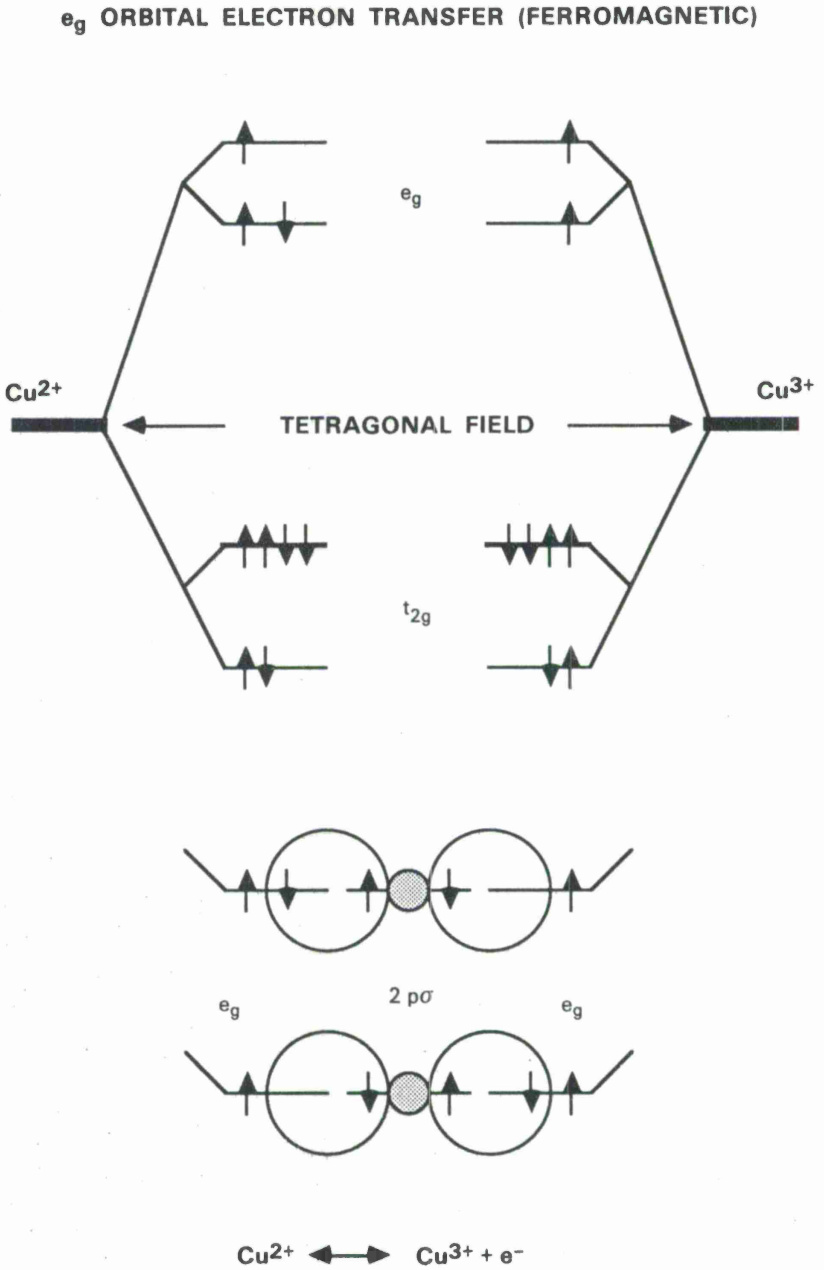

Figure 4. Proposed orbital electron transfer ($Cu^{2+} \leftrightarrow Cu^{3+} + e^-$) for the perovskite case. Ferromagnetic coupling is assumed for illustrative purposes.

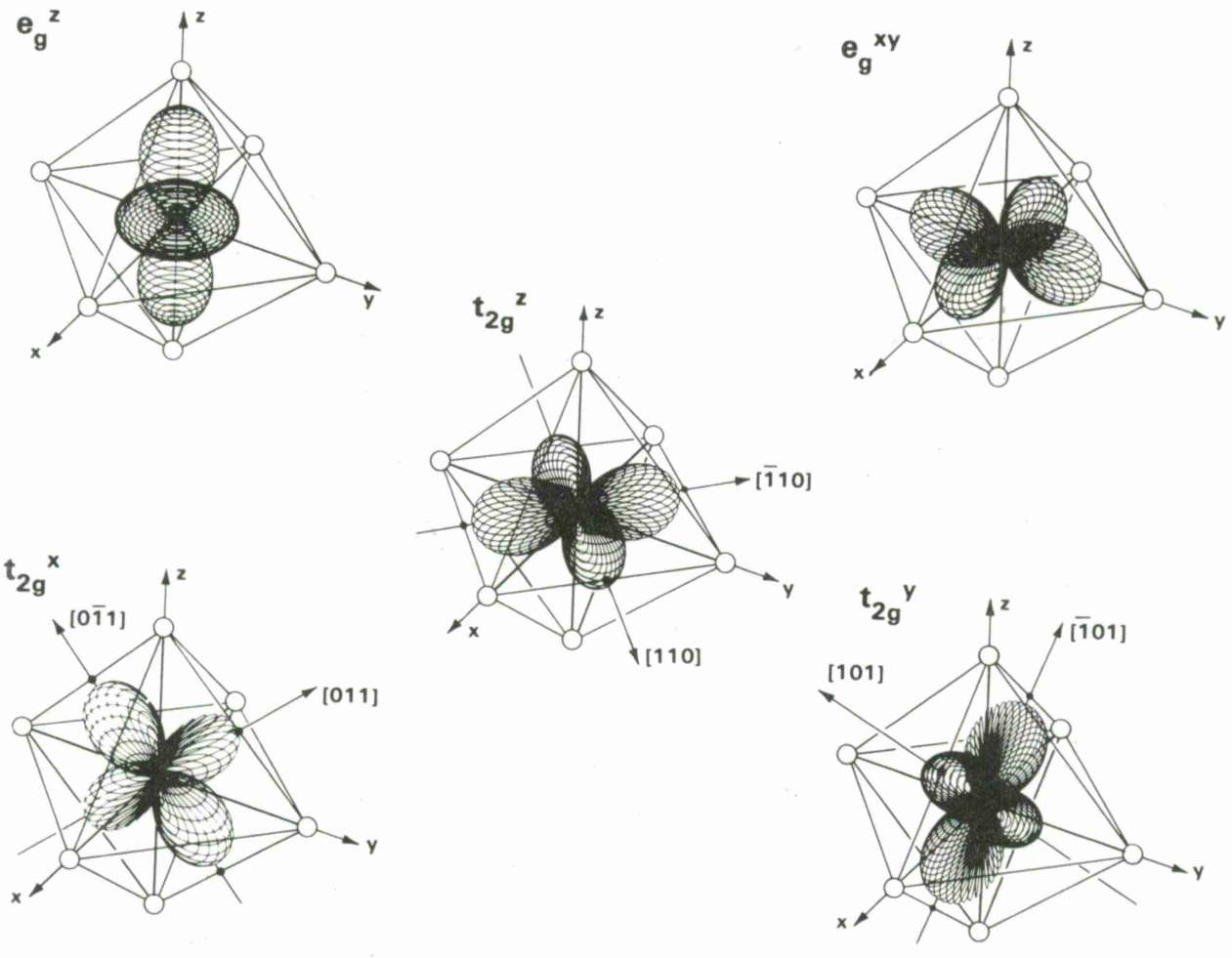

Figure 5. d-Electron orbital wave functions pictured in an octahedral site, with z as the axis of quantization (and axis of tetragonal distortion) directed along the [001] cubic axis. In this frame of reference, the relative energies of the five orbitals may be discerned from their proximities to the ligands, with the two e_g states higher than the three t_{2g} states.

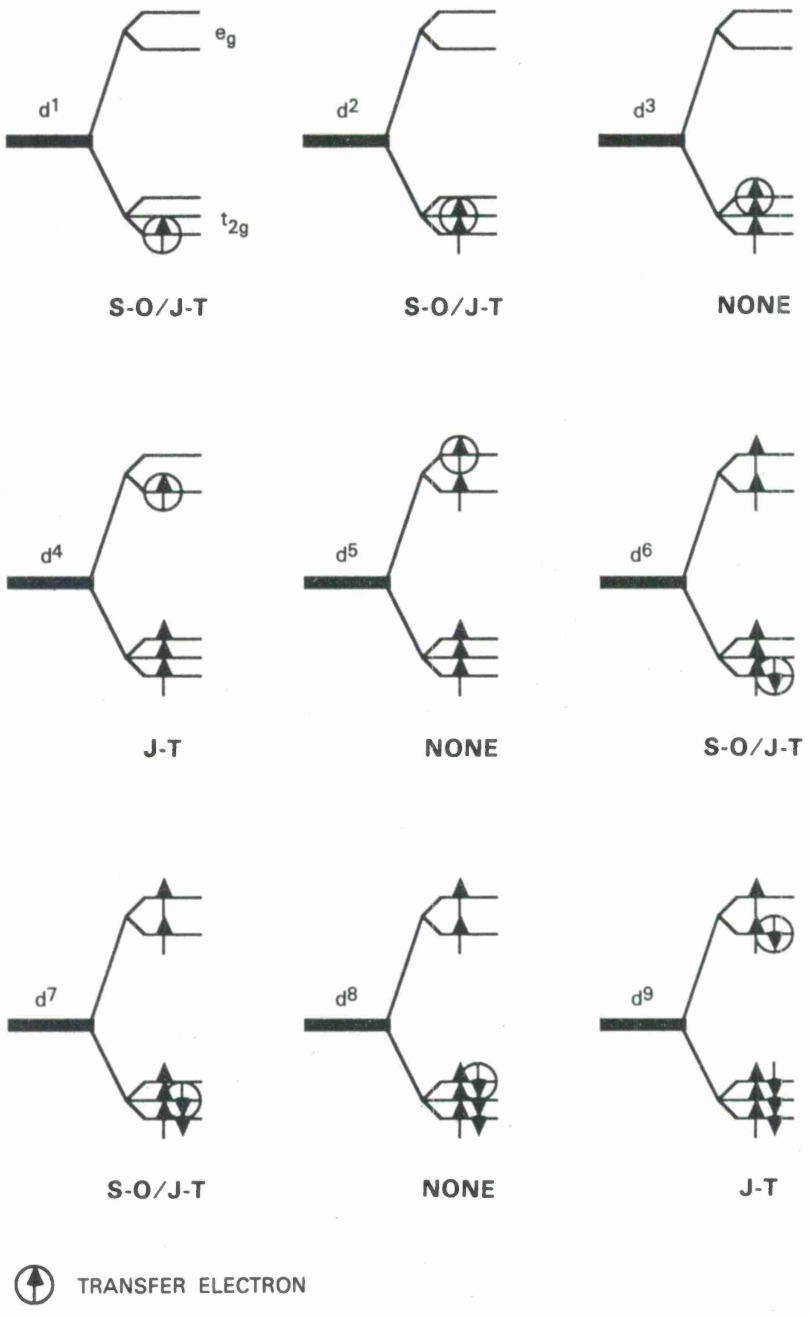

Figure 6. High-spin state electron occupancy diagrams for the $3d^n$ iron-group transition-metal ions in an octahedral crystal field.

TABLE I

d^n Ion Mixed-Valance B-Site Exchange Properties in Oxides

Transfer Pair		S_L n(p)	Bond	Dq[a] eV	b[a] eV	J_{PL} ↑⇑	$E_{ex}(\sim J_{LL}S_L{}^2)$[b] ⇑⇓
$d^1 \rightarrow d^0$	**$Ti^{3+(4+)}$ $Nb^{4+(5+)}$ $Ta^{4+(5+)}$**	**0(1/2)**	**t_{2g}-pπ**	**0.25**		**II**	**None (small)**
$d^2 \rightarrow d^1$	$V^{3+(4+)}$	1/2 (1)	t_{2g}-pπ	0.22		II	Small (small)
$d^3 \rightarrow d^2$	$V^{2+(3+)}$	1 (3/2)	t_{2g}-pπ	0.15		II	Small (small)
$d^4 \rightarrow d^3$	$Cr^{2+(3+)}$	3/2 (2)	$e_z{}^2$-pσ	0.17	0.14	II	Small (med)
	$Mn^{3+(4+)}$			0.26	0.22	II	Small (med)
$d^5 \rightarrow d^4$	$Mn^{2+(3+)}$ $Fe^{3+(4+)}$	2 (5/2)	$e_x{}^2{}_{-y}{}^2$-pσ	0.10	0.32	II	Med (large)
$d^6 \rightarrow d^5$	$Fe^{2+(3+)}$	5/2 (2)	$(t_{2g}$-p$\pi)^c$	0.12	0.41[c]	III	Large (large)
$d^7 \rightarrow d^6$	$Co^{2+(3+)}$	2 (3/2)	$(t_{2g}$-p$\pi)^c$	0.12	0.41[c]	III	Large (large)
$d^8 \rightarrow d^7$	$Ni^{2+(3+)}$	3/2 (1)	$(t_{2g}$-p$\pi)^c$	0.11	0.35[c]	III	Large (med)
$d^9 \rightarrow d^8$ (high-spin)	$Cu^{2+(3+)}$	1 (1/2)	$e_z{}^2$-pσ	0.16	0.13	III	Med (small)
$d^9 \rightarrow d^8$ (low-spin)	**$Cu^{2+(3+)}$**	**0 (1/2)**	**$e_x{}^2{}_{-y}{}^2$-pσ**	**0.16**	**0.39**	**II**	**Small (none)**
$d^{10} \rightarrow d^9$	$Cu^{1+(2+)}$ $Ag^{0(1+)}$	1/2 (0)	$e_x{}^2{}_{-y}{}^2$-pσ	0.16	0.39	III	Small (none)

a Based on data and estimates from Anderson's paper;[10] b is determined for specific transfer orbitals, (5/2)Dq for $e_x{}^2{}_{-y}{}^2$-pσ bonds and (5/6)Dq for $e_z{}^2$-pσ bonds in the x-y plane of a perovskite lattice; t_{2g}-pπ bonds have little overlap and negligible b integral.

b Based on criteria outlined in Reference 14, Table XII.

c Since the e_g orbitals are unoccupied in these ions (see Figure 6), and additional excitation U is required to effect a transfer by promoting the electron to the e_g shell in order to utilize the pσ bonding overlap in the 180-degree case. As a consequence, the likelihood of superconduction is remote regardless of the type of resultant magnetic exchange. For the 90-degree case, the roles of the t_{2g} and e_g orbitals are reversed to some extent with regard to σ and π bonding, and a direct t_{2g}-$t_{2g}\sigma$ can produce a significant b value.

same element, the path traversed may be examined by considering the types of superexchange configurations involved. In Fig. 7, the cases of 90-degree and 180-degree bond angles are presented to illustrate the importance of the t_{2g} and e_g orbitals and their interaction with the oxygen 2p orbitals. The 90-degree case represents the spinel configuration B-O-B (see Fig. 8), that tends to be magnetically parallel because of the two sublattice ferrimagnetism where the dominant antiferromagnetic $Fe^{2+}_B \leftrightarrow O^{2-} \leftrightarrow Fe^{3+}_B$ interaction forces the two individual sublattices into a parallel alignment, while the 180-degree case is characteristic of the generic cubic perovskite B-O-B (see Fig. 9). In this latter structure, the e_g orbitals directly overlap the $p\sigma$ orbitals and create a favorable geometry for electron transfer; the t_{2g} orbitals overlap in a $p\pi$ superexchange arrangement that would be less effective in contributing to a conduction mechanism.

As a consequence, orbital transfer would be most efficient with a $d^9 \rightarrow d^8$ ion pair in the perovskite structure, because the e_g orbitals are not only partially occupied, but the specific electron involved in the transfer already occupies an e_g orbital that directly overlaps a 2p oxygen orbital. For the 180-degree bonding geometry, this situation does not occur to this extent in the other combinations listed in Table I (except for the $d^{10} \rightarrow d^9$ case to be discussed later). Therefore, the $d^9 \rightarrow d^8$ pair (embodied in $Cu^{2+} \leftrightarrow Cu^{3+} + e^-$) should be the most probable candidate for orbital transfer in the perovskite structure. It is interesting that in the 90-degree spinel case, the t_{2g} orbitals would overlap the $p\sigma$ orbitals and consequently would play a greater role in any electron transfer, in conjunction with the direct t_{2g}-t_{2g} overlapping that can exist between B-B sites. As suggested by Goodenough,[22] this direct cation-cation interaction is the most probable delocalization exchange mechanism for the 90-degree case. According to Table I, the end member for this geometry would be $d^1 \rightarrow d^0$ (e.g., $Ti^{3+(4+)}$).

D. Transfer-Cation Spin Configurations

In general, where correlation exchange effects are strong (e.g., type I), the spin alignments would be antiferromagnetic. According to Table I, the $d^9 \rightarrow d^8$ case is expected to feature antiferromagnetism for high-spin d^8 configurations. If these antiparallel spin alignments impose energy expense requirements for electron transfer, the details of this coupling must be examined more closely. Figure 10 presents four possible scenarios of single electron transfer between the e_g orbitals of the two cations in a tetragonal or orthorhombic crystal field with coordinate axes along the cubic $\langle 100 \rangle$ directions. In Case (a) the coupling is assumed to be ferromagnetic with the

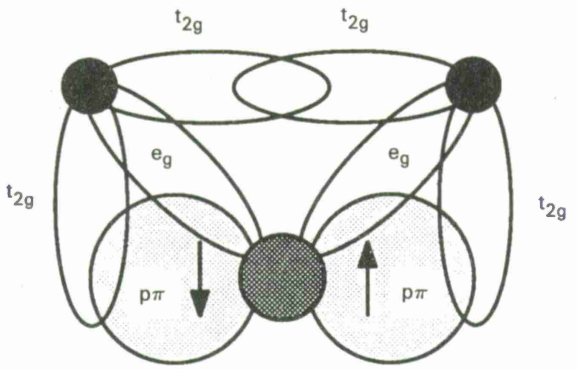

90-DEGREE BOND (SPINEL)

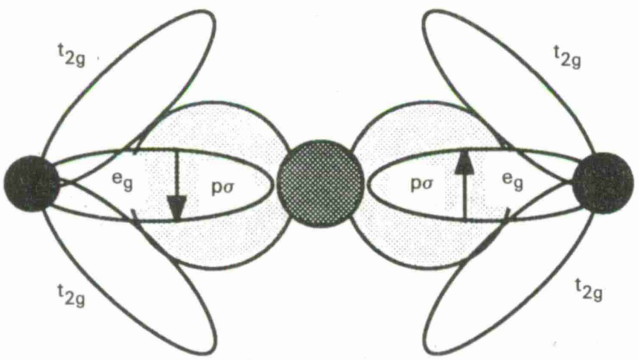

94292-6

180-DEGREE BOND (PEROVSKITE)

Figure 7. B-O-B orbital overlaps for 90- and 180-degree bond angles.

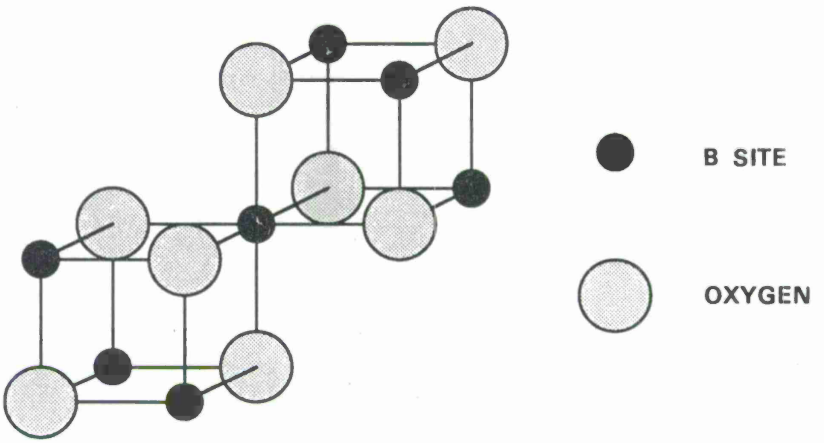

90-DEGREE BONDS (SPINEL OCTAHEDRAL SITE)

94292-7

Figure 8. 90-degree B-O-B bonding in spinel lattice surrounding an octahedral site.

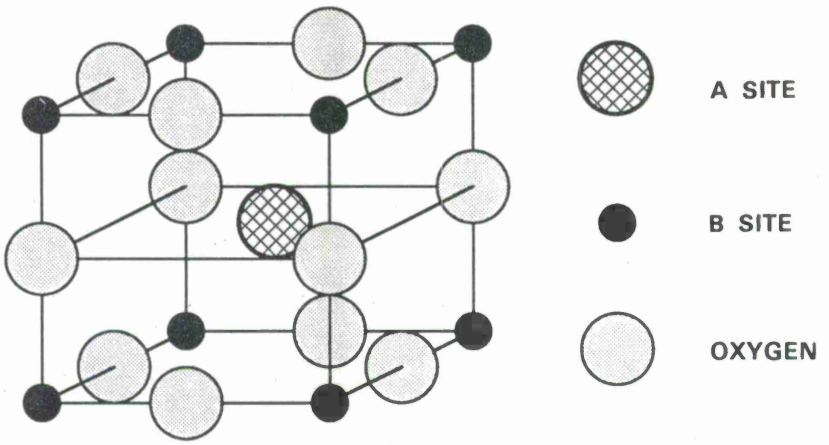

180-DEGREE BONDS (CUBIC PEROVSKITE A SITE)

94292-8

Figure 9. 180-degree B-O-B bonding in basic cubic perovskite (ABO_3) unit cell.

(a) FERROMAGNETIC (HIGH-SPIN) CASE

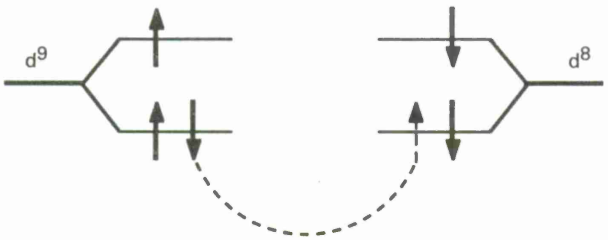

(b) ANTIFERROMAGNETIC (HIGH-SPIN) CASE

(c) FERROMAGNETIC (LOW-SPIN) CASE

(d) MONOVALENT Cu CASE

94292-9

Figure 10. Single-electron orbital transfer arrangements. Note that (d) is a $Cu^{1+} \leftrightarrow Cu^{2+} + e^-$ *transfer that is dependent on circumstances described in Appendix B.*

electron transfer occurring between the two lower e_g levels, with a type III delocalization coupling at the lower e_g level. For a host lattice of Cu^{2+} ions, characteristic of the first high-temperature superconductor $La^{3+}_{2-x}(Ba,Sr)^{2+}_x(Cu^{2+}_{1-x}Cu^{3+}_x)O_4$,[2] at least the short-range antiferromagnetic order of Case (b) would be present, with a spin-flip excitation required for electron transfer to an immediate nearest neighbor cation. Alternatively, the dynamic antiferromagnetism in the x-y plane of the perovskite, recently suggested by the neutron diffraction measurements of Shirane et al.[23] with La_2CuO_4 may evolve from magnetic disorder among ions with local antiferromagnetic coupling, typical of the B-site Fe^{3+} ions in paramagnetic $Zn[Fe_2]O_4$.[24] Here the local coupling could accommodate an electron transfer by flipping the spin to satisfy local exchange requirements and give rise to a type of moving-electron spin wave. With a Cu^{3+} "hole" of S = 0, a moving polaron could thus create the illusion of a magnon.

Based on the findings of Goodenough et al.[25] for the trivalent B-site end member $La^{3+}Sr^{2+}Cu^{3+}O_4$, Case (c) is a probable transfer scheme. In this work, it was concluded that the strong tetragonal distortion of the octahedron creates a "low-spin" state (S = 0 instead of 1 for Cu^{3+}), with a filled lower e_g orbital in violation of Hund's rule. (The implications of a possible local orthorhombic symmetry at the B-sites and other considerations are discussed in Appendix A). The effect of this spin configuration is readily seen in Fig. 10c, where the Cu^{3+} upper state is empty and the transfer would now take place at this level, receiving the electron from a corresponding half-filled orbital of an adjacent Cu^{2+} ion. Since the $d^9 \rightarrow d^8$ (low-spin) couplings for the 180-degree perovskite bond would be type II-$e_g p\sigma$, delocalization exchange would result if magnetic order were not present in the planes normal to the c axis. The possibility of superconductivity in the x-y plane would then exist where the weak exchange field of the lattice ions is neutralized by the magnetic dilution effects of higher concentrations of diamagnetic Cu^{3+} low-spin ions, in the manner of the exchange isolation effects of Co^{2+} in ferrimagnetic oxides.[26]

An exotic possibility is depicted in Case (d), which could arise if B^{1+} cations were to appear. According to Fig. 10d, the transfer situation for a $Cu^{1+(2+)}$ pair would involve a type III-$e_g p\sigma$ exchange, with the Cu^{1+} ion diamagnetic (similar to the "receptor" Ti^{4+}, except that it has all d orbitals filled instead of empty) and essentially independent of the magnetic state of its environment. Similar to the $Cu^{2+(3+)}$ low-spin case, however, antiferromagnetic order could be a limitation on its ability to participate in the transfer process, if the spins of the Cu^{2+} ions in the host lattice are antiparallel. The likelihood of these ion pairs participating in superconduction will be discussed later in connection with double-electron transfer.

Each of the above spin arrangements could theoretically produce delocalization electron transfer. However, from examination of the specific orbital lobe directions (see Appendix A), a curious conclusion emerges. Since the lower state is d_{z^2} for the tetragonal perovskite with c/a > 1, transfer between lower e_g orbitals would be along the z direction (i.e., the c axis), but in the x-y plane for upper $d_{x^2-y^2}$ state transfers. Accordingly, superconductivity would be along the c axis in Cases (a) and (b), but in the x-y plane for Cases (c) and (d). From an inspection of the tetragonal unit cell in Fig. 1, it is clear that c-axis transfers are not available because of the absence of 180-degree Cu-O-Cu bonds. As a result, it is concluded that Case (c) would be the most probable situation for $Cu^{2+} \leftrightarrow Cu^{3+} + e^-$ orbital electron tranfer in tetragonal perovskite.

The results of the above discussion are summarized in Table II, which also includes two additional possibilities that involve the transfer of electron pairs ($d^{10} \rightarrow d^8$ or $d^2 \rightarrow d^0$), according to the discussion given in Appendix B.

TABLE II

Summary of Electron Transfer Situations

	Spin Alignment	Transfer Orbital	Direction
$d^9 \rightarrow d^8$ (high-spin)	↑↑	d_{z^2}	c-axis
	↑↓	d_{z^2}	c-axis
$d^9 \rightarrow d^8$ (low-spin)		$d_{x^2-y^2}$	In-plane
$d^{10} \rightarrow d^9$		$d_{x^2-y^2}$	In-plane
$d^{10} \rightarrow d^8$ (high-spin)		d_{z^2}, $d_{x^2-y^2}$	c-axis, in-plane
$d^{10} \rightarrow d^8$ a (low-spin)		$d_{x^2-y^2}$	In-plane

a The two spins could behave as a coupled pair (See Figure 32).

3. POLARON STABILIZATION AND ITINERANCY

For electrical conduction in metallic oxides, two energy requirements must be considered: (i) the excitation energy of a band gap (where present), and/or (ii) the activation (stabilization) energy of a polaron. In the former case, conduction requires the creation of charge carriers through the expense of an excitation energy U (see Fig. 2), in the manner of an intrinsic semiconductor. Since the initial and final states differ, energy is not conserved, and superconduction is improbable. Except for the case of static antiferromagnetism, however, energy is conserved in the case of polarons generated by mixed-valence, with no net absorption (i.e., U = 0). In this situation, polarons move between equivalent sites, and the initial and final energy states are identical.* There remains, however, the activation energy that would at least reduce the probability of an orbital electron transfer.

For a typical nonmagnetic polaron in an ionic lattice, this activation energy (E_{hop}) results from an elastic strain effect on the immediate environment of the "impurity" ion. Where transition-metal ions with partially-filled d shells are involved in an ionic/covalent bonding combination, other contributions to E_{hop} are present. Magnetic exchange between the polaron ion and lattice ions and among lattice ions themselves, as well as ligand-field interactions (enhanced by spin-orbit and Jahn-Teller stabilizations) must be considered.

A. Magnetic Exchange Stabilization

Any spin ordering of the equal-valenced host lattice ions would arise from type I coupling (half-filled↔half-filled orbitals) and would be antiferromagnetic. For host ions with filled (Cu^{1+}) or empty (Ti^{4+}) d orbitals, there would be no lattice magnetic exchange. However, if a polaron ion of spin S_P resides in a magnetically ordered lattice of fixed spins S_L, the magnitude of its coupling energy to the exchange field at site i will add to the trapping energy according to the standard relation

$$E_{ex} = -2\sum_{i,j}{}' J_{ij} S_i S_j \quad , \tag{1}$$

* This situation is analogous to a mechanical "see-saw" or electrical "flip-flop" circuit.

where J_{ij} is the exchange constant between the i and j cations. For the coplanar situation depicted in Fig. 11, the exchange energies at sites 1 and 2 are given by

$$E_{ex}^{(1)} = -2(4)J_{PL}S_PS_L \tag{2a}$$

and

$$E_{ex}^{(2)} = -2(3)J_{LL}S_LS_L + 2(1)J_{PL}S_PS_L \quad , \tag{2b}$$

where J_{PL} and J_{LL} are the respective exchange constants between polaron and lattice ions, and between lattice ions themselves.

The exchange stabilization energy may then be estimated by subtracting these individual quantities to obtain

$$\Delta E_{ex} = 6S_L \left| J_{LL}S_L - J_{PL}S_P \right| \quad . \tag{3}$$

If $J_{PL} \approx J_{LL}$, $\Delta E_{ex} \approx 6S_LJ_{LL}(1/2)$, since $\left| S_L - S_P \right| = 1/2$ for a single electron transfer. For the $Cu^{2+(3+)}$ case, $S_L = 1/2$ and $\Delta E_{ex} \approx 6J_{LL}(1/2)^2 \approx 0.08$ eV.* Where $S_P = 0$, this result also applies if $J_{PL} \approx -J_{LL}$.

To minimize ΔE_{ex}, the molecular or exchange field for spin ordering embodied in the average J_{LL} (commonly called the molecular-field coefficient $\mathcal{N}_{LL}$) should cancel through disorder, usually resulting from magnetic dilution when polarons of $S_P = 0$ appear in concentrations sufficient to break down the cooperative exchange effects. According to Table I, only Ti^{4+}, Cu^{3+} (low-spin), and Cu^{1+} offer an $S_P = 0$ magnetic dilution capability to satisfy conditions required to nullify $\mathcal{N}_{LL}$.

For electron transfer in a magnetic lattice with either static or dynamic spin alignments, the various possibilities are summarized in Table III. For superconduction, the polaron ion must couple to the lattice ions either ferromagnetically (types II or III exchange) or nonmagnetically (type II). Where $J_{LL} \neq 0$, magnetic contributions to polaron stabilization exist and a net activation

---

* From Anderson's rationale for estimating exchange constants,[10] $J_{LL} = b^2/2S_L{}^2U$, which yields

$$\Delta E_{ex} \approx 3b^2/U \quad ,$$

where b = 0.39 eV (see Table I), and U = 5.9 eV for Cu (see Table I of Reference 10). In this context, U represents the energy difference between the ionic ground and excited states involved in the exchange perturbation term.

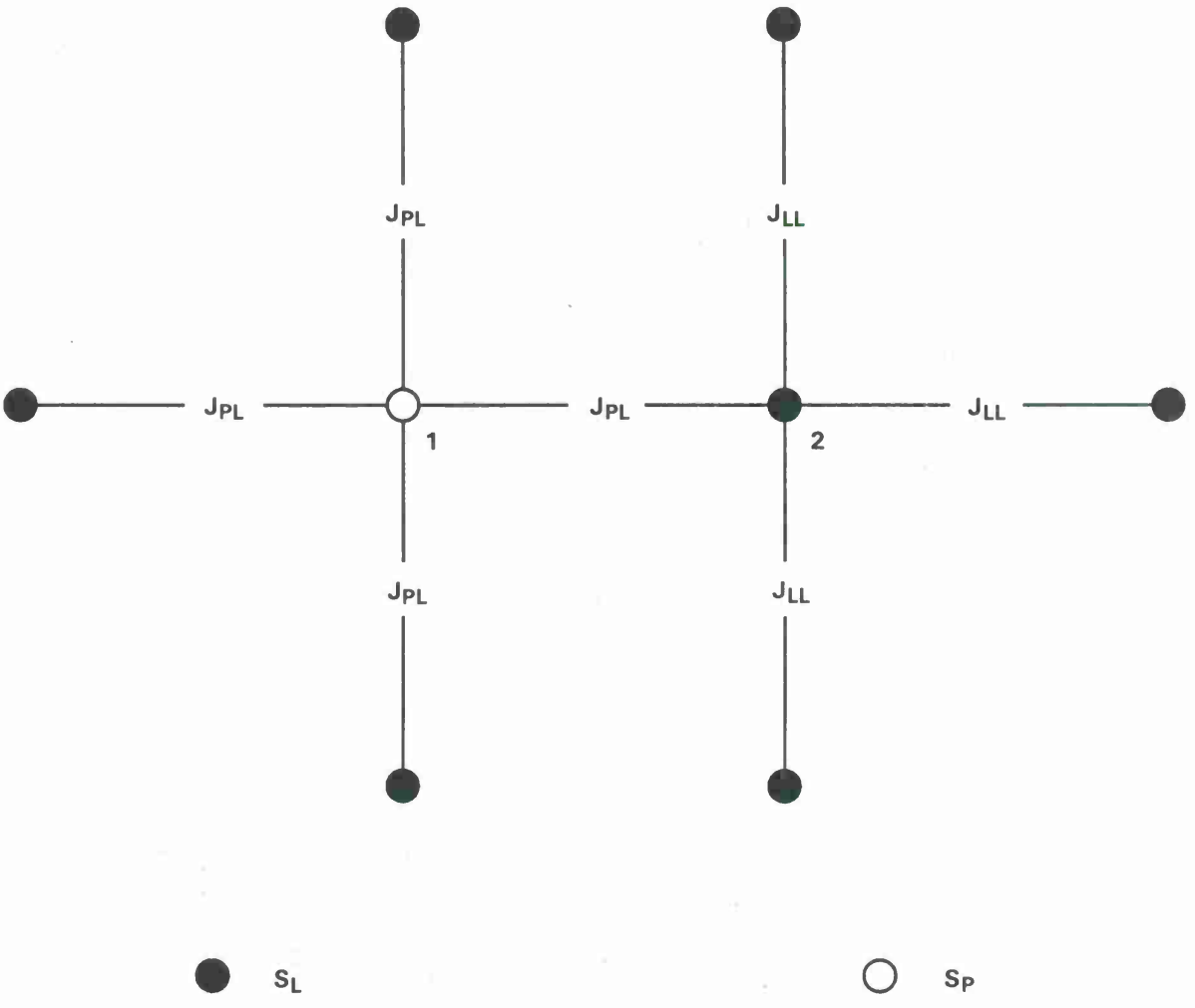

Figure 11. Schematic diagram showing magnetic exchange couplings between adjacent Cu^{2+} and Cu^{3+} ions involved in an electron transfer.

TABLE III

Magnetic Ordering and Excitation Energy

	$J_{LL} \geq 0$		$J_{LL} < 0$	
$J_{PL} \geq 0$	$\uparrow$—●—	$U = 0$	$\uparrow\Uparrow\bullet\Downarrow$	$U \neq 0$
	$-\Uparrow\bullet\Uparrow$	$U = 0$	$\uparrow\Uparrow\times\Downarrow$	$U = 0$
	$\uparrow\Uparrow\bullet\Uparrow$	$U = 0$	$-\Uparrow\times\Downarrow$	$U = 0$
$J_{PL} < 0$	$\uparrow\Downarrow\bullet\Downarrow$	$U \neq 0$	$\uparrow\Downarrow\bullet\Uparrow$	$U \neq 0$
			$\uparrow\Downarrow\times\Uparrow$	$U = 0$

$\Uparrow\bullet\Uparrow$ Statically coupled ferromagnetic lattice

$\Downarrow\bullet\Uparrow$ Statically coupled antiferromagnetic lattice

$\Downarrow\times\Uparrow$ Disordered or dynamically coupled antiferromagnetic lattice

$\uparrow$—●— Type II ferromagnetic exchange ($S_p \neq 0$ polaron in nonmagnetic lattice)

$-\Uparrow\bullet\Uparrow$ Type II ferromagnetic exchange ($S_p = 0$ polaron in ferromagnetic lattice)

energy results; where J_{PL} and/or $J_{LL} < 0$ in a statically ordered state, polaron ion spin reversals are required for transfer and an excitation energy ($U \neq 0$) must be supplied, thus rendering superconduction unlikely.

B. Ligand-Field Stabilization

The ligand-field (called crystal-field for the point-charge approximation) energy level splittings differ for the $Cu^{2+(3+)}$ pair in the manner shown in Fig. 12. For the conventional case of Cu^{2+} (d^9), the cubic splitting of 10 Dq has been measured as 12600 cm^{-1} in an octahedrally coordinated oxygen site (actually H_2O in solution)[27] and provides a lower doublet with stabilization energy of 6 Dq (= 7560 cm^{-1}). Subsequent distortions and spin-orbit coupling create a net stabilization $E_{lf}(Cu^{2+}) \sim 8500\ cm^{-1}$.

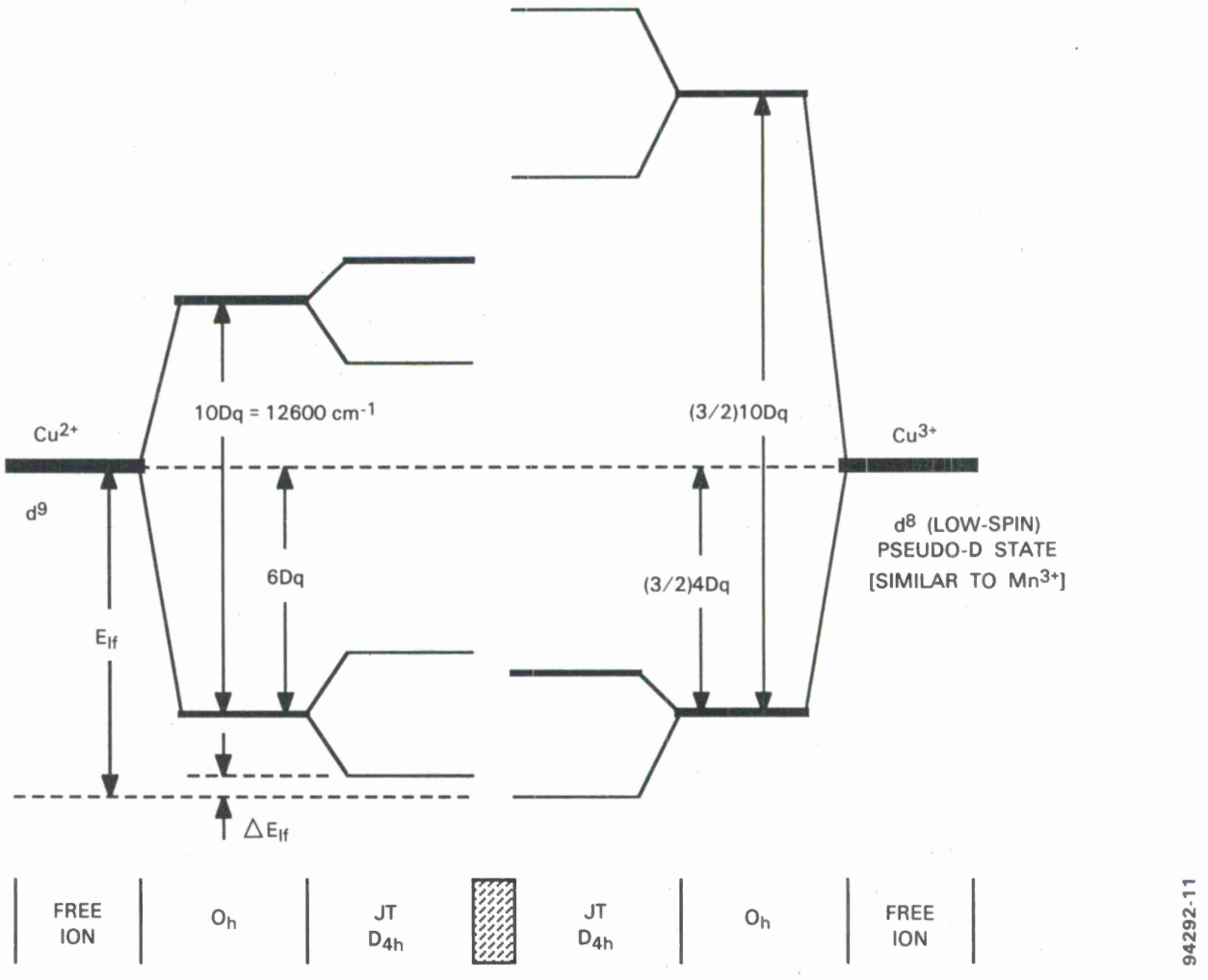

Figure 12. Proposed energy level diagrams of Cu^{2+} and Cu^{3+} ions to illustrate the source of a ligand-field stabilization energy ΔE_{lf}.

The low-spin Cu^{3+} (d^8) ion presents a more interesting situation. In the high-spin state, d^8 has a ground F term, typical of Ni^{2+}. With S = 0, however, the eight d electrons are completely paired and the energy level occupancy becomes exactly double that of a d^4 (Mn^{3+}) ion, with its ground D term and a cubic field structure inverted from the Cu^{2+} case. Since this ion is trivalent (as opposed to divalent Cu^{2+}), the level splittings are magnified by a factor of 3/2,[28] which theoretically produces an effective 10 Dq of 18900 cm^{-1}. In support of this estimate is the measured splitting of 21000 cm^{-1} for Mn^{3+}.[10] With the level inversion putting the triplet lower, the cubic stabilization is weighted by a factor of 4 instead of 6 and the equivalent cubic splitting becomes (3/2)4 Dq = 6 Dq, identical to that of Cu^{2+}.

Similar arguments may be applied for the lower symmetry fields, i.e., D_{4h} or D_{2h}, and the conclusion reached is that the ligand-field stabilization energies of the $Cu^{2+(3+)}$ transfer pair should be nearly identical to a first-order approximation. As a consequence, ΔE_{lf} may not be significant for the copper perovskite system.

C. Spin-Orbit and Jahn-Teller Stabilizations

Where spin collinearity exists, the occurrence of cooperative lattice distortions that reduce the energy of the ground-state orbital term through the spin-orbit coupling can become significant in lattices of cubic symmetry.[29] In these situations, the splitting of a ground triplet would leave an orbital doublet lowest in those cations indicated in Fig. 6. Therefore, the stabilization energies of the two cations with unequal valence would be affected. Thus, above the Curie temperature, differing local crystal-field effects (from SO distortions) between transfer cations would act as perturbations on the ligand-field stabilization ΔE_{lf}.

Distortions of cubic symmetry can also be caused by Jahn-Teller effects which are counterparts or competitors to SO stabilizations also where the cubic crystal field leaves a triplet as the ground state. Since these phenomena result from orbit-lattice interactions, they are independent of magnetic ordering, but contribute to the electron-phonon interactions that would determine hopping-electron transition probabilities (frequencies). Here the system energy is also reduced by a spontaneous deformation of the local environment, but the sign of the distortion is opposite to that of the SO stabilization because the ground state orbital must be nondegenerate (a singlet).[29] Where the SO perturbation energy dominates the JT term, it is still possible that the resulting orbital doublet may be split by a JT effect of lower symmetry (e.g., tetragonal or trigonal to orthorhombic).[30] For static JT effects, thermal considerations are important and the distortions will become cooperative at a temperature signaled by a lattice phase transition.

In the context of energy barriers to orbital electron transfer, the presence of local lattice distortions above temperatures where the deformations are cooperative would also be detrimental. In lattices of lower symmetry, e.g., the tetragonal Cu perovskites, however, the effects of these stabilizing distortions can be reduced by the existence of a natural lattice symmetry. Where additional cooperative JT stabilizations take place at Cu^{2+} sites, the crystal-field distortions should carry over to the ligands of neighboring Cu^{3+} transfer partners, and the elastic environments should be similar.

As indicated in Fig. 12, without an unpaired electron there is no JT effect for d^8 (Cu^{3+}). With S = 0 in the low-spin configuration, there is no SO stabilization. For Cu^{2+}, the JT effect may be overridden by the existing D_{4h} symmetry, but may contribute to a D_{2h} orthorhombic distortion where Cu^{2+} concentration is largest. In addition, it may be shown that the energy of the e_g levels is unaffected by the spin-orbit coupling perturbation, so that spin-orbit effects are absent in both Cu^{2+} and Cu^{3+}. As a consequence, it may be assumed that SO and JT stabilizations (ΔE_{so} and ΔE_{JT}) have little effect in this system.

D. Ionic Bond and Elastic Stabilizations

For all crystal systems, the polaron ion stabilization energy has a contribution from the elastic deformation of its local environment, i.e., contraction or extension of bond lengths. If the bonds are purely ionic, the forces involved are electrostatic and may be represented by the energy function[31]

$$E_{ion} = - z_c z_a q^2/r_{ca} + Bq^2/r_{ca}^n \quad , \qquad (4)$$

where q is the electron charge, r_{ca} is the cation-to-anion bond length, z_c and z_a are the respective cation and anion valences which determine the Madlung constant, B is the Born repulsion constant, with the empirical exponent n ~ 9. Since Cu^{3+} is smaller than Cu^{2+} and carries a larger cation charge, its contribution to the attractive term of Eq. (4) is larger and its ionic stabilization should be greater.

In an isolated octahedral-site normally occupied by the larger Cu^{2+} ion, Cu^{3+} can be further stabilized if its ligands move closer and reduce the effective values of r_{ca}. It is this adjustment of the lattice surrounding the impurity that gives rise to an elastic stabilization effect often called "Landau" trapping. According to the conventional wisdom on this somewhat vague concept

$$\Delta E_{ion} = \alpha(h\nu) \quad , \tag{5}$$

where $h\nu$ is the phonon equivalent of the Landau stabilization energy, and α is a proportionality constant related to the phonon spectrum density and increases monotonically with the purity of the ionic bonding.[32]

From the fundamental theory of lattice vibrations, it follows that $\nu \propto M^{-1/2}$, with M representing the average nuclear mass of the ionic constituents. From Eq. (5) the ionic bond contribution to the polaron activation energy becomes

$$\Delta E_{ion} \propto M^{-1/2} \quad . \tag{6}$$

The implications of Eq. (6) will be pointed out later in relation to isotope and other ionic mass effects on superconducting properties.

The combination of these ionic bond and Landau trapping effects provides the basic polaron stabilization in mixed-valence ionic systems and normally determines the electron hopping conductivity. Since

$$E_{hop} = \Delta E_{ex} + \Delta E_{lf} + \Delta E_{so} + \Delta E_{JT} + \Delta E_{ion} \quad , \tag{7}$$

estimates of the ΔE_{ion} contribution is not readily separable for transition-metal oxides, and it is perhaps more instructive to examine its influence as part of the total stabilization energy, to be discussed in Appendix C where a review of experimental results suggests that its value is substantially less than 0.1 eV for the $Cu^{2+(3+)}$ system even for a relatively small polaron concentration.

Based on the foregoing discussion, the condition for polaron itinerancy through delocalization exchange may be defined as

$$b' = b - E_{hop} \geq 0 \quad . \tag{8}$$

Physically, this relation indicates that the broadening of the transfer orbital level must exceed the polaron activation energy. According to the estimates in Table I, b = 0.39 eV for the $Cu^{2+(3+)}$ case with $d_{x^2-y^2}$ as the transfer orbital. Since the largest term in Eq. (7) is likely to be $\Delta E_{ex} \approx 0.08$ eV,

and the combined contribution of the remaining terms could be considerably smaller (and perhaps of opposite sign), it may be argued that the total magnitude of E_{hop} in the isolated polaron approximation should remain in the 10^{-2} eV range, and the condition specified by Eq. (8) should be satisfied.

4. SUPERCONDUCTION AND THE NORMAL TRANSITION

A. Superconducting Cells and Electrostatic Homogeneity

If an isolated "impurity" ion with a localized or bound charge carrieris a small polaron, this physical situation of carriers moving about the lattice through overlapping orbits may be treated as the expanded polarons described above, where the boundaries of the mobile polarons may extend for several bond lengths depending on the magnitude of the b' parameter and the strength of the electrostatic attraction to the local sources of the polarons (e.g., mixed valence A-site ions). The boundaries of each mobile polaron would then define a superconduction cell centered about the source ion of the Cu^{3+} hole (e.g., a Sr^{2+} ion or O^{2-} vacancy in a perovskite), as pictured in Fig. 13. The superconduction carrier density would therefore vary inversely with the average volume of these cells along the current path, and the spatial variation of the current density within the cell would follow the radial distribution of the polaron wave function. In this sense, the cell radius would resemble a coherence length.

A schematic illustration of the relationship between effective cell radius r_p and the orbital transfer energy threshold given by $b' \geq \Delta E_C$ here defined as the increase in Coulomb energy incurred as a polaron moves away from its source, is given in Fig. 14. The crystal-field energies of the e_g and t_{2g} orbitals (separated in energy by 10 Dq) increase stepwise as the polaron charge moves through sites of increasing distances from its source. In the 180-degree configuration, the e_g levels are broadened by an amount b' through the covalent interaction (e_g-pσ), and the spatial range for energy-free electron transfer in these orbitals is fixed by matching of the band top at the origin to the band bottom at the r_p boundary. For a quantitative estimate of ΔE_C as a function of the various parameters involved, the four equally-spaced negative charges shown in Fig. 15 approximate a chain of isolated A^{2+} ions that determine the electrostatic environment of the positive Cu^{3+} polaron charges. The net electrostatic attractive energy of this abbreviated one-dimensional system as a function of polaron position is then given by

$$\Delta E_C = -(q^2/K)[(1/h - 1/h_o) + (1/i - 1/i_o) + (1/j - 1/j_o) + (1/k - 1/k_o)] , \qquad (9)$$

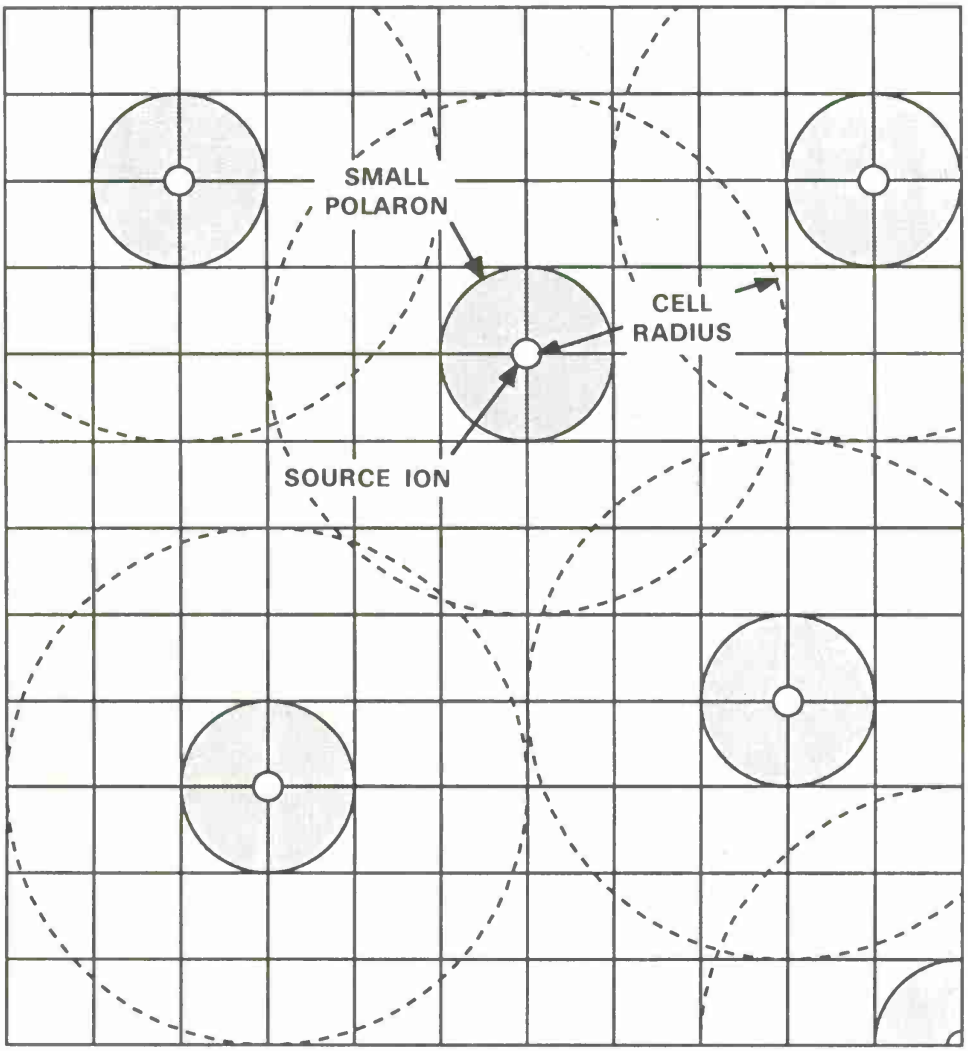

94292-12

Figure 13. Overlapping superconduction cells of mobile polarons.

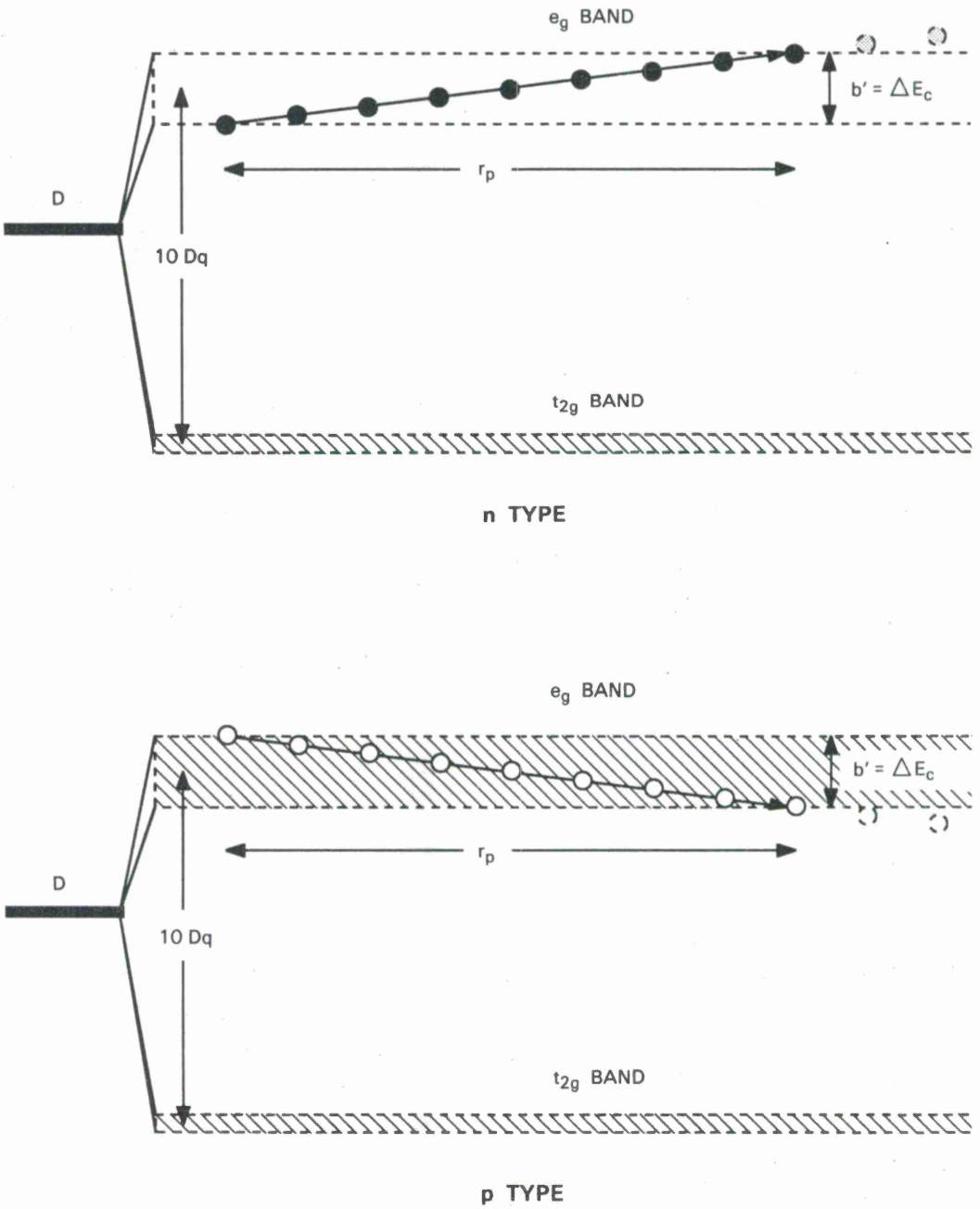

Figure 14. Illustration of ligand-field e_g-level broadening ($b' \approx b$) from covalent bonding and the increase in electrostatic energy ΔE_c as a polaron propagates from its source, for the n-type case of a half-filled polaron level within an empty band (type II) and the p-type case of a half-empty level in a filled band (type III). Other cases include: n-type filled level in half-filled band (type III), and p-type empty level in half-filled band (the type II $Cu^{2+(3+)}$ case). The boundary r_p of the superconducting cell is established at $b' = \Delta E_c$.

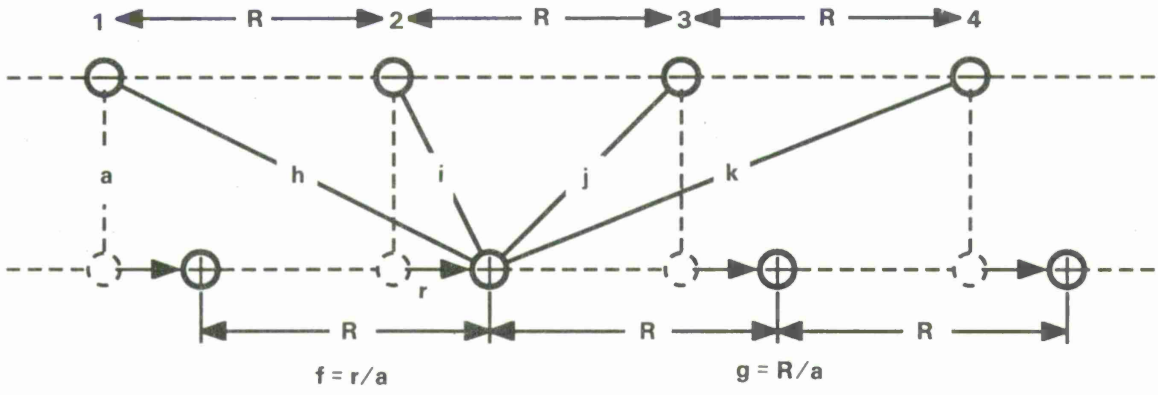

Figure 15. Itinerant polarons (positive holes) tethered to negatively charged stationary sources (i.e., causes of the mixed valence), spaced at intervals of distance R.

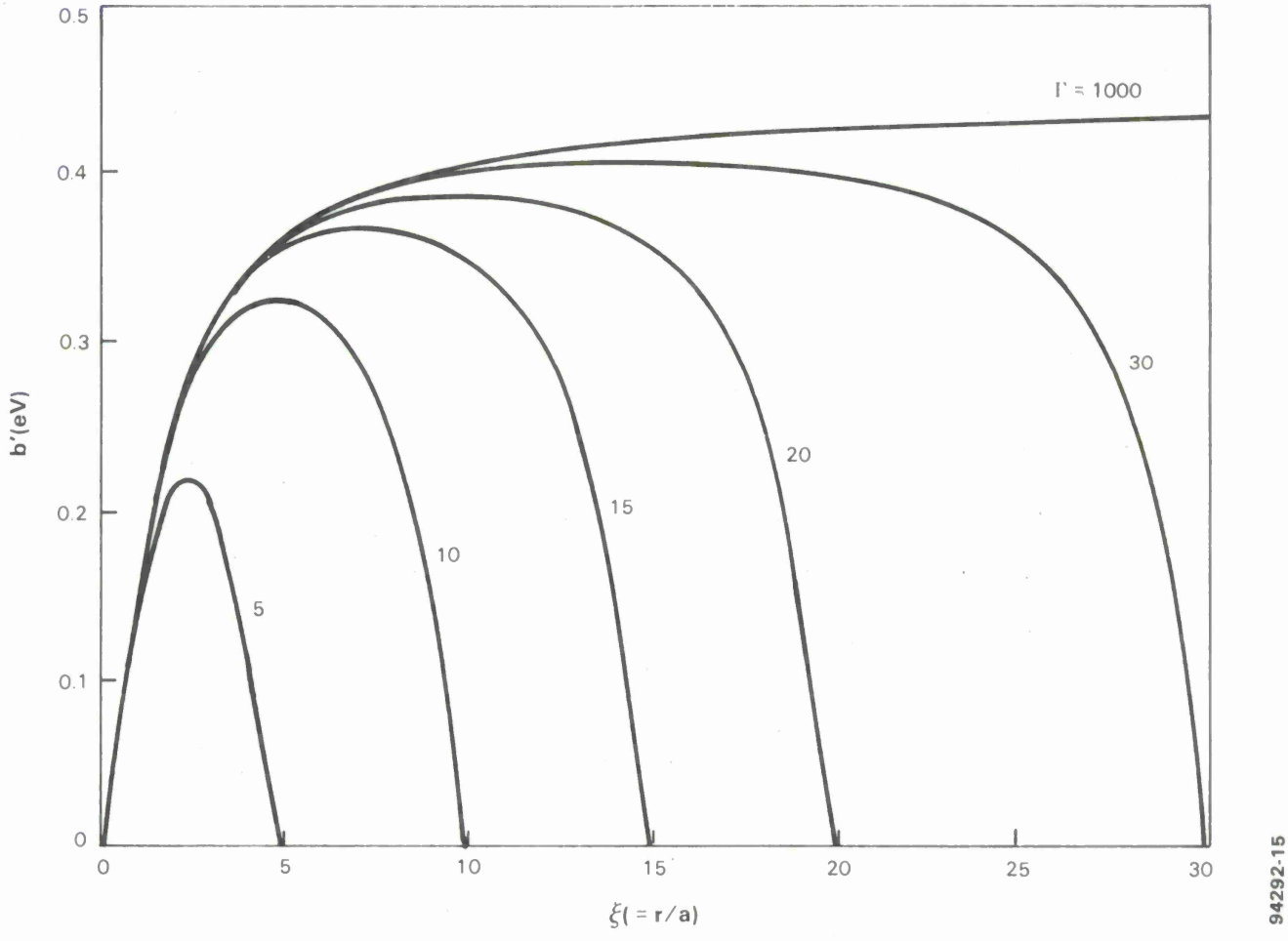

Figure 16. Polaron Coulomb attractive energy (linear four-charge approximation) E_c as a function of reduced polaron-charge displacement ξ (= r/a) from its source, for various reduced source-charge separations Γ (= R/a). Energy barriers are periodic with Γ.

where $(1/h - 1/h_o) = (1/a)[(1 + \Gamma^2 + \xi^2 + 2\Gamma\xi)^{-1/2} - (1 + \Gamma^2)^{-1/2}]$,

$(1/i - 1/i_o) = (1/a)[(1 + \xi^2)^{-1/2} - 1]$,

$(1/j - 1/j_o) = (1/a)[(1 + \Gamma^2 + \xi^2 - 2\Gamma\xi)^{-1/2} - (1 + \Gamma^2)^{-1/2}]$,

$(1/k - 1/k_o) = (1/a)[(1 + 4\Gamma^2 + \xi^2 - 4\Gamma\xi)^{-1/2} - (1 + 4\Gamma^2)^{-1/2}]$.

The symbol Γ is the reduced source separation distance (= R/a) with a lower limit of 1.0, ξ is the reduced polaron charge displacement (= r/a), and q and K are the Coulomb charge and dielectric constant, respectively. In Eq. (9), repulsive energy contributions have not been included. Since the fixed source charges are stationary and the supercurrent occurs through mutual repulsion of the mobile hole charges, with the polarons retaining their separation as they propagate, there is no net change in repulsive energy as a function of r.

For a = 4 A (c-axis distance between an A and B cation as estimated from crystallographic data) and K = 8*, for example, ΔE_c is plotted as a function of ξ in Fig. 16 to illustrate the polaron electrostatic potential barriers for various values of polaron separation R (in terms of numbers of A-O-B bond lengths). An upper limit of b' = 0.39 eV is included to suggest the appropriate range of r_p values for this system. Since $\xi_p = \Gamma/2$ represents the reduced cell radius in bond lengths (r_p/a, with a lower limit of 0.5), the Coulomb energy reaches a maximum ΔE_c^m which may be expressed as

$$\Delta E_c^m = -2(q^2/K\Gamma a)[(1 + 9\xi_p^2)^{-1/2} + (1 + \xi_p^2)^{-1/2} - (1 + 16\xi_p^2)^{-1/2} - (1+4\xi_p^2)^{-1/2} - 1] \quad . \qquad (10)$$

In Fig. 17, Eq. (10) is plotted with a b' value of 0.39 eV to indicate the range of ξ_p for which $b' \geq \Delta E_c$*. Here ξ_p would reach a maximum of 11 (i.e., $r_p \leq 44$ A), in general accord with the measured coherence length of 34 A and threshold carrier concentration of $x_t \approx 0.08$ to be discussed later.

The superconducting state could thus be viewed as the result of coupled wave functions (molecular orbitals) that extend over sections of the lattice determined by the location of A^{2+} ions

* This value for K is representative of a typical oxide dielectric. A more realistic value for the perovskite system might be somewhat larger (for the related spinel and garnet families it is in the range of 12 to 15). It may also be argued, however, that the effective $d_{x^2-y^2}$ bandwidth should be b/2, since for Cu^{2+} this band is "half-filled" in a collective-electron scheme. These changes would tend to offset each other in the above estimate of ξ_p.

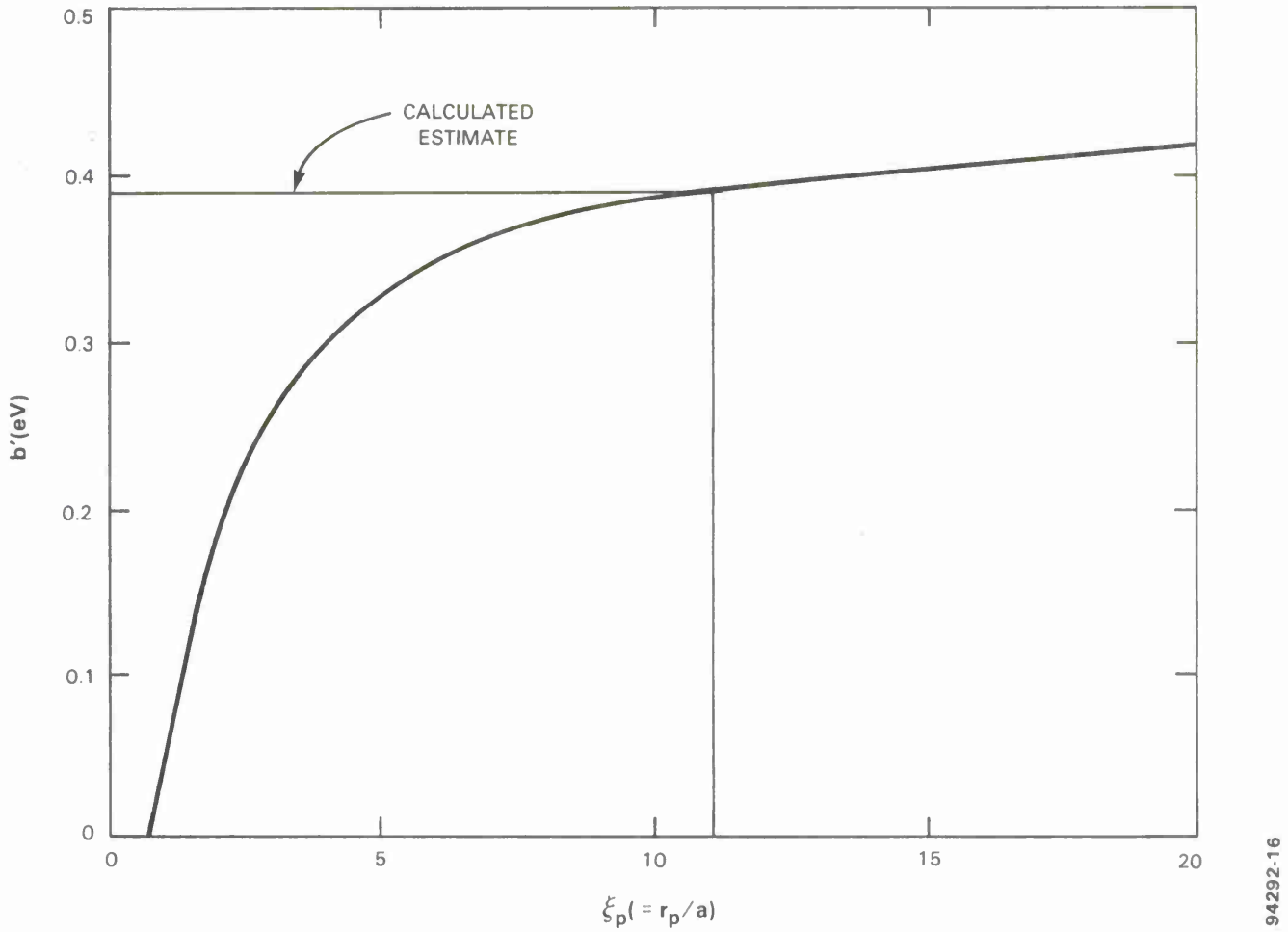

Figure 17. Energy barrier peak values E_c^m versus reduced polaron radius $\xi_p (= r_p/a)$. The calculated estimate of $b' = 0.39$ eV is included to suggest a range of ξ_p values.

or other sources that generate mixed-valence B cations, depicted in Fig. 18 for an isolated cell in a one-dimensional chain with alternating A^{2+}-A^{3+} ions. When these cells merge, the entire lattice could become superconducting at a percolation threshold, with persistent currents established as the cells form intact loops. In this sense, there would be no distinguishable Cu^{3+} ions, only probabilities of particular cation sites having +2 or +3 valences. As a consequence, the extent of superconduction would depend on the degree of dispersal (ordering) of the $Cu^{2+(3+)}$ pairs (or A^{2+} ions).

In Fig. 19, a two-dimensional lattice model illustrates the mechanism by which the superconducting state may be sustained in an x-y plane. In this idealized situation of a linear chain with polaron boundaries of only one bond length, there is a 1:3 ordering of A^{2+}-A^{3+} cations with accompanying B^{3+} ions to act as receptors for the transfer electrons. Pairing of B^{3+} ions, dictated by pairing of associated A^{2+} should be minimized. Therefore, electrostatic homogeneity is a requirement to maintain a continuous current path. Optimization of electrostatic neutrality through chemical homogeneity produces maximum Madlung energies where different ions of a common element exist in the same lattice,[33] and departures from homogeneity would represent higher energy states of the system. In opposition to electrostatic ordering, the minimization of elastic energy where cations of different size compete for the same site, and where SO or JT stabilizations require accommodation, the resulting disorder could become an important factor in determining the onset of superconductivity, as discussed in the sections that follow.

B. Resistivity in Superconducting Oxides

For transition-metal oxides, there are two mechanisms for electron transfer between mixed-valence cations, one mediated by covalent bonding and the other by lattice vibrations.* In

* As pointed out by Goodenough,[12] spin collinearity (ferromagnetism) in these mixed-valence situations allows an electrostatic excitation energy $U = 0$ and a tunnelling transfer probability proportional to the square of the orbital interaction energy and inversely proportional to the polaron trapping energy (i.e., $\tau_{tun}^{-1} \propto b^2/E_{hop}$). Thus, in the special case of limiting large orbital interaction energy and small trapping energy, this tunnelling mechanism at low temperatures could produce orbital electron transfer. At low temperatures the ratio of conductivities $\sigma_{tun}/\sigma_{hop} \sim (b/E_{hop})\exp(E_{hop}/kT)$ and σ_{tun} should be the dominant mechanism where b/E_{hop} is large. Since strong covalency will produce a large b and weak magnetic exchange energy will yield a small but non-vanishing E_{hop}, $Cu^{2+(3+)}$ ions are logical candidates to fill these requirements. For a detailed examination of polaron conduction mechanisms, the reader is encouraged to consult Sections II.E.3 and IV.B.3 of Reference 12.

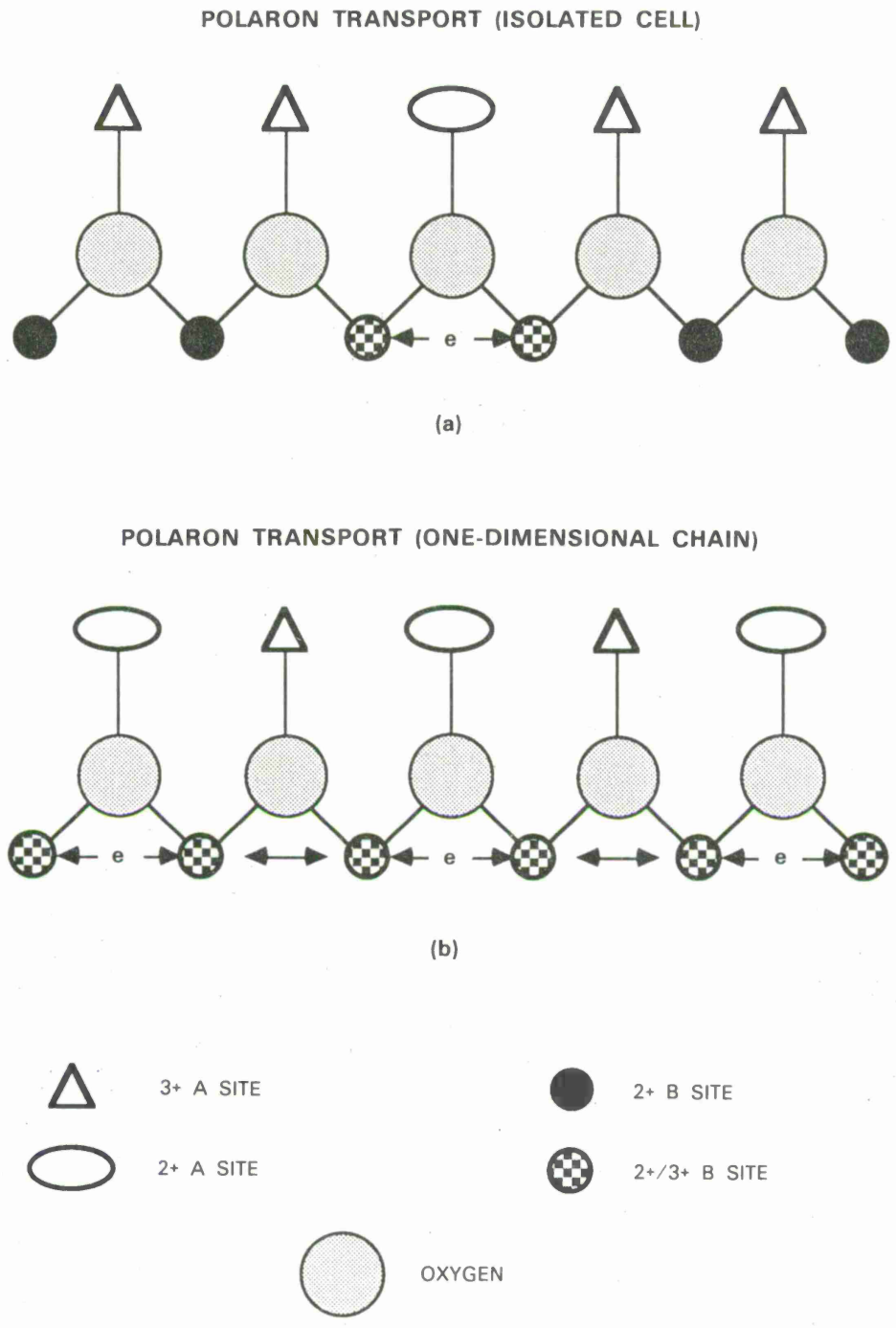

Figure 18. Geometrical schematics of electron delocalization: (a) isolated A^{2+} ion, and (b) one-dimensional chain with alternating A^{2+} and A^{3+} ions.

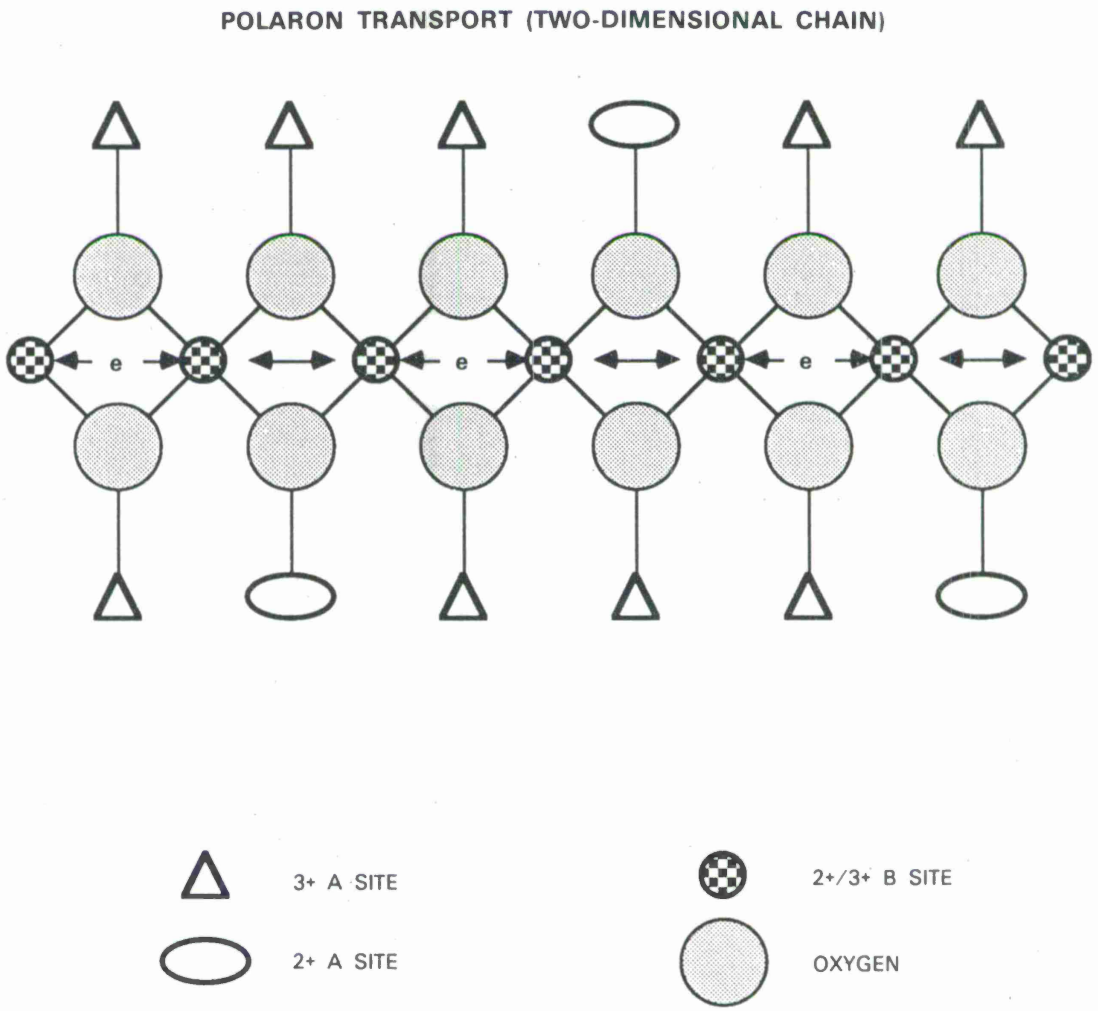

Figure 19. Two-dimensional schematic of continuous orbital transfer with density ratio of $A^{2+}/A^{3+} = 1/3$.

competition with the orbital transfer mechanism which is driven by the covalent orbital interaction, normal conduction in transition-metal oxides results from thermal excitation, where the electron leaves its orbit on one cation and diffuses or hops to a higher-valence cation in a different lattice site, with the resulting current limited by a finite mobility.[34] Since the normal resistivity decreases with temperature, mixed-valence oxides are considered to be semiconductors (hopping semiconductors), but differ from conventional Fermi band-theory semiconductors in the temperature dependence of the mobility.*

In Fig. 20, the physical situation is sketched in an x-y plane to illustrate these alternative conduction mechanisms, described more fully in Appendix C. For metal oxides with mixed-valence cations (e.g., $Li^{1+}_{x}Cu^{2+}_{1-2x}Cu^{3+}_{x}O$), a measurable electrical resistivity exists and was determined by Heikes and Johnston[35] as

$$\rho_n = \rho_o \exp(E_{hop}/kT) \quad , \tag{11}$$

where $\rho_o \propto (Ne\mu_n)^{-1}$, and N is the nominal carrier density. Since the incidence of a successful hop is proportional to the product of the carrier and receptor concentrations,[36] the effective carrier concentration x must be reduced by the factor (1 - x). The mobility $\mu_n = eD/kT$, where the diffusion constant $D = d^2/\tau_{hop}$, with d as the diffusion length (average hop distance) and τ_{hop} as the carrier lifetime (inverse hopping frequency, related to ν). The symbols e and k represent the electron Coulomb charge and Boltzmann constant, respectively. Since d should increase with the density of trapping centers, i.e., the jumps will get longer if the competition for available receptor sites increases, d will be assumed to vary modestly as $x^{1/2}$ over the range of interest in this discussion. As a result, Eq. (11) will be expressed as

---

* There are important differences between conventional semiconductors, i.e., Ge and Si, and mixed-valence oxides. The former feature covalent bonding which dictates a band-theory analysis. Ions do not exist in the ground state of these materials, and carriers consist of intrinsic electron-hole pairs or charges from ionized impurities, with external (thermal) excitation required in either case. With ionic-bonded oxides, carriers arise from mixed valence independent of temperature, but propagate through a type of ionization/recombination process governed by $\exp(-E_{hop}/kT)$. In the band-model semiconductors, the carrier density is controlled by kT and the mobility is relatively fixed; in the hopping semiconductors, it is the reverse situation that prevails.[36]

$$\rho_o = C\,kT/x^2(1 - x) \quad , \tag{12}$$

and

$$\rho_n = [C\,kT/x^2(1-x)]\,\exp(E_{hop}/kT) \quad , \tag{13}$$

where C is a proportionality constant in appropriate units.

The above arguments apply to the normal case where electron hopping is the only conduction mechanism. If it is assumed that the material is made up of a mixture of normal (with mobility μ_n) and superconducting (with $\mu_s \rightarrow \infty$) cells, the density of normal and superconducting electrons in an ordered system would be given respectively by

$$n_n = N\,\exp(-E_{hop}/kT) \quad , \tag{14}$$

and

$$n_s = \eta N\,[1 - \exp(-E_{hop}/kT)] \quad , \tag{15}$$

where $\eta \leq 1$ is the efficiency of the orbital transfer mechanism and is related to the orbital interaction parameter b'. Since the model involves only isolated polarons, Fermi statistics that are required to describe state occupancies of collective electrons are not invoked here. Each mobile polaron has a single charge carrier that does not have to compete for an available state; when it moves into an adjacent cell, it inherits the environment of the exiting polaron that is being expelled through electrostatic repulsion.

The basic concept is stated as follows: *where d-orbital interaction between mixed-valence cations satisfies the orbital transfer condition ($b \geq E_{hop}$) in a system where polaron cells can merge, superconduction is an operating mechanism, with quenching occurring by thermal excitation of the electrons out of their bonding orbitals into the semiconductor hopping mode.* The role of phonons is thus reversed here: instead of making superconduction possible by mediating the formation of electron pairs, lattice vibrations disrupt superconduction by activating the electrons out of their orbital states into the hopping conduction mode.

To estimate the resistivity above the transition or critical temperature, consider the elementary approximation of a cylinder of length L and cross-sectional area A sketched in Fig. 21. If all of the uniformly dispersed cells are grouped in two separate regions, i.e., as two resistors in series, the total resistance would be approximated by

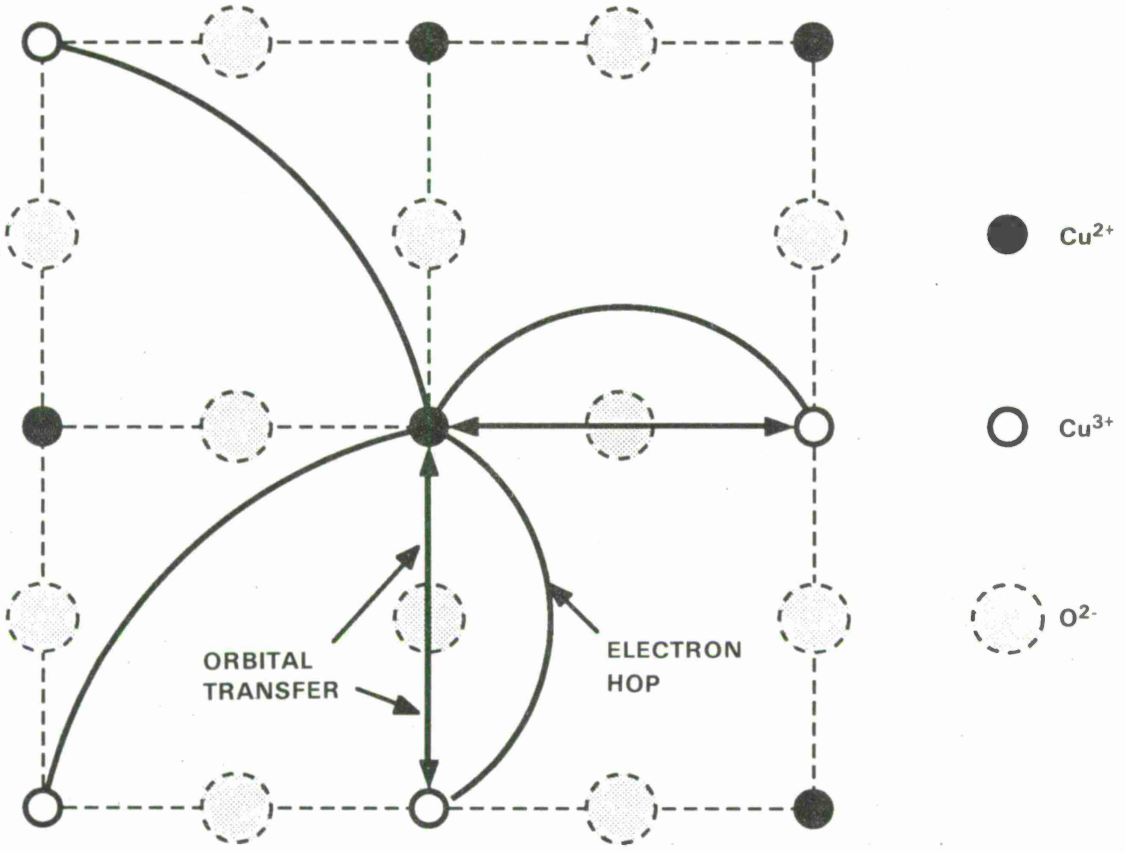

94292-19

Figure 20. Alternative electron transfer mechanisms: orbital delocalization between nearest neighbors and conventional semiconductor hopping between both nearest and farther neighbors in the x-y plane.

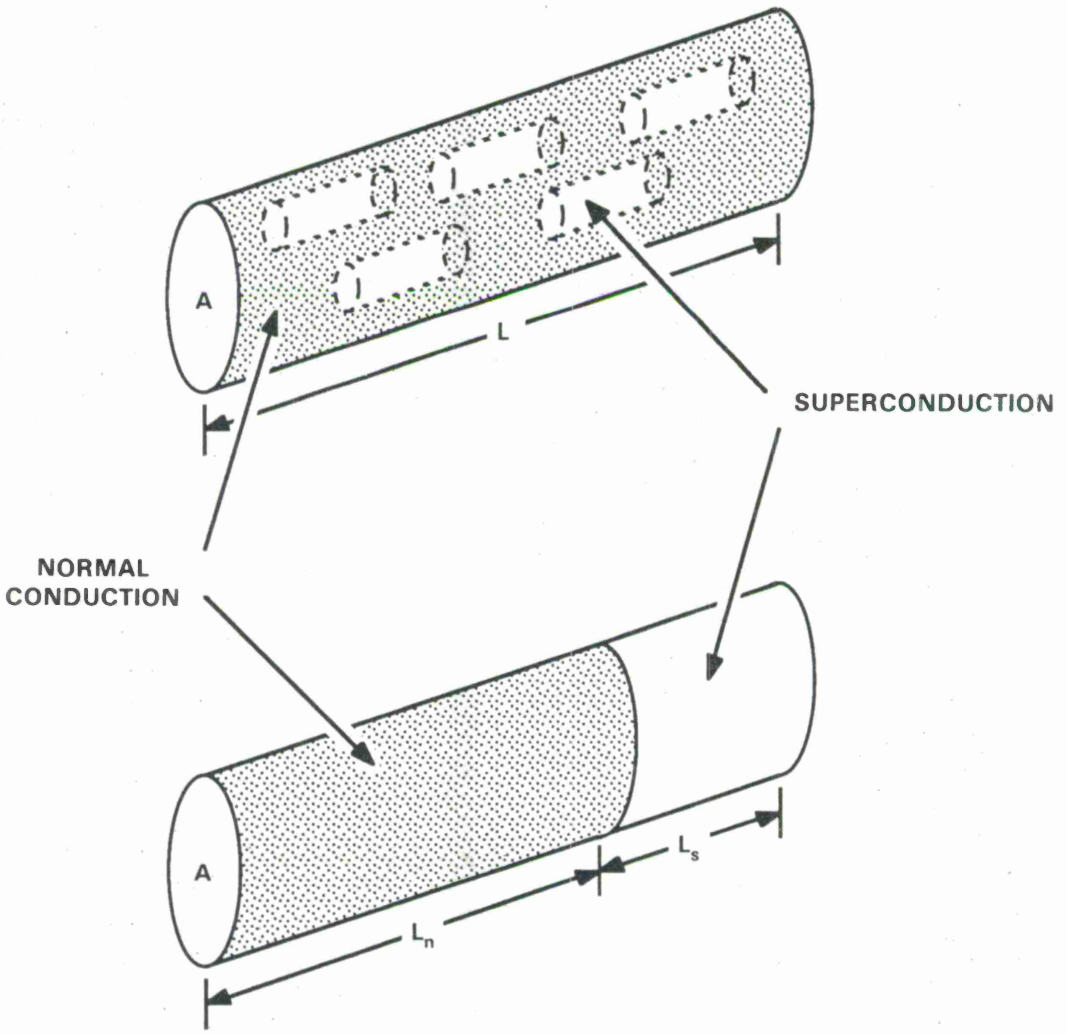

Figure 21. Simple model of the segregation of superconducting and normal regions for the purpose of estimating electrical resistivity above the transition temperature.

$$R = \rho L/A = \rho_n L_n/A + \rho_s L_s/A \quad . \tag{16}$$

Since $\rho_s = 0$ (assuming optimum transfer conditions),

$$\rho = \rho_n[L_n/(L_n + L_s)] = \rho_n[(L - L_s)/L] \quad . \tag{17}$$

Since L and L_s are respectively proportional to N and n_s, and Eq. (17) will be expressed as

$$\rho = \rho_o [\eta + (1 - \eta) \exp(E_{hop}/kT)] \tag{18a}$$

or

$$\rho = [C\, kT/x^2(1-x)] [\eta + (1 - \eta) \exp(E_{hop}/kT)] \quad . \tag{18b}$$

In the limiting cases of $\eta = 0$ (no superconduction) and $\eta = 1$ respectively, Eq. (18) reduces to Eqs. (11) and (12):

$$\rho = \rho_o \exp(E_{hop}/kT) \tag{19a}$$

and

$$\rho = \rho_o = C\, kT/x^2(1 - x) \quad . \tag{19b}$$

From the arguments in Appendix C, Eq. (18) can be refined to include cation clustering effects by incorporating the results for n_s and E_{hop} from Eqs. (C-2) and (C-3), with the result that

$$\rho = [C\, kT/x^2(1 - x)] [P + (1 - P) \exp(E_{hop}/kT)] \quad (\text{for } \eta = 1) \quad , \tag{20}$$

where $E_{hop} = E_{hop}{}^o [1 - 2(1 - P)]$ and P is the B-cation clustering probablity, as defined in Appendix C. It should be noted here that the hopping mechanism would be less sensitive to ordering, and the (1 - x) in Eq. (20) is not modified by the probability variable, since a random distribution, i.e., P = 1, should represent a reasonable average for this conduction mode. Both Eqs. (19) and (20) indicate a metallic temperature dependence with approximately linear slope that varies inversely with the density of charge carriers. These results are in general accord with the experimental results reported for the LaSrCu and YBaCu perovskite systems and, in particular, Eq. (20) predicts some of the more subtle variations in resistivity at lower temperatures suggested by

the Tarascon et al. data.[4]

In the context of the above, the temperature dependence of normal conduction is explainable by the residual amounts of local superconductivity. It was pointed out earlier that semiconducting Fe spinels exhibit the expected increasing conductivity with temperature, while the superconducting Cu perovskites have the opposite temperature dependence. Since the Cu perovskites feature superconducting cells above the transition temperature that decrease in number as the temperature is increased, the decrease in normal conductivity occurs because of the steady removal of the "short circuits" as more of the transfer electrons become activated to the normal state. With the strong antiferromagnetic exchange coupling of the $Fe^{2+(3+)}$ pairs in ferrites, no superconducting cells should be anticipated and only normal conduction is present, with the population of hopping electrons causing increased conductivity in typical semiconductor fashion at higher temperatures.

To compare this phenomenological theory with experiment, the results[4] for the $La^{3+}_{2-x}Sr^{2+}_{x}(Cu^{2+}_{1-x}Cu^{3+}_{x})O_4$ system with x = 0.10, 0.15, and 0.30 are plotted in Fig. 22 together with the calculations based on Eq. (20). Values of C = 1.60 mΩ cm/eV, E_{hop}^{o} = 7.7 meV and α = 0.6 were found to provide a good fit. A similar agreement between theory and the data of Cava et al.[5] for $Y^{3+}Ba^{2+}_{2}(Cu^{2+}_{3-3x}Cu^{3+}_{3x})O_y$ for y = 6.9 (representing an average x = 0.267 for charge balance) is shown in Fig. 23. In this case, C = 1.35 mΩ cm/eV, E_{hop}^{o} = 7.7 meV and α = - 0.11.

C. Critical Temperature

From the arguments presented in the previous sections, orbital electron transfer may be considered as a resistanceless conduction mechanism that can be quenched by thermal activation of electrons to the normal state. In effect, the superconducting mode acts as a thermally controlled "short circuit" to the resistance of the normal conduction path, in a manner similar to the "two-fluid model" of Gorter and Casimir.[37] It is logical that for widespread continuous superconduction to exist, a threshold density n_t of transfer pairs (polarons) must be reached.

For a density N of uniformly dispersed $B^{2+(3+)}$ pairs (i.e., ideal ordering), the density n_s of superconducting electrons would be given by Eq. (15). If the superconducting transition occurs when $n_s = n_t$ (the minimum required $B^{2+(3+)}$ pair density), then the critical temperature may be estimated by

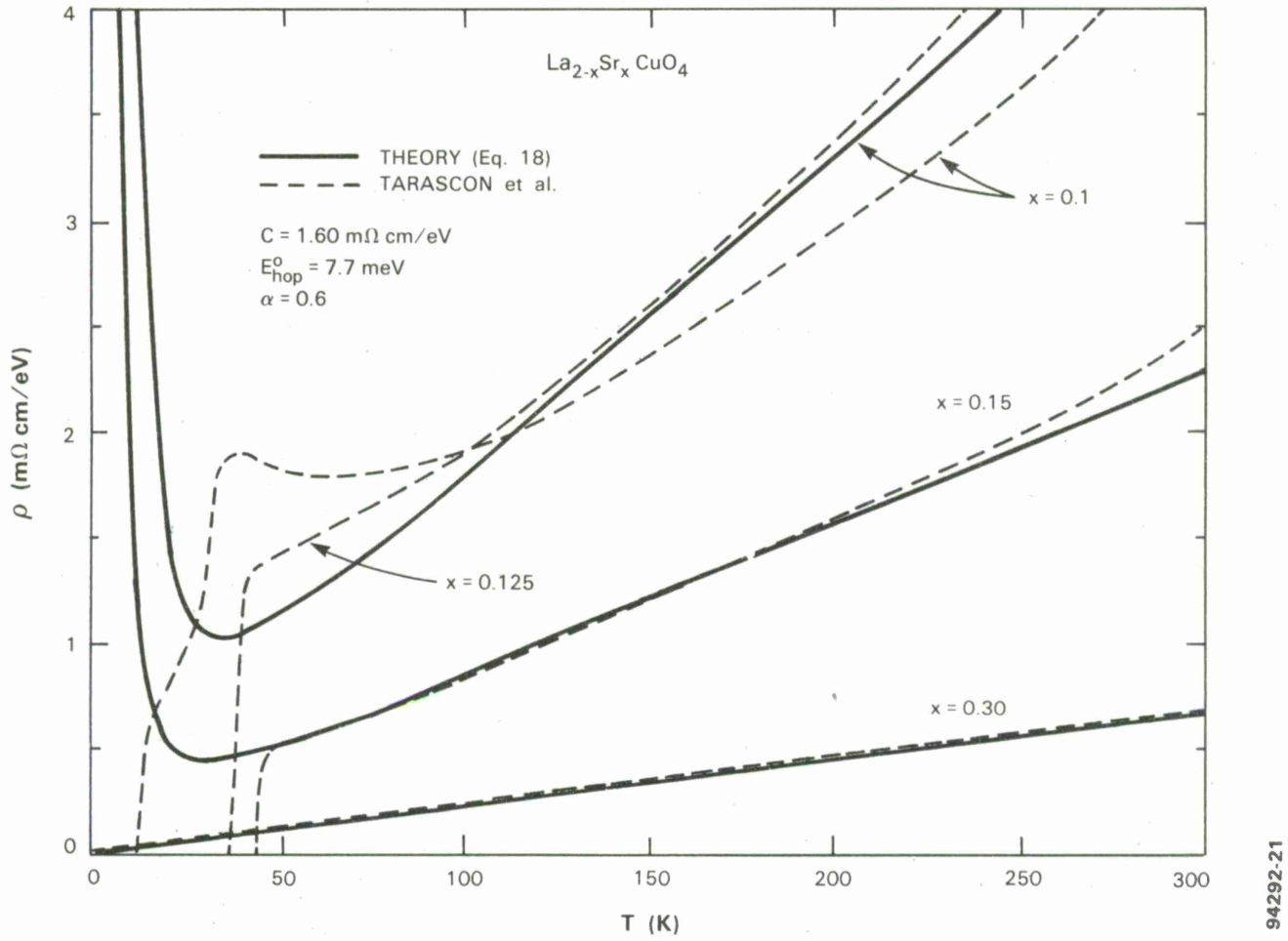

Figure 22. Comparison of theory and experiment for ρ as a function of T: $La^{3+}_{2-x}Sr^{2+}_x(Cu^{2+}_{1-x}Cu^{3+}_x)O_4$. (Data of Tarascon et al., Reference 4)

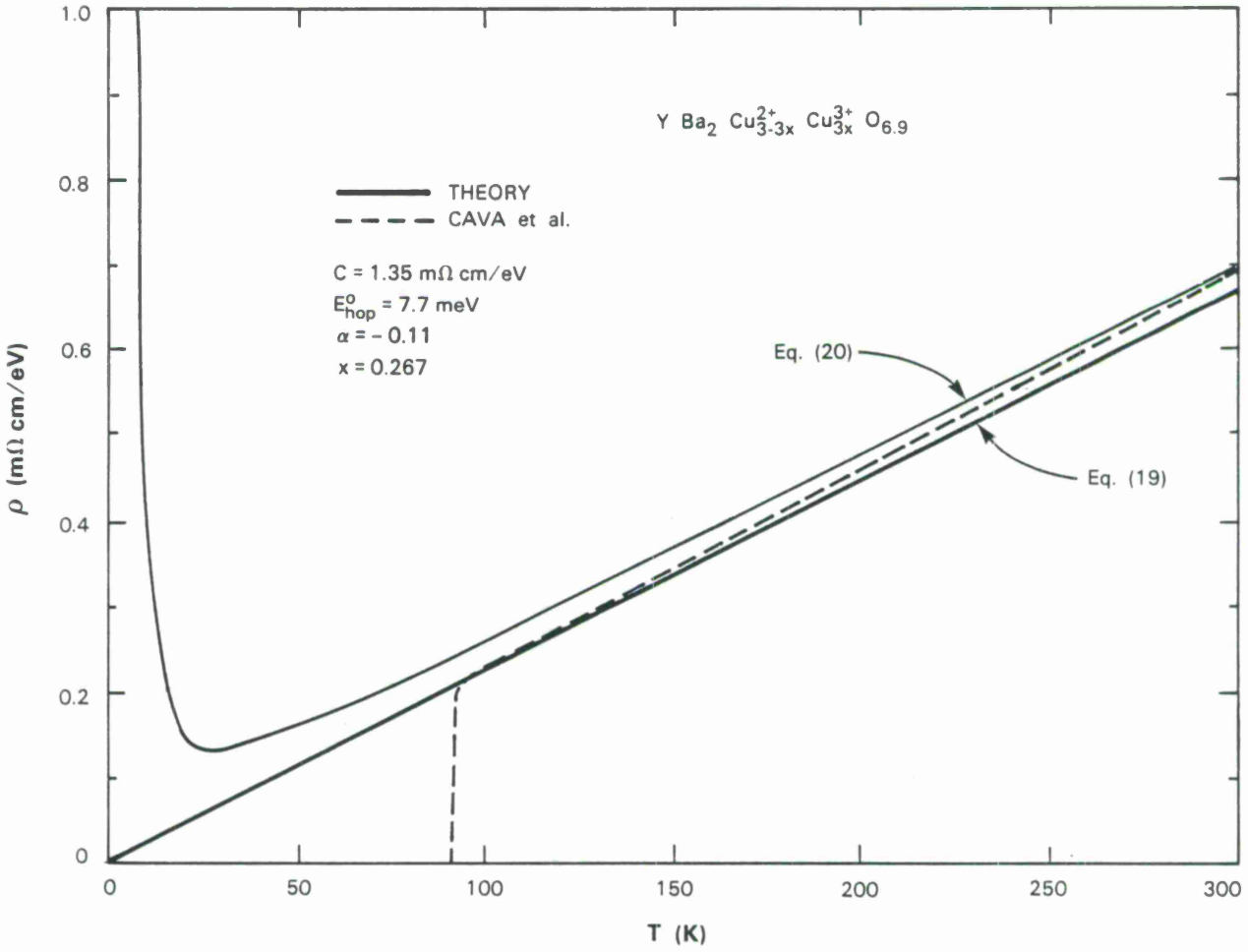

Figure 23. Comparison of theory and experiment for ρ as a function of T: $Y^{3+}Ba^{2+}{}_2(Cu^{2+}{}_{3-3x}Cu^{3+}{}_{3x})O_y$. (Data of Cava et al., Reference 5).

$$T_c = \frac{E_{hop}}{k \ln(1 - n_t/\eta N)^{-1}} \quad . \tag{21}$$

As discussed in Appendix C, Eq. (21) represents the case of perfect B-cation ordering. The more complete expression contains the probability P that accounts for the effects of cation disorder and is obtained by substituting Eqs. (C-2) and (C-3) into Eq. (21):

$$T_c = \frac{E_{hop}}{k \ln(1 - n_t/\eta NP)^{-1}} = \frac{E_{hop}}{k \ln(1 - x_t/\eta xP)^{-1}} \quad . \tag{22}$$

Figures 24 and 25 present results computed from Eq. (22) fitted to data from measurements on the LaSr and YBa systems. In both cases, ideal transfer efficiency was assumed ($\eta = 1$) and $x_t \approx 0.08$.* In Fig. 24, T_c versus x as calculated from Eq. (22) is compared with the reported data[4] for $La^{3+}_{2-x}Sr^{2+}_x(Cu^{2+}_{1-x}Cu^{3+}_x)O_4$. The agreement for this system, where T_c reaches a maximum of 39 K at x = 0.16, is optimum with $E_{hop}^o = 7.7$ meV and $\alpha = 0.6$, the same parameters used for the normal resistivity temperature dependence fitting in Fig. 22. For the $RE^{3+}Ba^{2+}_2(Cu^{2+}_{3-3x}Cu^{3+}_{3x})O_y$ system plotted with data[38] in Fig. 25, showing a maximum T_c of 94 K at y = 7.08 [corresponding to an x value in the Cu(2) planes of 0.27, as determined by Eq. (D-2)], the fit is also optimum with the parameter values used in the ρ calculations of Fig. 23, $E_{hop}^o = 7.7$ meV and $\alpha = -0.11$.

As discussed in Appendix D, the ordering of Y and Ba on separate A-O_4 planes may create different oxygen vacancy distributions, thereby altering both x and α values above and below the nominal for the Cu-O_4 planes sandwiched between (i) two Ba-O_4 planes and (ii) one Y-O_4 and one Ba-O_4 plane. As a consequence, there may be more than one superconducting system in the same specimen, with different effective x and α values. This effect could account for the reported anomalies and discontinuities in T_c at low x values.[39]

* It was assumed that a percolation threshold value of x would be slightly less than the lowest value x = 0.1 for which superconductivity was reported in the LaSr system. The assumed minimum concentration ($x \approx 0.08$) suggests that the maximum radius of a superconduction cell may be as large as seven Cu-O-Cu bond distances. In the context of the analysis in Section 3D, $x_t \sim 1/2\xi_p$, and falls within the range of ξ_p estimates calculated in Section 3D. With coherence lengths of 34 A (equivalent to about eight Cu-O-Cu bond distances) reported for the basal planes of the YBa system,[40] this threshold concentration is also consistent with the magnitude of the coherence length.

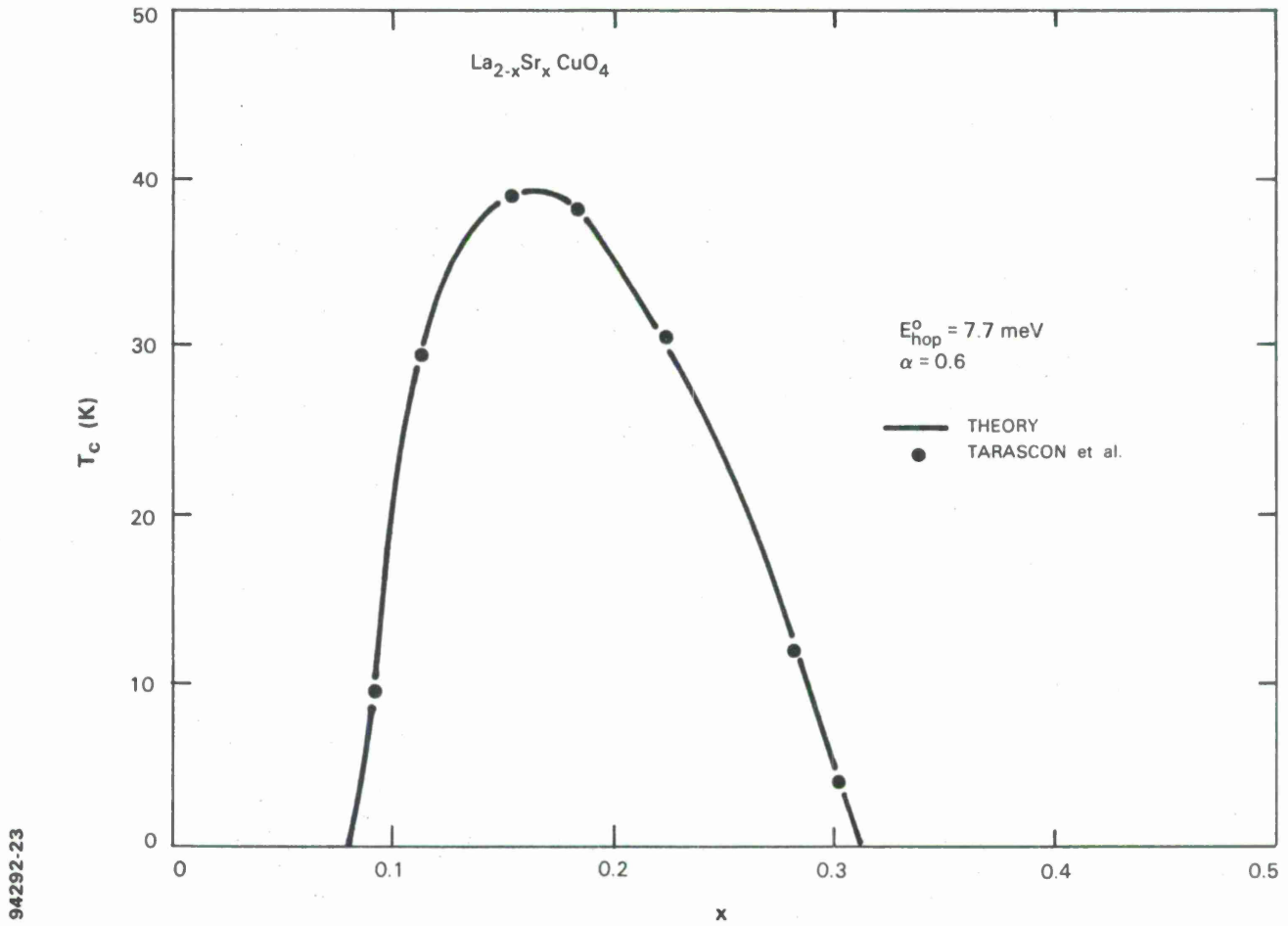

Figure 24. Comparison of theory and experiment for T_c as a function of x: $La^{3+}_{2-x}Sr^{2+}_x(Cu^{2+}_{1-x}Cu^{3+}_x)O_4$. (Data of Tarascon et al., Reference 4)

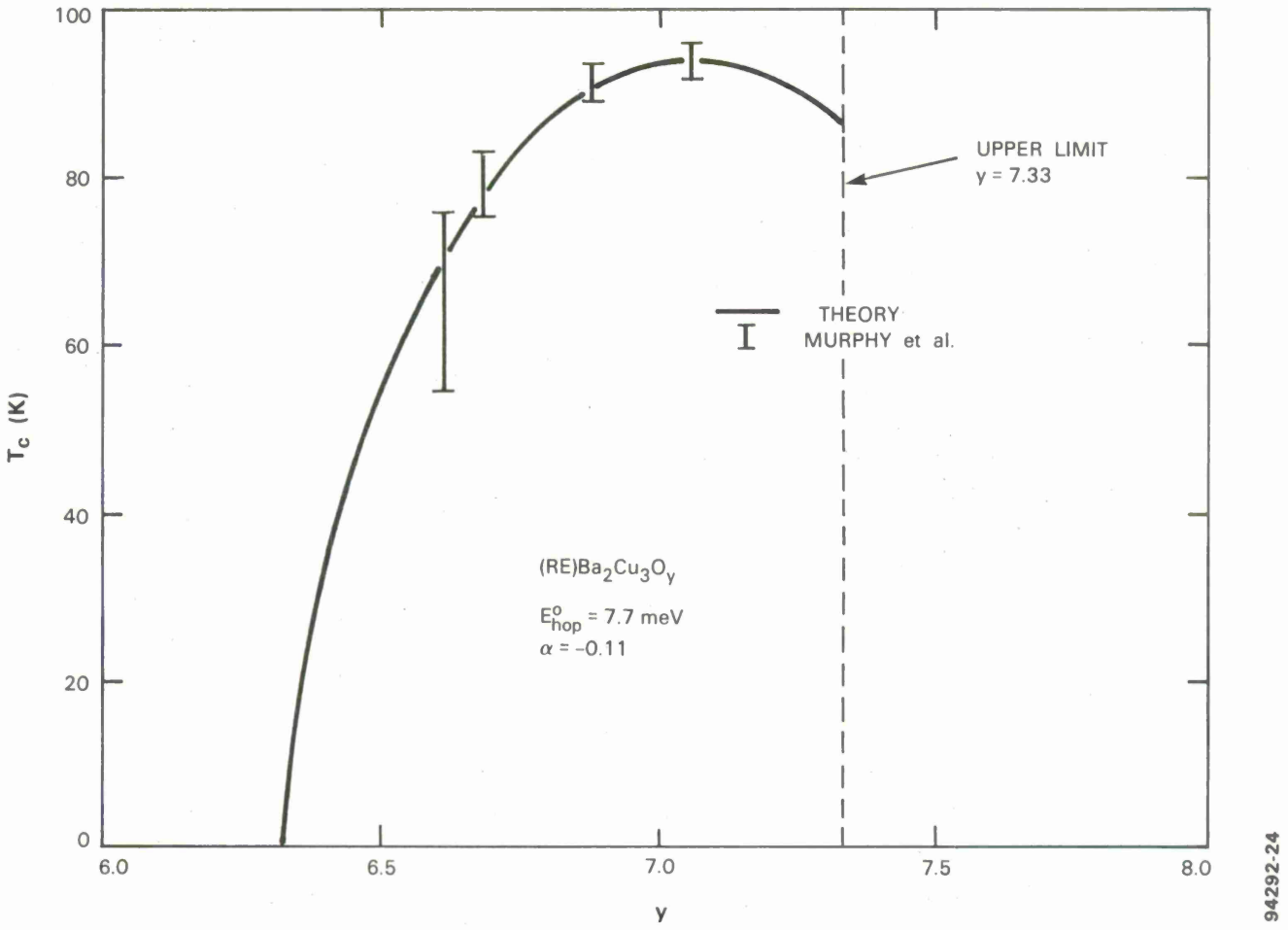

Figure 25. Comparison of theory and experiment for T_c as a function of y: $RE^{3+}Ba^{2+}{}_2(Cu^{2+}{}_{3-3x}Cu^{3+}{}_{3x})O_y$. (Data of Murphy et al., Reference 38). The upper limit of y = 7.33 is discussed in Appendix D.

The sensitivity of T_c to ordering may be seen in Figs. 26 and 27, where T_c is plotted as a function of α with x = 0.16 and 0.27, and as a function of x for selected values of α between -1 and +1, respectively. In Fig. 26, the data points[41] on the x = 0.27 curve for $Y(Ba_{1-z}Sr_z)_2Cu_3O_y$ suggest that $\alpha \rightarrow 0$ with a 40 % substitution of Sr for Ba (it is assumed that Sr and Ba share the same plane according to Appendix D); the $T_c \approx 30$ K data point on the x = 0.16 curve is from the original work[1] on $La_{2-x}Ba_xCuO_4$ and suggests that α begins to approach 1 with the large Ba^{2+} ion in place of Sr^{2+}. Both situations point to greater disorder, the former likely caused by elastic compensation from the ionic size mismatch, and the latter from the interplanar ordering considerations discussed in Appendix D. A more complete picture of the interdependence of T_c, x, and α is presented in Fig. 27. As $\alpha \rightarrow -1$, the curves suggest that T_c values exceeding 300 K could be obtained with improved cation ordering.

As a final comment regarding the relationship between the critical temperature and cation ordering, the following observation will be made about the shape of the ρ versus T curve. At the critical temperature for a homogeneous material, i.e., uniform α throughout, the resistivity should fall vertically to zero (or some minimum residual value) as the superconducting state is percolated simultaneously across the specimen. In practical cases, particularly in multicomponent systems such as these oxides, homogeneity is imperfect and the ordering parameter varies in the sample. As a consequence, there exists a distribution of T_c values manifested by the rounded knee and more gradual transition (see Fig. 28) to the superconducting state (a type II or "hard" superconductor). Evidence of this phenomenon is suggested in the measured curves of Fig. 22, and also in numerous other examples from the burgeoning literature on this subject. Therefore, the problem of producing a high-temperature superconductor with a well-defined transition becomes a task of not only optimizing the value of α, but just as important, controlling its uniformity throughout the material.

D. Critical Magnetic Field and Current Density

The application of an external magnetic field will quench superconductivity when it exceeds a threshold value H_c. The mechanism for this effect is believed to relate to the perfect diamagnetism property of the superconducting current, which is manifested by the expulsion of all magnetic flux from the material in the superconducting state (Meissner effect). As a consequence, the current may be sustained only where the applied field does not exceed the diamagnetic field induced by the

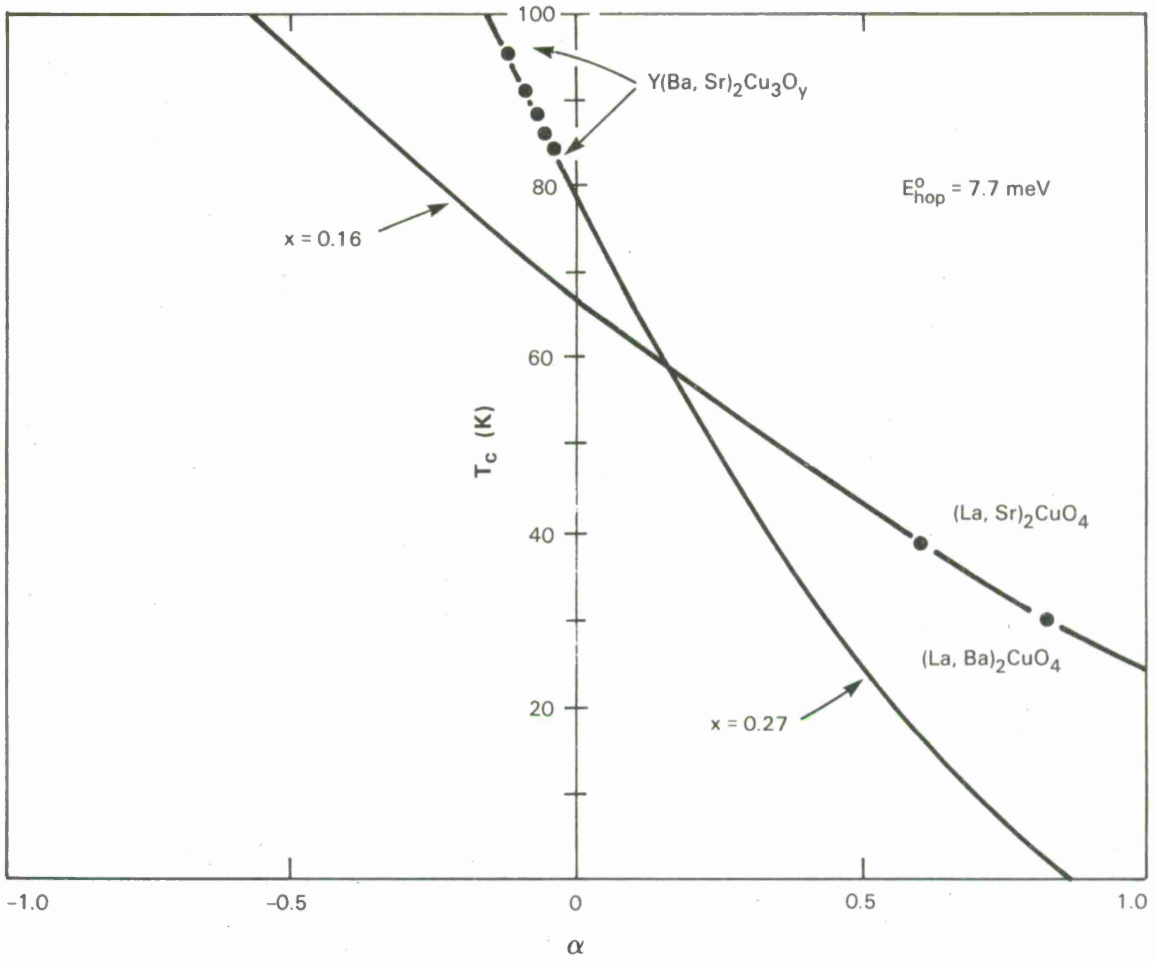

Figure 26. Theoretical estimates of T_c as a function of α for values of x = 0.16 and 0.27 to indicate the potential effects of improved ordering on the magnitude of the critical temperature. For x = 0.16, data are from Bednorz and Muller, Reference 1, and for x = 0.27, data are from Wada et al., Reference 41.

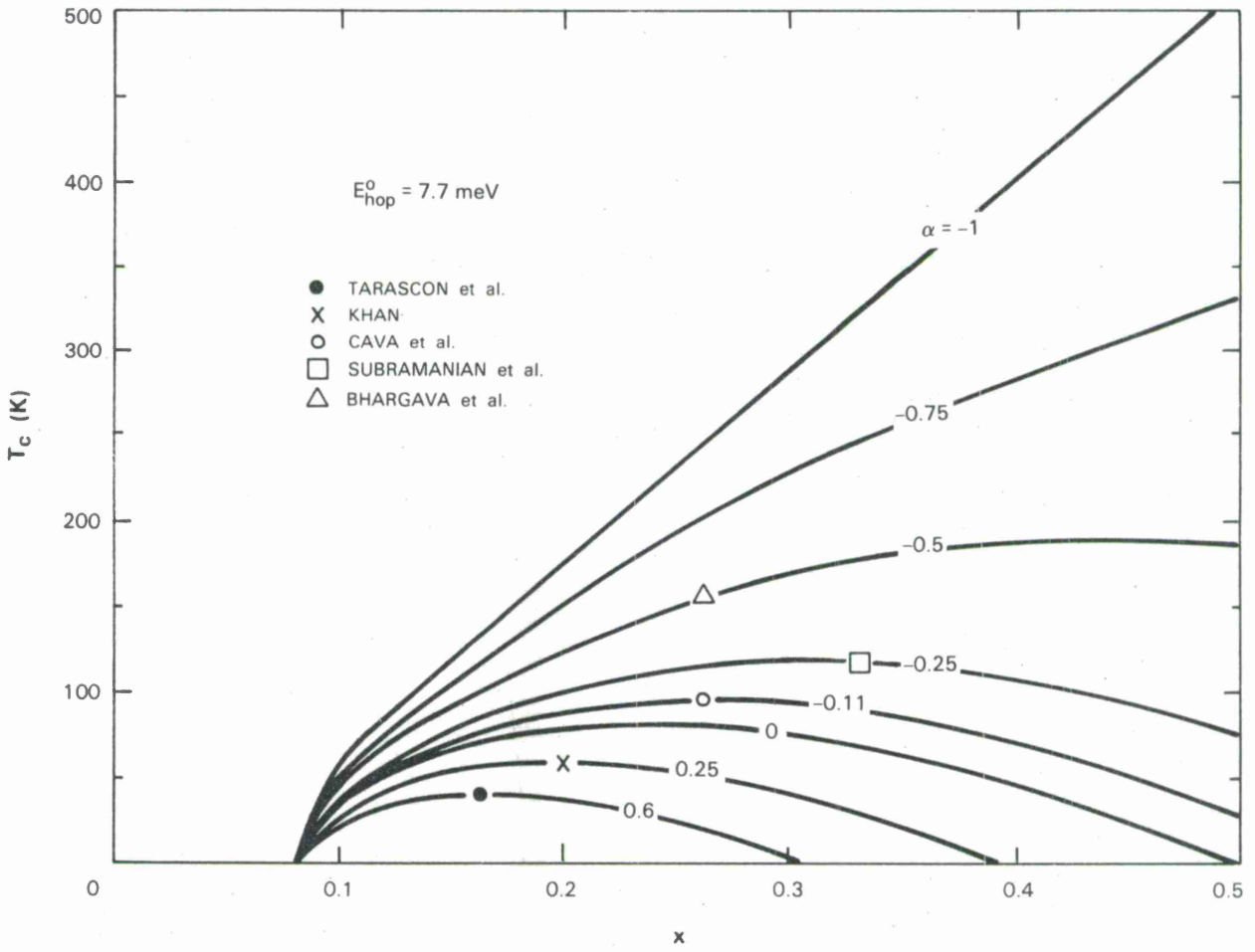

Figure 27. Computed values of T_c plotted as a function of x for full range $-1 \leq \alpha \leq 1$. Experimental data points: T_c = 39 K for α = 0.6 (Reference 4), T_c = 66 K for α = 0.25 (Reference 47), T_c = 94 K for α = -0.11 (Reference 5), T_c = 116 K for $\alpha \approx$ -0.25 (Reference 52), and T_c = 159 K for $\alpha \approx$ -0.5 (Reference 48).

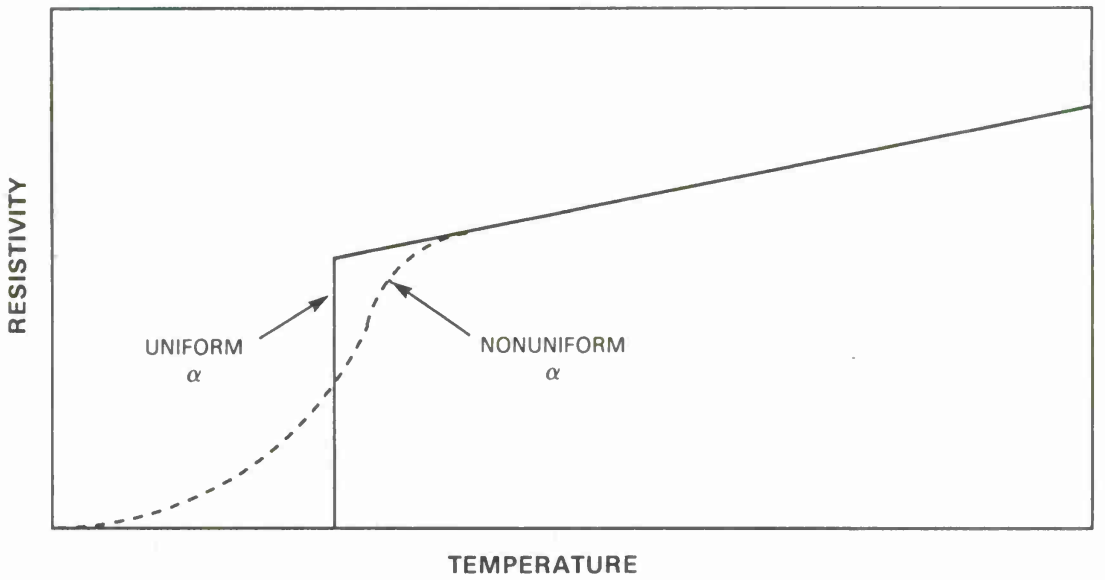

94292-36

Figure 28. Sketch of the normal to superconduction transition region, showing the influence of inhomogeneous α.

current. Any combination of insufficent superconducting current density or excess magnetic field will therefore destroy the superconducting state. From thermodynamic arguments, the following phenomenological relation between magnetic field and temperature has been found to fit data in many cases:[42]

$$H_c/H_c^o = 1 - (T/T_c)^2 \quad , \tag{23}$$

where H_c^o is the thermodynamic critical field extrapolated to T = 0. For the metallic elements, an empirical relation $H_c^o \approx 60\ T_c^{1.3}$ may be derived from experiment.[43]

In terms of the present model, the superconducting current density I_s would be proportional to the density of transfer carriers n_s from Eq. (C-2) and the ratio of current density to critical current density would be given by

$$I_s/I_t = n_s/n_t = \frac{[1 - \exp(-E_{hop}/kT)]}{[1 - \exp(-E_{hop}/kT_c)]} \quad , \tag{24a}$$

or

$$I_s/I_t = n_s/n_t = \frac{[1 - \exp(-W/V)]}{[1 - \exp(-W)]} \quad , \tag{24b}$$

where $W = E_{hop}/kT_c$ and $V = T/T_c$.

For the magnetic effects described above, the critical field will be considered as proportional to the excess electron density over the critical value, i.e., $n_s - n_t$, and the thermodynamic field would then be proportional to $\eta N - n_t$, with the result that

$$H_c/H_c^o = (n_s - n_t)/(\eta N - n_t) = 1 - \exp[(E_{hop}/kT) - (E_{hop}/kT_c)] , \qquad (25a)$$

or

$$H_c/H_c^o = 1 - \exp(W/V - W) \quad . \qquad (25b)$$

In Eqs. (24) and (25), there is an implicit assumption that the superconducting electron velocity is constant over the temperature and electron density ranges. Variations in velocity undoubtedly are present and would directly affect the nature of these simple relations. In this model, T_c is dependent on the effective carrier concentration x in addition to the activation energy E_{hop}, which also varies with x. For these oxide systems, therefore, a universal relation between H_c/H_c^o and T/T_c, as stated in Eq. (23) should not be expected. In Fig. 29, curves for these equations are plotted together with that of Eq. (23) for comparison. The values W = 1.04 and 0.45 correspond to the optimum T_c cases for the LaSr and YBa systems, respectively, with the effective $E_{hop} \sim 5$ meV in both cases.

From these relations for critical temperature, magnetic field, and current density as functions of polaron activation energy, the dependence on ionic or isotopic mass (referred to as the isotope effect) may be established from the discussion in Section 3D. If $E_{hop} \propto M^{-1/2}$, it follows that T_c also varies as $M^{-1/2}$, while for H_c/H_c^o and I_s/I_t the dependence is somewhat less direct, as dictated by Eqs. (24) and (25) when the substitution is made for E_{hop}.

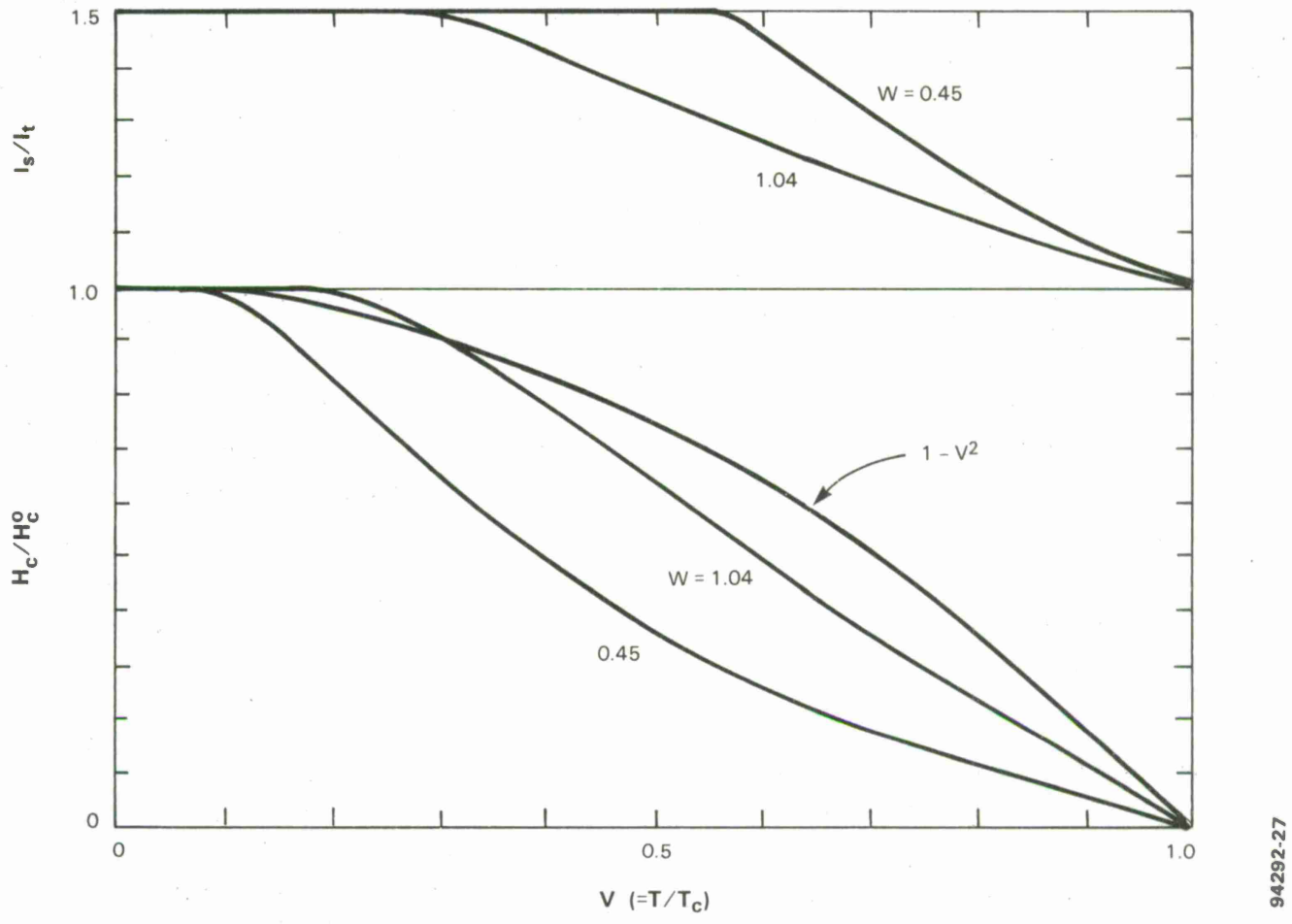

Figure 29. Theoretical estimates of I_s/I_t and H_c/H_c^o as functions of U (= T/T_c) for W = 0.45 (YBa system) and 1.04 (LaSr system).

5. SUPERCONDUCTING OXIDE SYSTEMS

A. General Criteria and Transfer-Pair Candidates

In summary, the foregoing analysis suggests that superconductivity may occur in select transition-metal oxides through the merging of itinerant polaron cells made possible by a uniform dispersal of stationary cations (or defects) of varying valence. Some idealized general conditions for continuous orbital electron transfer may now be established:

1. The initial and final states of the electron transfer must be virtually identical in energy.
   a. Mixed-valence cations of the same element must occupy the same sublattice to form isolated polarons at low concentrations.
   b. Crystallographic identity should exist between the transfer cation sites; SO and/or JT stabilizations (if present) should be cooperative and similar for both sites.
   c. Ferromagnetic order or magnetic disorder (including dynamic spin fluctuations associated with the electron transfers) permit delocalization transfer. Static antiferromagnetic ordering, however, requires a spin-flip excitation energy ($U \neq 0$).

2. For polarons to be mobile, the orbital exchange energy between transfer ion pairs must exceed the polaron activation energy (i.e., $b \geq E_{hop}$).
   a. To maximize b values, the greatest orbital wave function overlap (e_g-pσ-e_g bonding) is desirable, by larger radial factors and shorter B-O-B or B-B bond lengths.
   b. From a geometrical standpoint, e_g-pσ-e_g may be obtained from 180-degree bond formations; an alternative source of large b would be direct t_{2g}-$t_{2g}\sigma$ overlaps in 90-degree formations.
   c. Magnetic interactions that arise from exchange between the transfer pair (J_{PL}) and among lattice ions (J_{LL}) contribute to E_{hop}.
   d. Differences in ligand-field and ionic crystal energy stabilizations must be small to limit E_{hop}.

3. The magnitude of E_{hop} has a mixed influence: it must be less than b for orbital transfer to occur, but it should be large to suppress hopping conduction and provide high T_c values. In other words, E_{hop} should be as large as the $b \geq E_{hop}$ requirement will permit.

4. For polaron cell radii large enough for percolation at low concentrations of mixed-valence cations, the excess orbital exchange energy must override the attractive energy of the polarons to their source (i.e. $b' = b - E_{hop} \geq E_c$).

5. Lower threshold concentrations (x_t) for superconduction may be obtained with larger itinerant polaron boundary radii (r_p) or improved mixed-valence cation ordering ($\alpha \rightarrow -1$).

6. Electrostatic homogeneity (B-cation $Cu^{2+(3+)}$ pair ordering) should exist as dictated by optimum Madlung energy through ordered mixing of $A^{2+}$and A^{3+} cations. Oxygen defects may also serve to ensure the dispersal of mixed-valence B cation pairs and reduce the occurrence of non-transfer pairs (i.e., $Cu^{3+(3+)}$) which limit the critical temperature value.

7. Compositions with larger proportions of B cations can increase the limiting density of transfer pairs N and correspondingly, the values of T_c, I_c, and H_c.

8. Combinations of B cations, either transition-metal or simple dilutants (e.g., Zn^{2+}), should only serve to reduce superconducting effects.

9. Superconductivity is expected in non-cubic phases (tetragonal or orthorhombic) and for the perovskites at least, limited to the plane normal to the c axis because of (i) the absence of B-O-B transfer bonds in the c direction, and (ii) the orientations of the bonding lobes of the filled d_{z^2} and unfilled $d_{x^2-y^2}$ orbitals.

Based on these guidelines, the most probable candidate for superconductivity in Table I is weakly exchange-coupled $d^9 \rightarrow d^8$ (or possibly $d^{10} \rightarrow d^9$) in a 180-degree configuration to take advantage of the most efficient e_g-pσ-e_g transfer bond. This is the case of the mixed-valence Cu perovskites. The second choice would be at the opposite end of the series $d^1 \rightarrow d^0$, with weaker exchange interactions. In addition to a t_{2g}-pπ-t_{2g} bond, this system would feature a direct t_{2g}-$t_{2g}\sigma$ bond formation in the 90-degree geometry (see Fig. 7) of a spinel lattice (see Fig. 8). These general conditions also exist for the rest of the lower half of the series, $d^2 \rightarrow d^1$, $d^3 \rightarrow d^2$, and $d^4 \rightarrow d^3$, each with a type II coupling, but with an increasing number of antiferromagnetic type I couplings, as more d orbital levels become half-filled in high-spin states. The case of $d^5 \rightarrow d^4$, as manifested in $La^{3+}{}_{1-x}Sr^{2+}{}_x(Mn^{2+}{}_{1-x}Mn^{3+}{}_x)O_3$ perovskite[7] which has an e_g-pσ-e_g bond arrangement, there is only normal conduction. The presence of three type I couplings apparently

create static antiferromagnetic interactions too large to permit the occurrence of superconductivity.

For the other combinations in the upper half of the series, $d^8 \rightarrow d^7$, $d^7 \rightarrow d^6$, and $d^6 \rightarrow d^5$, the number of type I couplings dictate significant antiferromagnetic ordering and little chance of superconductivity. This group includes the common ferrite conduction pair $Fe^{2+(3+)}$, which shows no evidence of superconductivity in spite of a type III-epσ 180-degree coupling in perovskite. In spinel Fe_3O_4, however, the $Fe^{2+} \leftrightarrow Fe^{3+} + e^-$ transfer takes place on adjacent octahedral (B) sites (see Fig. 8) which have a parallelism induced by the strong $Fe^{2+}{}_B \leftrightarrow O^{2-} \leftrightarrow Fe^{3+}{}_A$ antiparallel sublattice couplings. Thus, the B-O-B group here features an imposed ferromagnetic alignment that does not require a spin flip for electron transfer, but the bonding angle is 90 degrees and the e_g-pσ-e_g covalence is not available.

B. Optimization of Superconduction Properties

In Table IV, some of the generic chemical formulae for transition-metal oxides that may harbor $B^{2+(3+)}$ transfer pairs are listed together with estimated formula unit volumes and the corresponding B-site number densities that would dictate the maximum densities of transfer electrons. It is clear from the maximum densities N_{max} that superconducting current densities will be limited in oxides, simply from the lack of charge carriers as compared with metals. Each of the perovskite forms would provide N_{max} values ~ $10^{22}/cm^3$; for metallic copper, the maximum electron density could approach $10^{23}/cm^3$.

The spinel case AB_2O_4 offers somewhat greater densities, but is limited by the 90-degree bond angles that would apply only to $d^1 \rightarrow d^0$ pairs such as $Ti^{3+(4+)}$ (see Table I). In contrast to the $Cu^{2+(3+)}$ perovskite case, $Ti^{3+(4+)}$ in 90-degree spinel or other structure suitable to provide direct t_{2g}-t_{2g} σ bonds would usually provide an n-type conduction because less-stable Ti^{3+} would be the dominant species and therefore act as a donor impurity. Since the host Ti^{4+} ions are diamagnetic, there would be no concerns about antiferromagnetic coupling between either host or transfer ions. It is interesting that the first and only transition-metal oxide other than Cu perovskite for which superconductivity has been reported is $Li^{1+}[Ti^{3+}Ti^{4+}]O_4$ spinel, with $T_c = 13.7$ K.[44]

The technique for creating the cation pairs may be stoichiometric or nonstoichiometric. In the A_2BO_4 system (the case of $La^{3+}{}_{2-x}Sr^{2+}{}_x(Cu^{2+}{}_{1-x}Cu^{3+}{}_x)O_4$),* the desired mix of B^{2+} and B^{3+}

* Mixed-valence B cations may also be obtained by nonstoichiometric creation of A-site deficiencies, normally represented in the chemical formula as excess oxygen (e.g., La_2CuO_{4+}).

TABLE IV

Transfer-Pair Densities in Superconducting Oxides

Formula	Symmetry	Formula Unit Volume[a] x 10^{-24} cm^3	B-site Density x $10^{21}/cm^3$	N_{max}[b] x $10^{21}/cm^3$
ABO_3	Cubic	~50	~20	~10
A_2BO_4	Tetragonal	~75	~13	~7.5
$A_2BB'O_6$	Tetragonal	~100	~20	~10
$A_2A'B_3O_9$	Tetragonal	~150	~20	~10
$A_2A'_3B_2O_8$	Tetragonal	~150	~13	~7.5
AB_2O_4	Cubic (spinel)	~75	~26	~13

a Based on average lattice parameter data

b N_{max} represents one-half of the B cation site density

ions is obtained by deliberately mixing the valences of the A-site ions in reverse proportion. This approach will normally provide single-phase material if the ions involved fall within the solubility limits of the phase. A mixed-valence situation has also been induced by rendering the composition oxygen deficient to form $Cu^{2+(3+)}$ pairs, at the risk of creating additional phases that would likely disrupt any long-range linkages between superconducting regions. Oxygen-defect systems have given the highest T_c values among the Cu perovskites, i.e., $Y^{3+}Ba^{2+}_2(Cu^{2+}_{3-3x}Cu^{3+}_{3x})O_y$, where $3x = 2y - 13$. Here the large Ba^{2+} ions share the A sites with smaller Y^{3+} ions in the ratio of 2:1.

From the results of the theory and experiment comparisons in Figs. 22 and 24, it appears that the LaSr system with $\alpha = 0.6$ represents a case of significant cation disorder (i.e., $P = 1 - 1.6x$), where local clustering of $La_2Cu^{2+}O_4$ and $LaSrCu^{3+}O_4$ would be expected to escalate into segregation of agglomerates[45] as x approaches 0.5, thereby eliminating most of the $Cu^{2+(3+)}$ transfer pairs. Since both La^{3+} and Sr^{2+} have radii $\approx$ 1.15 A, the clustering is more likely of electrostatic origin or possibly from grouping of Cu ions according to size differences between the two valences. Where Ba^{2+} (radius = 1.35 A) is used in place of Sr^{2+}, elastic energy accommodation increases clustering ($\alpha \rightarrow 1$), as shown in Fig. 26. Further evidence of this tendency is reflected in the lower T_c values when Ca^{2+} ions (radius $\approx$ 0.93 A) replaces Sr^{2+} in this system.[46] The variability of the α parameter within a fixed chemical system is indicated by the

recent data of Khan,[47] who reported incipient superconduction for $La_{1.8}Sr_{0.2}CuO_4$ (x = 0.2) at 66 K. According to Fig. 27, this result would occur for $\alpha \approx 0.25$ and suggests that the clustering of Sr^{2+} ions can be decreased in at least local regions, even if thermodynamically unstable.

With the creation of mixed-valence Cu by introduction of oxygen deficiencies, the YBa system offers a more complex situation (see Appendix D). With $\alpha = -0.11$ established from the data fittings in Figs. 23 and 25, P = 1 - 0.89x and the distribution of mixed-valence Cu(2) cations is slightly better than random, yielding a greater effective density of transfer pairs and a correspondingly higher T_c value. The importance of cation ordering was further demonstrated by Bhargava et al.[48] in temperature cycling experiments which yielded an incipient T_c value as high as 159 K, suggesting an $\alpha \approx -0.5$ for the same x = 0.27 (see Fig. 27). However, the role of oxygen defects in imposing a more ordered distribution of Y^{3+} and Ba^{2+} ions results in a high sensitivity of T_c to oxygen content and chemical instability when subjected to atmospheric constituents.

The dependence on oxygen defects, therefore, presents a dilemma: excess defects will induce a chemical instability that will eventually destroy the superconducting phase because of the natural oxygen affinity (gettering) of Y, Ba, and other highly reactive metals; but fewer defects may increase cation clustering. To achieve higher critical temperatures, therefore, improved cation ordering will be necessary. If oxygen defects obtained by decreasing y will contribute to this ordering, it is also clear that the advantages of such ordering will be offset by the attendant reduction of x to lower the density of transfer pairs. In addition, since each defect will create a nearby $Cu^{2+(2+)}$ pair to preserve local charge neutrality, there is an obvious limit to the effectiveness of this technique for dispersing Cu^{2+} and Cu^{3+} ions.

Since cation vacancies are likely to be less sensitive to environmental factors, compounds with A-site deficiencies may be worthy of investigation. Cations from a higher transition series, i.e., $4d^n$ or $5d^n$, will be accommodated in B sites where ionic radii are compatible with lattice parameters. To reduce the radii below ~ 0.80 A, higher valence numbers would be required. One example of a $d^1 \rightarrow d^0$ transfer situation would be heavily A-site defect perovskite containing Nb or Ta, e.g., $\varnothing_{7/6-z}La^{3+}{}_{1/3+z+x}Sr^{2+}{}_{1/2-x}(Nb^{4+}{}_{3z+x}Nb^{5+}{}_{2-3z-x})O_6$.[49,50] In spite of the dependence on t_{2g}-pπ or direct t_{2g}-$t_{2g}\sigma$ bonds, the greater radial extent of these outer-shell wave functions may still provide b exchange integral values large enough to satisfy the $b \geq E_{hop}$ condition for superconduction. With the e_g orbitals empty, however, orbital transfer would be less likely for this 180-degree bond structure. A more desirable situation might be a spinel type with 90-degree bond angles in the octahedral sublattice, perhaps $Zn^{2+}[\varnothing_{0.8-0.2x}Nb^{4+}{}_xNb^{5+}{}_{1.2-0.8x}]O_4$ or $Li^{1+}[\varnothing_{0.6-0.2x}Nb^{4+}{}_xNb^{5+}{}_{1.4-0.8x}]O_4$, in the manner of $Fe^{3+}[\varnothing_{1/3}Fe^{3+}{}_{5/3}]O_4$ defect spinel

(γFe_2O_3). In relation to these proposals, it should be mentioned that high-temperature superconduction in Nb oxides ($T_c > 44$ K) has been reported by Ogushi and Osono for sputtered Nb-Ge-Al-O films.[51]

For multication oxides the likelihood of clustering is expected to be significant, particularly where site stabilization energies vary. Since random ordering would be the best hope even in the unlikely case of complete energy equivalence, the problem of raising the critical temperature could be formidable. According to Fig. 27, the maximum T_c for $\alpha = 0$ in the Cu perovskites is below 90 K. If cation ordering is indeed necessary for higher critical temperatures and probably higher current densities, tailoring of the A-cation distribution (perhaps by selection of constituents or development of creative processing methods) appears to be essential for developing the full potential of transition-metal oxide superconductors. Inexpensive A-site cations, such as the larger Bi^{3+} and Ca^{2+}, and smaller Al^{3+}, Ga^{3+}, and V^{5+} (which could replace Cu(1) ions in B sites of the nonsuperconducting layers) that have been used successfully as substitutes for rare-earth and iron ions in magnetic garnets[45] may also have beneficial effects on both chemical stability and cation ordering. Most recently, the results of structure and chemical analysis of another Cu-O_4 layered superconducting system $Bi^{3+}{}_2Sr^{2+}{}_{2.33}Ca^{2+}{}_{0.67}(Cu^{2+}{}_{1.33}Cu^{3+}{}_{0.67})O_{8+y}$ that features an incipient $T_c = 116$ K were reported by Subramanian et al.[52] Since $x = 0.33$ (making $y = 0.33$ for charge balance), α is estimated at - 0.25 for this system. In order to compare this result with the previous work and place it the context of the above models, the data point is also plotted in Fig. 27.

6. CONCLUSIONS

Superconductivity in transition-metal oxides arises from the orbital transfer of d-electrons through covalent bonds where mixed-valence cations of the same element share nearest-neighbor sites with identical local environments. The presence of static antiferromagnetism from correlation exchange between half-filled orbitals should hinder orbital electron transfer by establishing an excitation energy ($U \neq 0$) associated with a spin flip. The $Cu^{2+(3+)}$ pair (i.e., $d^9 \rightarrow d^8$ configuration with d^8 in a low-spin state) appears to offer the most favorable situation in a 180-degree bonding arrangement (perovskite). Another possibility is the $Ti^{3+(4+)}$ (also $Nb^{4+(5+)}$ or $Ta^{4+(5+)}$) pair ($d^1 \rightarrow d^0$ configuration) in a 90-degree bonding geometry (e.g., spinel). In both of these situations, there is no magnetic exchange coupling between transfer ions, but antiferromagnetism could be expected between $Cu^{2+(2+)}$ pairs (together with Jahn-Teller stabilizations). The transport of charge carriers of $S = 0$ (i.e., the Cu^{3+} hole) through this antiferromagnetically coupled lattice may give the appearance of a dynamic antiferromagnetism, simulating a type of magnon but actually representing a travelling polaron .

The transition from superconduction to normal states occurs when the population of superconducting cells (mobile polarons) becomes too small to sustain continuous linkages. Higher temperatures increase the numbers of electrons excited from the bonding orbitals with energies sufficient to surmount the effective hopping activation energy. This competition between conduction mechanisms is readily seen in the metallic temperature dependence of the superconducting oxides, where orbital transfer centers act as short circuits to the conventional hopping semiconductor behavior. To obtain widespread superconductivity below a critical temperature, a threshold density of superconducting cells is required. For this occurrence, the density of transfer electrons as determined by the density of ion transfer pairs $Cu^{2+(3+)}$ must be maximized, with minimum clustering of the sources of mixed valence. The importance of cation ordering is magnified by its direct influence on both the effective transfer pair density and the hopping activation energy, which jointly influence the critical temperature and other properties.

With optimized chemical composition and cation ordering, room-temperature superconductivity could be possible (reports of isolated higher temperature regions of short duration have already suggested this), with current densities increased in proportion to the effective transfer pair densities. Since the dependence on oxygen defects for the creation of the mixed-valence condition presents a nonequilibrium compositional balance that is subject to

deterioration in the presence of atmospheric constituents, alternative techniques for accomplishing the formation and dispersal of $Cu^{2+(3+)}$ pairs should be sought. Thermodynamic equilibrium represented by Madlung and elastic energy optimizations must conform to the desired cation ordering, and would require a specific mixture of A-site ions (or vacancies) based on valence and ionic size. To achieve these objectives, chemically stable crystallographic structures with 180-degree B-O-B bonds should be investigated for B cations within the $3d^n$, $4d^n$, and $5d^n$ transition series, particularly where larger activation energies occur without unwanted magnetic exchange couplings. If the predictions of Fig. 27 are reasonable estimates of the reality involved, the degree of ordering for superconductivity in the Cu perovskites at even 150 K could require molecular engineering methods yet to be developed.

ACKNOWLEDGMENTS

The author acknowledges the inspiration gained from his association with Dr. John B. Goodenough, Professor of Materials Science and Engineering at the University of Texas at Austin and former M.I.T. Lincoln Laboratory colleague, whose enormous contributions to the chemistry and physics of magnetic oxides made possible the discovery of superconductivity in the copper perovskites.

APPENDIX A - Orbital States of Cu Ions in $La_{2-x}Sr_xCuO_4$

For the $d^9 \rightarrow d^8$ exchange pair in $La^{3+}_{2-x}Sr^{2+}_x(Cu^{2+}_{1-x}Cu^{3+}_x)O_4$, the superexchange couplings may be examined in terms of the end members, $La^{3+}_2Cu^{2+}O_4$ and $La^{3+}Sr^{2+}Cu^{3+}O_4$. The basic perovskite tetragonal B site for this system is shown in Fig. 30, with $c/a > 1$. For this case, the orbital energy level diagram may be readily discerned from the sizes and directions of the five d-orbital eigenfunction lobes.[21] Since the lower t_{2g} levels are filled for Cu^{2+} and Cu^{3+}, the focus is on the two upper e_g levels which are split in the tetragonal field, with d_{z^2} of lower energy than $d_{x^2-y^2}$. If the splitting is large enough, the Cu^{3+} ion can violate Hund's rule and enter a "low-spin" state, with d_{z^2} filled and $d_{x^2-y^2}$ empty. Under these conditions, the occupancy required for orbital electron transfer with a type II delocalization coupling are satisfied (see Fig. 10c).

From the crystallographic data of Longo and Raccah[53] for $La^{3+}_2Cu^{2+}O_4$ and of Goodenough et al.[25] for $La^{3+}Sr^{2+}Cu^{3+}O_4$ (the Cu^{3+} B-site end member), the ratio $c/a \sim 1.2$ (within the individual octahedra), but a further complication is present — the octahedra are distorted by almost 15 percent in the x-y plane, rendering the overall symmetry orthorhombic with ratios of in-plane Cu-O bond lengths approaching 1.4. Since the octahedra feature unequal axes that alternate between x and y directions, Goodenough et al. have interpreted this situation by assuming a reversal in energy of the e_g orbitals, with d_{z^2} becoming d_{x^2} or d_{y^2} and alternating in the x-y plane, as shown in Fig. 31.

For the analysis of a Cu-O-Cu three-ion system, however, the above choice of basis vectors is inappropriate because the frame of reference must be rotated through 90 degrees at each cation site. A more suitable approach would be to use the basis vectors of the tetragonal case of Fig. 30. Since the only difference is the off-center O^{2-} locations that cause the alternating in-plane distortions, the same coordinate axes may be used at each cation site. The d_{z^2} orbital would then be a filled lower state and, an empty upper state. Because of the z-axial symmetry of the d_{z^2} orbital and the identical x and y lobes of $d_{x^2-y^2}$, these eigenfunctions have the same energy at each cation site. The half-filled $d_{x^2-y^2}$ of the Cu^{2+} ion should form a type II delocalization superexchange coupling with the equi-energetic empty $d_{x^2-y^2}$ orbital of the adjacent Cu^{3+} ion and superconductivity should be possible in the x-y plane.

For orbital electron transfer to occur in the direction of the c axis, the two e_g orbitals would have to be reversed in energy, according to Fig. 30. In this case, the sign of the tetragonal field

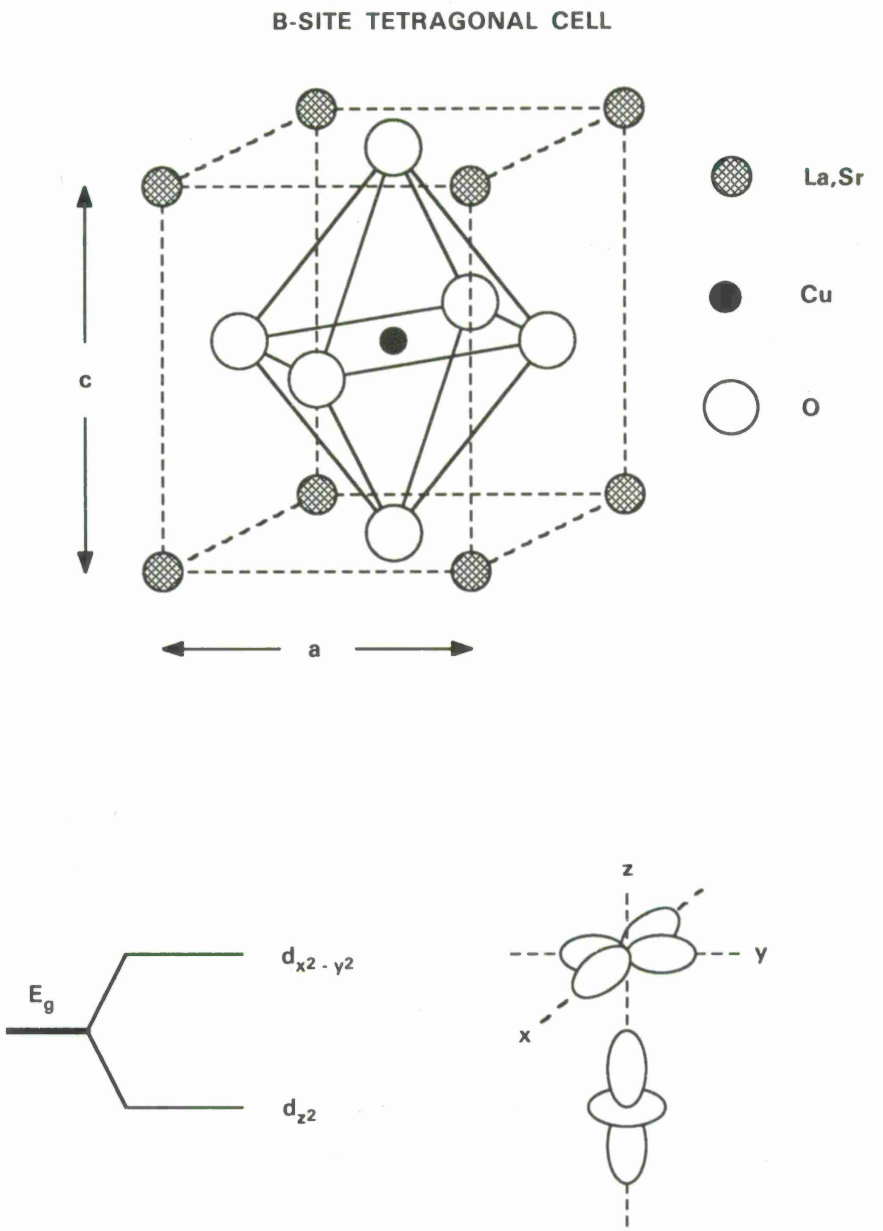

Figure 30. Octahedral site with tetragonal distortion (c/a > 1) that splits E_g term. If splitting is large enough, Hund's rule can be violated to produce a filled lower d_{z^2} orbital and an empty upper $d_{x^2-y^2}$ orbital in a d^8 cation to create a low-spin (S = 0) state.

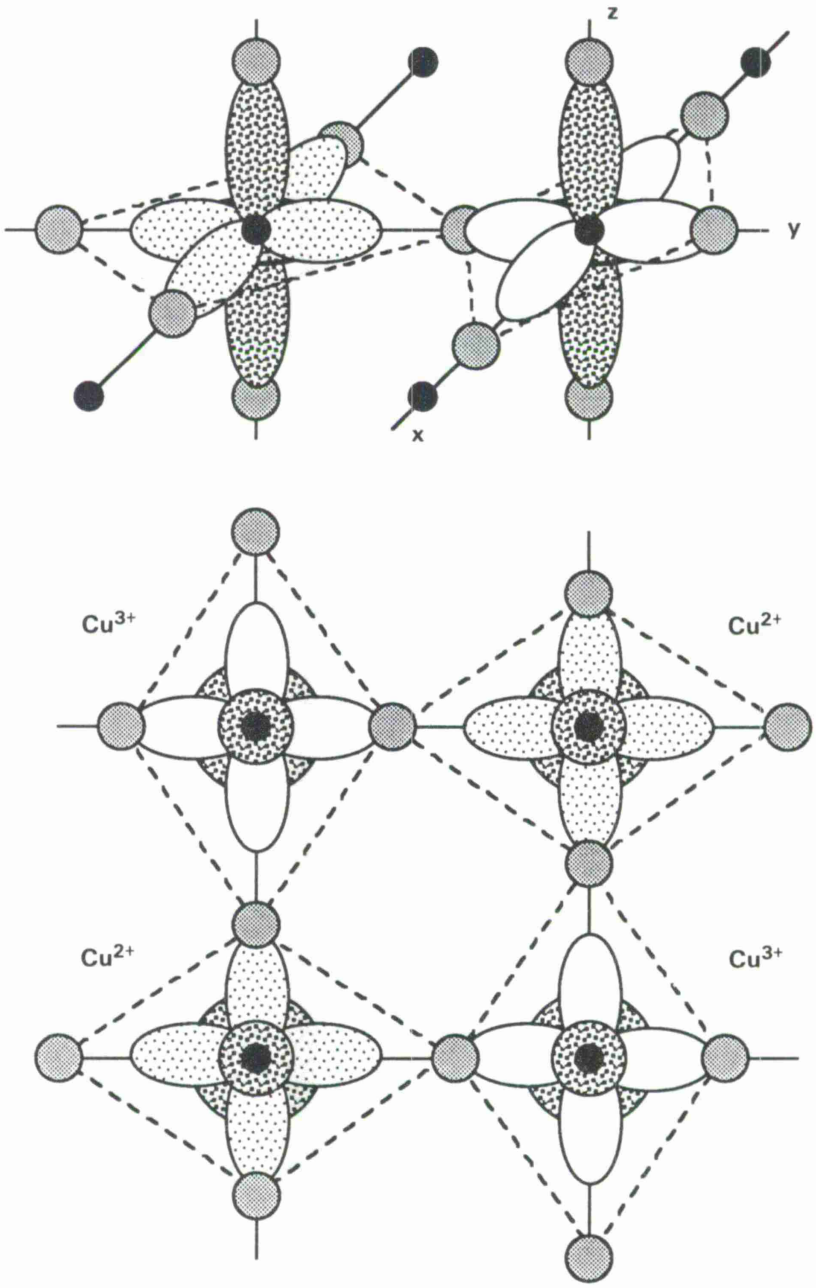

94292-29

Figure 31. Orbital wave functions for the $Cu^{2+} \leftrightarrow Cu^{3+} + e^-$ transfer in the x-y plane, indicating exchange coupling between half-filled and empty orbitals made possible by a d^8 low-spin state in Cu^{3+}.

would be changed or the presence of a stronger in-plane (orthorhombic) distortion would alter the order of the energy levels. If the Cu^{3+} ion were in a high-spin state, however, (ignoring any local antiferromagnetic coupling to Cu^{2+}), electron transfer would take place between d_{z^2} orbitals, now the higher energy states, and the conduction would be along the c axis. This situation is hypothetical for the lattice discussed here, however, because there are no superexchange linkages between B ions in the c direction (see Fig. 1).* Such a possibility would exist for the $YBa_2Cu_3O_y$ system which more closely resemble a stacked cubic lattice with cells of the type shown in Fig. 9. A summary of orbital configurations for these ion combinations, including the double-electron case discussed in Appendix B, is given in Table II.

* A discussion of electrical properties for this general system in terms of a half-filled (Cu^{2+}) $d_{x^2-y^2}$ band was given earlier by Goodenough,[9] and more recently the question of tetragonal to orthorhombic phase transitions and their dependence on the ratio of A-O to B-O bond lengths has been examined by Singh, Ganguly, and Goodenough.[54] The orthorhombic model pictured in this latter work, however, still retains the Cu-O_4 basal square-planar coordination that would not only maintain a lower d_{z^2} orbital, but probably enhance its stabilization.

APPENDIX B - Double-Electron Transfer

In Fig. 32, the special case of $d^{10} \rightarrow d^8$ double-electron orbital transfer ($Cu^{1+} \leftrightarrow Cu^{3+} + 2e^-$) is outlined for both high- and low-spin d^8 configurations. Since d^{10}, i.e., the Cu^{1+} ion, is diamagnetic with a filled $3d^n$ shell, the question of magnetic exchange coupling is absent between the transfer ions. For the low-spin situation, the transfer would involve "paired " spins, probably the closest available analog to pair conduction in the BCS sense. As pointed out by Goodenough,[9] copper ions may occur as 1+, 2+, or 3+, with the attendant differences in ionic radii. The likelihood of either static or dynamic reactions of the type $2Cu^{2+} \leftrightarrow Cu^{1+} + Cu^{3+}$ are present in these perovskite systems was strongly suggested by the recently reported appearance of an approach to superconductivity in $La^{3+}{}_2Cu^{2+}O_4$.[55] (The metallic resistivity temperature dependence determined in earlier measurements by George et al.[56] also suggested an incipient superconductivity). With this multi-ion B-site occupation, there is a complex electron transfer mechanism involving $d^{10} \rightarrow d^8$, as well as $d^{10} \rightarrow d^9$ and $d^9 \rightarrow d^8$, each with its own individual electrostatic, magnetic, and elastic energy constraints.

In the superconductng compositions reported to date, however, it is improbable that the Cu^{1+} ions appear in abundance, at least in a static situation that would require low temperatures. The radius of Cu^{1+} is very large (~ 0.96 A) for occupancy of an octahedral site in a metal oxide* and its existence in spinels[57] is still an unresolved question. In addition, the marginal superconductivity in the above-mentioned pure $La^{3+}{}_2Cu^{2+}O_4$ composition indicates little $2Cu^{2+} \leftrightarrow Cu^{1+} + Cu^{3+}$ formation. The occurrence of monovalent copper in perovskites may, however, confound to some extent the effective concentrations of transfer pairs and lead to errors in the quantitative interpretations of resistivity and critical temperature as carried out in this report.

An alternative situation that involves a double-electron transfer would be $d^2 \rightarrow d^0$ ($Ti^{2+} \leftrightarrow Ti^{4+} + 2e^-$). Here t_{2g} orbitals are involved with 90-degree bonds, and may be at least partly responsible for the superconductivity reported for $Li^{1+}[Ti^{3+}Ti^{4+}]O_4$.[44]

---

* There is also, of course, the possibility that oxygen vacancies reduce the coordination numbers of B sites and make room for these larger cations.

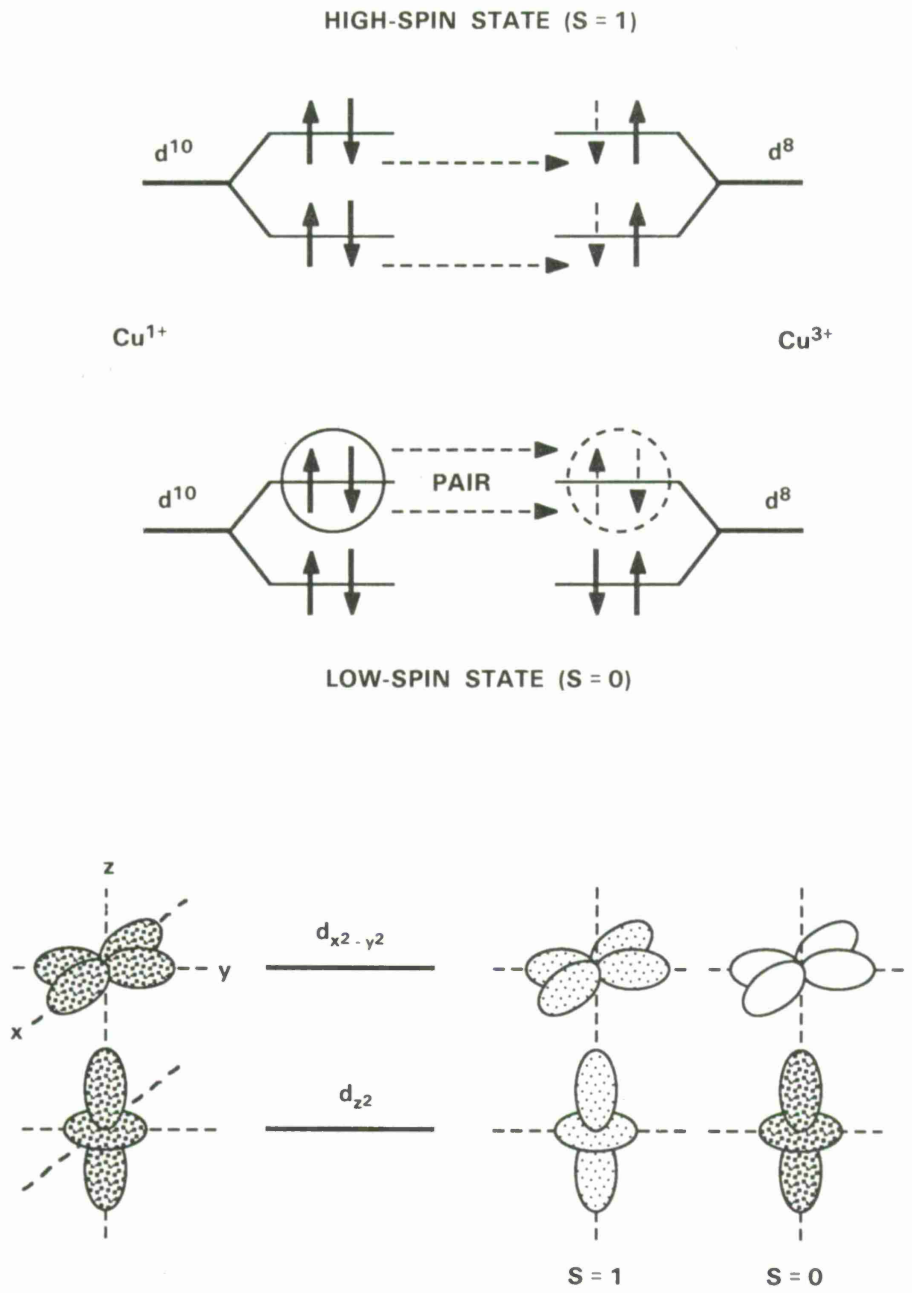

Figure 32. d-Orbital states and occupancies for $d^{10} \rightarrow d^8$ double-electron transfers.

APPENDIX C - Cation Clustering and Activation Energy

The general question of cation distribution is critical in the determination of superconductivity and will be examined here in relation to an "effective" density of transfer pairs or polarons. Elastic energy variations resulting from differing cation sizes (Cu^{2+} is larger than Cu^{3+}) and SO or JT cooperative stabilizations can override electrostatic considerations, even with ordering of the A-site cation combinations, i.e., La^{3+}-Sr^{2+} and Y^{3+}-Ba^{2+}. In addition, magnetic exchange between Cu^{2+} ions (antiferromagnetic), as well as between Cu^{2+} and Cu^{3+} ions (ferromagnetic or nonmagnetic for the low-spin S = 0 case) can affect cation ordering.

For ideal ordering, typified by the case of alternating Cu^{2+} and Cu^{3+} ions in the limiting case where x = 0.5, as in a NaCl lattice, the probabilities of $Cu^{3+(3+)}$ and $Cu^{2+(3+)}$ pairing for nearest neighbors are zero and unity, respectively. To estimate the random effects of pairing, consider an individual Cu^{3+} ion with its four neighboring B-site cations in the x-y plane. With a Cu^{3+} concentration equal to x, the random probability of any of these neighbors also being a Cu^{3+} is exactly x, so that the effective density of $Cu^{2+(3+)}$ pairs is determined by weighting x with the probability factor (1 - x). Therefore, the effective transfer pair density for random distribution would be simply N = x(1 - x)/V, where V is the volume of a formula unit.

Enhanced $Cu^{3+(3+)}$ pairing can result from elastic energy minimization[58] or from tendencies to increase $Cu^{2+(2+)}$ clustering to maximize antiferromagnetic couplings and create cooperative JT stabilizations, particularly where electrostatic (Madlung energy) ordering is not strong among the A-site cations. For these situations, we define a parameter α to represent the departure from random cation distribution, according to a disorder probability*

$$P = 1 - (1 + \alpha)x \quad , \tag{C-1}$$

where $-1 \leq \alpha \leq 1$. In simplest terms, $\alpha = 1$ represents the case where all nearest neighbors of a given B cation are of the same valence (clustering) and $\alpha = -1$ is the case for neighbors of the

* The possibility of a nonlinear term arising from enhanced clustering, where the disorder parameter is also a function of impurity concentration, i.e., $\alpha = \alpha_0 + \beta x$, should not be ruled out. Such an effect might be expected where strong magnetic and cooperative elastic effects may enhance clustering. The introduction of this additional term to Eq. (C-1) could account for the measured variation of T_c with x without even considering the reduction in trapping energy with cation clustering. In such a situation, E_{hop} could be relatively insensitive to x.

opposite valence (perfect ordering).

As the composition approaches equal densities of Cu^{2+} and Cu^{3+} ions (x = 0.5), the validity of these approximations declines where $\alpha \rightarrow 1$, but the physical situations may be seen more clearly, as modeled in the hypothetical x-y plane distributions in Fig. 33 with α values indicated. When $\alpha \rightarrow -1$, P = 1 and perfect ordering would be the case, with all $Cu^{2+(3+)}$ pairs as nearest neighbors and superconduction as the dominant transfer mechanism. When $\alpha \rightarrow 1$, $P \rightarrow 0$ and denotes the case of maximum disorder with mainly $Cu^{2+(2+)}$ and $Cu^{3+(3+)}$ pairs among nearest neighbors and fewer $Cu^{2+(3+)}$ orbital transfer pairs available for superconduction; in this case, conduction would occur between Cu^{2+}-Cu^{3+} ions linked by hopping paths to produce the highest resistivity. It should be pointed out that this type of disorder may fall within the general definition of a single-phase material, and clustering of the type detectable as isolated inhomogeneities through microstructural or x-ray analysis is not necessarily a requirement.

These results may now be applied to Eq. (15) for the effective density of superconducting electrons, where

$$n_s = NP\,[1 - \exp(-E_{hop}/kT)] = (xP/V)\,[1 - \exp(-E_{hop}/kT)] \quad , \qquad \text{(C-2)}$$

which is then used to derive the modified expression Eq. (20) for the effective normal resistivity.

In addition to determining the effective transfer pair density, cation clustering is expected to control the magnitude of the activation energy.[59] The activation energy E_{hop} for electron hopping has been shown experimentally to decrease with $B^{2+(3+)}$ pair concentration for a variety of transition metal cations.[35] In particular, the Cu case was found to have the lowest activation energy of the group that included antiferromagnetically coupled Mn, Co, and Ni, and also the lowest sensitivity to temperature, suggesting that antiferromagnetic exchange energies are minimal for the Cu system. The small value of E_{hop} for normal conduction and the metallic behavior of La_2CuO_4 was confirmed by George et al.[56] and measured in the superconducting system between 4 and 10 meV by several workers.[60-62]

In Section 3 of the text, the activation energy is attributed to several factors, including magnetic and elastic effects. Landau trapping[63] of polarons, i.e., the elastic compensation of the lattice to accommodate a different-sized ion, has been suggested by Heikes and Johnson[35] as important in this case. From their results reproduced in Fig. 34 for mixed-valence simple oxides $Li^{1+}{}_xM^{2+}{}_{1-2x}M^{3+}{}_xO$, E_{hop} decreases monotonically (i) with the number of antiferromagnetic

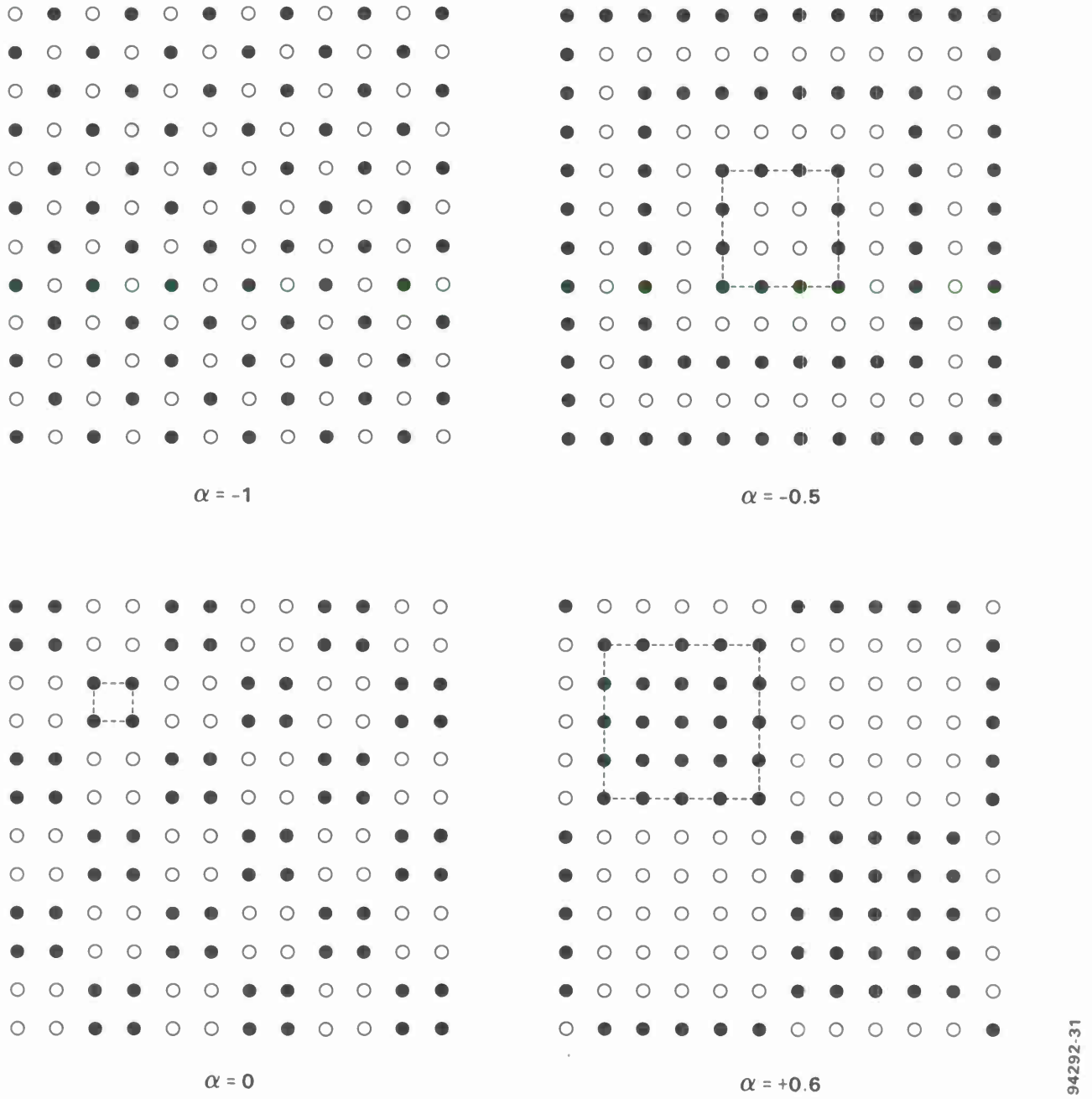

Figure 33. Idealized cation ordering models in the x-y plane for the maximum "impurity" concentration of x = 0.5: α = -1 (ideal), - 0.5, 0, and + 0.6.

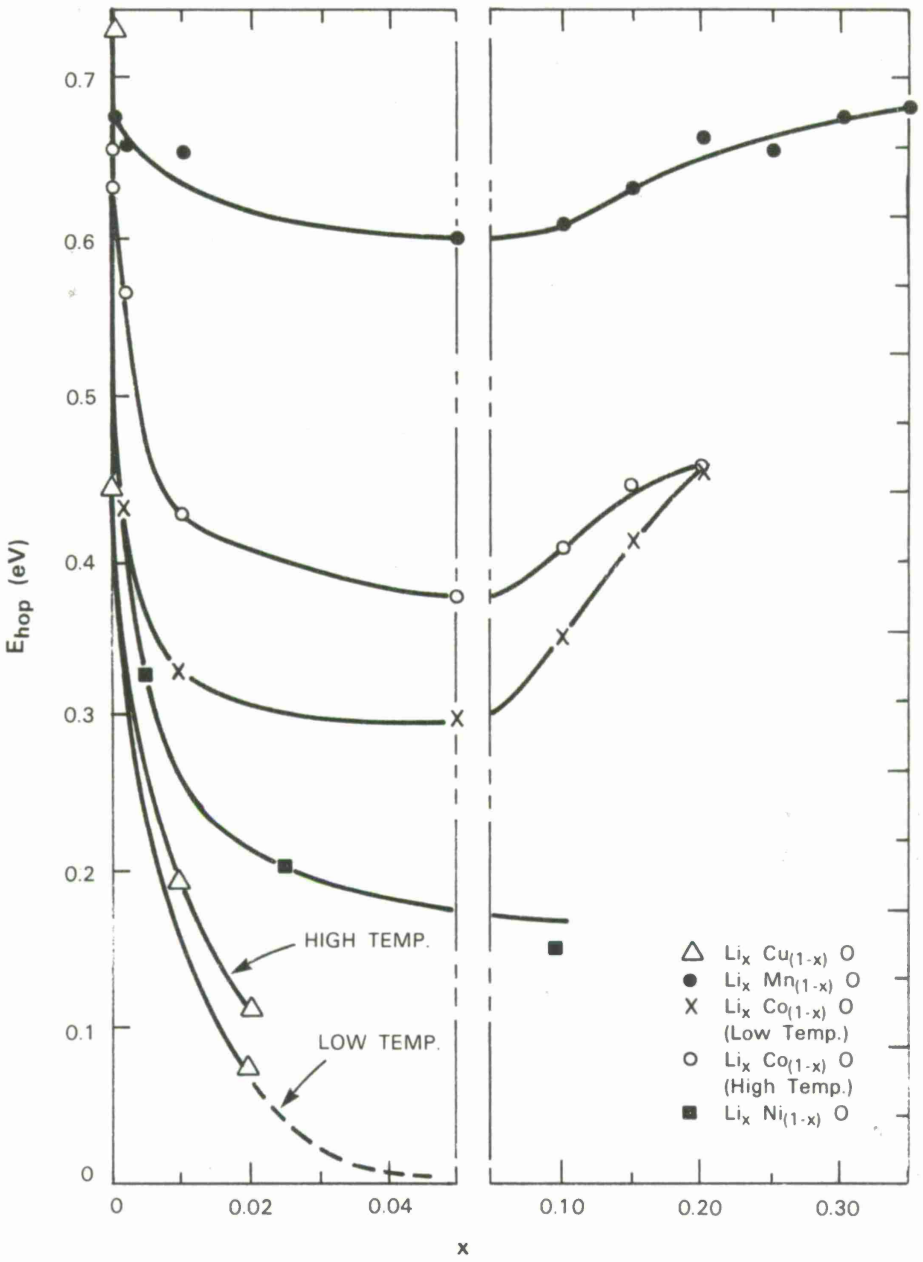

94292-32

Figure 34. Mixed-valence transition-metal oxide activation energy as a function of composition for $Li^{1+}{}_xM^{2+}{}_{1-2x}M^{3+}{}_xO$. *(Data of Heikes and Johnston, Reference 35)*

couplings per ion through the iron group for Mn, Co, Ni, and Cu, and (ii) with the concentration of 3+ ions (designated by x), which may result from $Li^{1+} + M^{3+}$ groupings that would produce substantial disorder. For the beginning part of this series, magnetic effects appear dominant and could account for the apparent rise in E_{hop} with both Mn and Co as x increases to values where polarons of the opposite sign may become significant. For Cu, however, these effects are small and the elastic compensation is probably more important.

In the earlier discussion on the magnetic (ΔE_{ex}) contributions to E_{hop}, it was reasoned that magnetic order would dictate higher values of these quantities where $J_{LL}S_L$ is large in the presence of SO stabilizations. Table I suggests that Mn, Co, and Ni in particular would initially feature greater E_{hop} values that would decline with increasing temperature and "impurity" concentration. For Cu^{2+} there is no SO stabilization, and any JT effect should be preempted by the tetragonal symmetry of the perovskite lattice; moreover, Cu^{3+} in an S = 0 state would serve to reduce ΔE_{ex} through magnetic dilution to yield a lower resultant E_{hop} than that given in Fig. 30 for CuO. It is also interesting that TiO, which should have minimal contributions from ΔE_{ex}, with no SO effects, is considered to be the most metallic of these simple transition-metal oxides.[64] Additional evidence that the activation energy is substantially lower in the mixed-valence perovskites may be found in Singh et al.[54] data, which indicate values for $E_{hop}{}^{o}$ as much as a factor of ten smaller than than those presented in Fig. 34.

Most recently, Pardavi-Horvath et al.[65] have used a model similar to that developed in the text to explain the behavior of Fe^{4+} polarons (i.e., $Fe^{3+(4+)}$ transfer pairs) in tetrahedral sites of a garnet lattice, where an activation energy below 10 meV was determined from experiment. With the orbital levels inverted from those shown in Fig. 6, this case would represent p-type conduction, with an empty polaron level in a half-filled t_{2g} band (type II). Since the lattice ions have S ground terms with no ligand-field stabilization, and the magnetic exchange energies are large for both ions, it is clear that substantial cancellation among the various contributors to E_{hop} must occur to produce such low net values. Although collinear spins in the tetrahedral sublattice imposed by the principal tetrahedral-octahedral ferrimagnetism provide a condition favorable for conduction, orbital transfer from direct cation-cation t_{2g} overlaps between neighboring tetrahedral sites should be inefficient and the polaron transport would likely be limited to thermally activated electron hopping.

According to the x-y cell models sketched in Fig. 35 for α = 1, 0, and -1 cases with x = 0, 0.25, and 0.5, trapping effects would be greatest with the "impurity" isolated. This would occur at

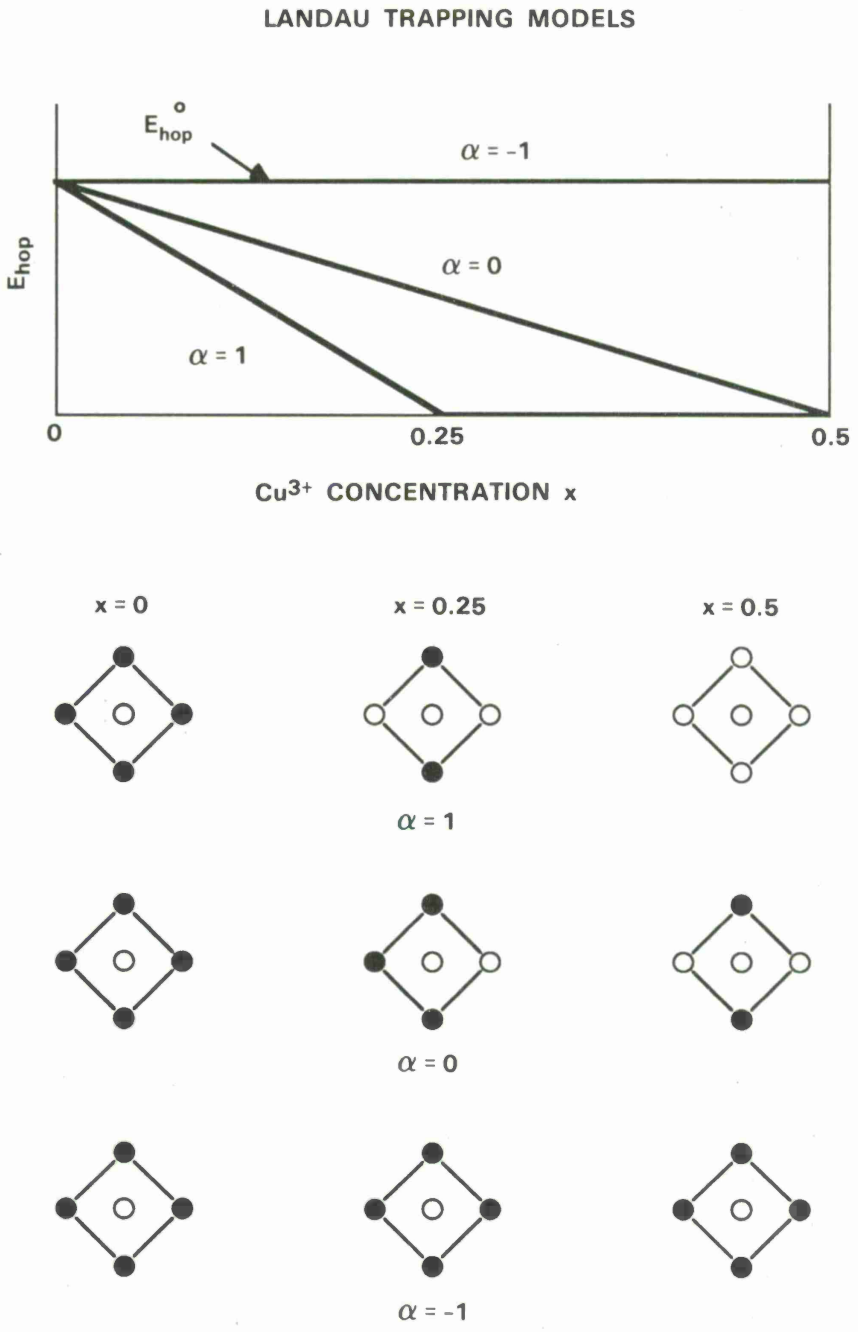

Figure 35. Model of polaron trapping as functions of composition and cation ordering.

$x \sim 0$, where Cu^{3+} is surrounded by only Cu^{2+} ions. Where a Cu^{3+} is surrounded by an equal number of Cu^{2+} and Cu^{3+} ions, the concept of a trapped carrier is no longer valid and the activation energy should be minimal. Where Cu^{3+} ions are surrounded entirely by other Cu^{3+} ions as part of a cluster, the concept of an impurity itself loses its meaning. Similar arguments could apply at least partially to the magnetic interactions between Cu^{2+}-O-Cu^{2+} (antiferromagnetic), Cu^{2+}-O-Cu^{3+} (ferromagnetic, if low-spin), and Cu^{3+}-O-Cu^{3+} (antiferromagnetic, if high-spin), but the magnetic interactions in general are probably less influential in the trapping process.

In Fig. 35, a linear model for the activation energy may be constructed for the $\alpha = 1$ case of maximum clustering, with E_{hop} bottoming at $x = 0.25$ (here assumed for convenience as $E_{hop} \sim 0$) and with a value of E_{hop}^{o} at $x = 0$. For the random distribution of Cu^{3+} ($\alpha = 0$), the curve would reach zero at $x = 0.5$, and would remain unchanged for ideal ordering ($\alpha = -1$) since the Cu^{3+} ions would always be surrounded by a full complement of Cu^{2+} neighbors. From this model, a simple approximation for E_{hop} evolves as

$$E_{hop} = E_{hop}^{o}\,[1 - 2(1+\alpha)x] \qquad 0 \le x \le 0.5 \qquad \text{(C-3a)}$$

limited by

$$E_{hop} = E_{hop}^{o}\,[1 - 2(1 - P)] \qquad \text{for } P \le 1$$

$$E_{hop} = 0 \qquad \text{for } P \ge 1 \quad . \qquad \text{(C-3b)}$$

APPENDIX D - Cation Valence and Ordering in $YBa_2Cu_3O_y$

The source of apparent increased $B^{2+(3+)}$ pair ordering in the YBa_2 system is an important question. Unlike the LaSr system, the crystal structure is not the naturally tetragonal K_2NiF_4 (Fig. 1), but rather a stack of cubic cells of the type shown in Fig. 9, with alternating A and B site layers. According to Hor et al.[66] and the careful crystallographic analysis of Bordet at al.,[67] the large (~ 1.35 A) Ba^{2+} ions and smaller (~ 0.93 A) Y^{3+} ions are segregated in different A planes, as shown in Fig. 36. Because of the 2:1 ratio of Ba to Y populations, it is appropriate to define two different Cu layers, Cu(1) sandwiched between Ba layers and Cu(2) between Y and Ba layers. Beginning with the hypothetical case of y = 9, each layer is intact and all Cu ions have the full complement of six O^{2-} ligands in octahedral coordinations. Oxygen vacancies first appear in the Y-O_4 planes as y decreases from 9 to 8, leaving the Cu(2) ions in pyramidal O_5 coordinations, but with Cu-O_4 planar bonding intact. With additional defects, an orthorhombic phase sets in as the Cu(1) layers suffer oxygen depletion to form linear chains of Cu-O-Cu at y = 7 (the regime of maximum T_c values in this system), until finally all of the oxygen is removed from the Cu(1) layers as $y \rightarrow 6$.[68]

Based on this accepted interpretation of the O^{2-} vacancy distribution, one result appears to be undisputed. Since filled d_{z^2} orbital lobes are directed along the c axis, with no connecting Cu ions, in addition to the oxygen depletion in the Y-O_4 plane, it is likely that the superconduction would have to be confined to the basal planes. This conclusion is supported by the coherence length measurements of 34 A in the basal plane and only 7 A in the c direction.[40] According to Fig. 36, therefore, in the superconducting region Cu(1) ions would have two-fold coordinations and Cu(2) ions would retain of four-fold (square-planar) coordinations, and the in-plane $d_{x^2-y^2}$ orbitals would have the highest energy in each case, with low-spin d^8 configurations for the Cu^{3+} ions. As discussed in Appendix A, these wave functions have lobes only in the x-y plane and would therefore be insensitive to environment changes along the c axis, with the result that the orbital transfer mechanism would be available between all of the Cu sites.

With this picture, there could be orbital transfer in either the Cu(1) or Cu(2) planes. There are, however, three important constraints on Cu(1) superconduction: (i) Cu(1) ions represent only one third of the total Cu content, thereby limiting the maximum current density, (ii) the conduction would follow linear and parallel chains that would impose a uniaxial feature determined by the orthorhombic phase that sets in for y ~ 7, an effect yet to be established by experiment, and (iii) for

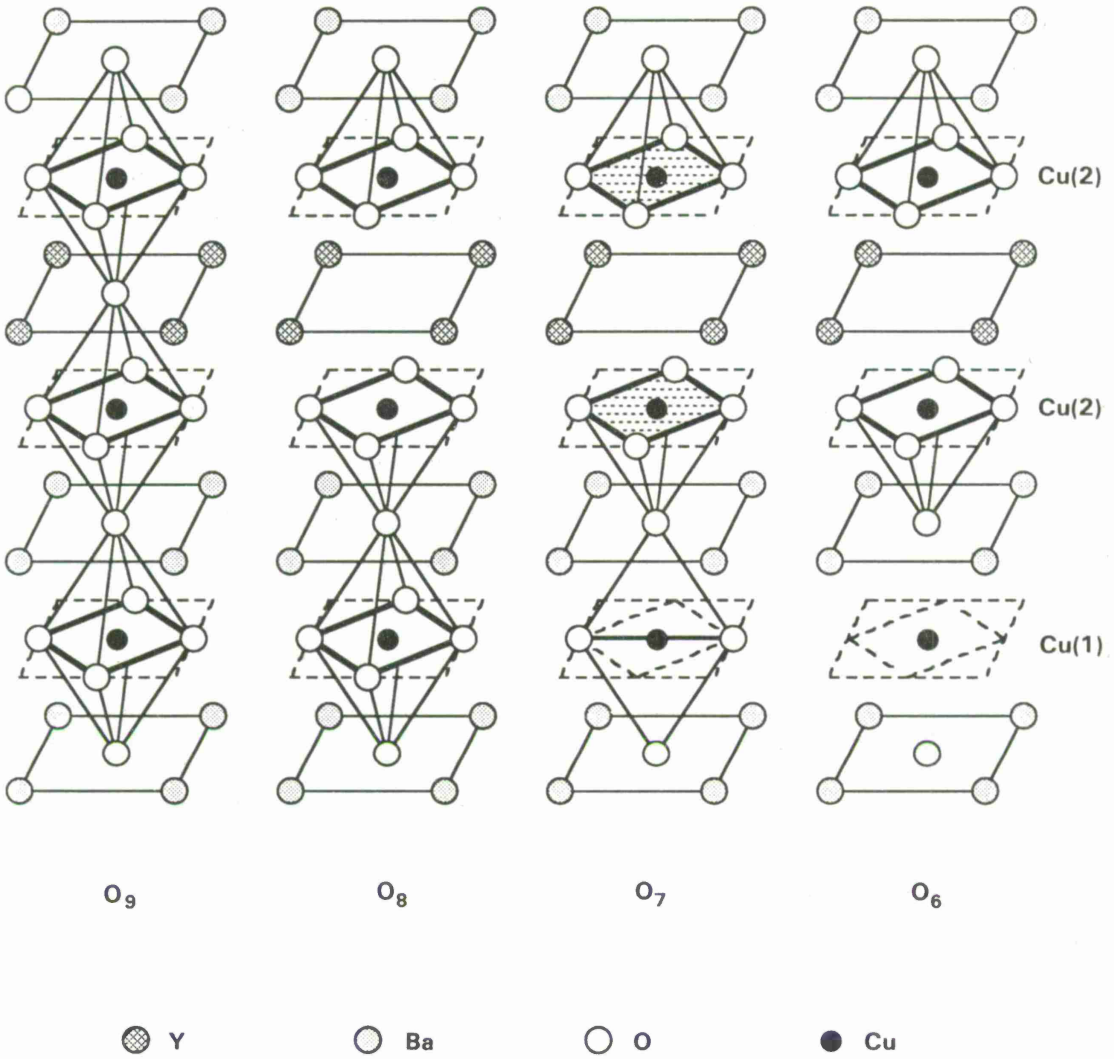

Figure 36. Ordered A-layer structure of $YBa_2Cu_3O_y$, showing breakdown of Cu-O_6 complexes as y decreases from 9 (hypothetical in this case). At y = 8, oxygen is removed from Y-O_4 planes and Cu(2) ions are square-pyramidally coordinated (i.e., Cu-O_5), but retain C_4 symmetry axis. At y = 7, Cu(1) ions become linearly coordinated in x-y plane (orthorhombic phase), with uniaxial superconduction expected; Cu(2) ions retain square-planar coordination in x-y plane, with planar superconduction possible. At y = 6, Cu(1) planes are fully depleted of oxygen and Cu(2) ions lose mixed-valence with only 2+ species present (see Fig. 37).

$y < 7$, O^{2-} vacancies begin to appear in the Cu(1) linear chains themselves, forcing the adoption of a tunnelling mechanism[68] to explain the superconduction effects at values of y that have been reported as low as 6.2.[39]

To investigate these situations with a more general approach, a model of the posssible Cu valence states may be estimated from the local electrostatic charge balance required to compensate for the O^{2-} defects. Figure 37 presents a chart of the B-cation valence, i.e., 2Cu(2) + Cu(1), required to balance the oxygen content. At y = 9, where the combined average valence is 3.67+ (= 11/3), we assume that valence states of only 4+ and 3+ are present. Since the B(2) planes are between Ba^{2+} and Y^{3+} layers, and the B(1) plane is between a pair of Ba^{2+} layers, it is assumed that the average valences of B(1) and B(2) ions are 4+ and 3.5+ respectively. As y drops to 8, the O^{2-} in the Y^{3+} layers is removed and the average valence of Cu(2) closest to the vacancies falls to 2.5+, while the Cu(1) valence remains unaffected at 4+ (fictitious for this particular element). For further reductions in y, the new defects occur directly in the Cu(1) planes where the more severe changes in valence are now expected to occur. For this approximation, it is logical to assume that the Cu(1) valence declines linearly from 4+ to its minimum possible value of 1+ as y decreases from 8 to 6, as depicted in Fig. 37. In conjunction with this drop in Cu(1) valence, the average Cu(2) valence must also decrease further to balance the total charge, with the result that the Cu(2) valence curve falls linearly from 2.5+ to 2+ over this range of y. This small additional reduction in Cu(2) valence is not surprising because these layers represent next-nearest neighbor cations to the Cu(1) layers where these latest O^{2-} vacancies appear and would be influenced by the charge deficiencies because of the relative proximity along the c direction.

With this model, the average Cu(2) valence, here defined as v, would be given by the relation

$$v = 0.25y + 0.5 \quad , \tag{D-1}$$

and v = 2.25+ at y = 7, in accord with the value established by neutron diffraction analysis.[67] In terms of the fraction of $Cu^{2+(3+)}$ transfer pairs x (= v - 2), the relation in Eq. (D-1) can be expressed as

$$x = 0.25y - 1.5 \quad . \tag{D-2}$$

If x = 0.08 is assumed to be the minimum value for superconduction, the lower threshold for y in $YBa_2(Cu_3)O_y$ would become ~ 6.3. Since the practical maximum Cu valence is 3+, the

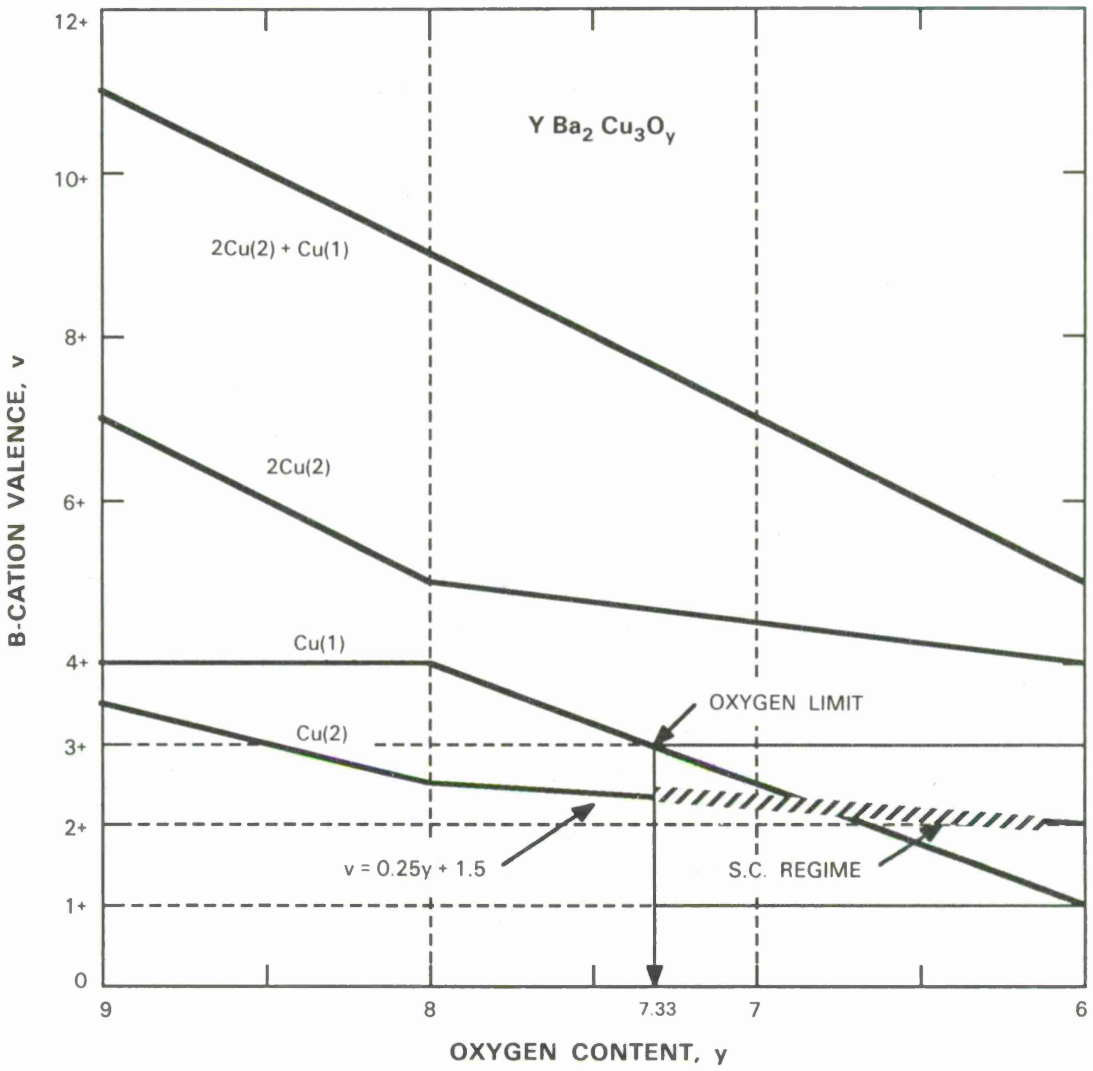

Figure 37. Proposed valence distribution of Cu(1) and Cu(2) as a function of the oxygen content variation and distribution depicted in Fig. 36.

theoretical oxygen upper limit not only for superconduction, but also for single-phase chemistry in this system would be y = 7.33 (see Fig. 37, and also the data and theory plotted in Fig. 25). As a consequence, the highest attainable $Cu^{2+(3+)}$ mix in the Cu(2) layers is x = 0.33. Therefore, with optimum ordering (P = 1, α = -1), the most optimistic T_c value for a structure based on $YBa_2(Cu_3)O_y$ may be determined from Eq. (22) to be 325 K (see also Fig. 27).

Since the distribution of Cu^{3+} cations is determined by the location of the oxygen vacancies, it is not surprising that the ordering is higher than random. The probability of oxygen defects being paired, for example, would be small based on structural integrity arguments. It is also curious that interplanar segregation of the Y^{3+} and Ba^{2+} probably enhances the Cu^{2+}-Cu^{3+} ordering, since any intraplanar mixture of these A-site ions could offset the oxygen vacancy effects. If the Y^{3+} and Ba^{2+} ions were mixed in a random fashion among the A planes, the Cu^{2+}-Cu^{3+} ordering would likely be reduced through Ba^{2+}-Cu^{3+} and Y^{3+}-Cu^{2+} clustering, both from charge balance and ionic size considerations.[58]

In the $Bi^{3+}{}_2Sr^{2+}{}_{2.33}Ca^{2+}{}_{0.67}(Cu^{2+}{}_{1.33}Cu^{3+}{}_{0.67})O_{8+y}$ system[52] (with x = 0.33 in this case) mentioned earlier, the Cu cations appear only in Cu-O_4 basal planes similar to the Cu(2) planes of Fig. 36, but without the fifth oxygen that forms the pyramidal coordination. In addition, these basal planes occur as pairs straddling a SrCa oxygen layer, with each pair segregated from neighboring pairs by highly ordered Sr-Bi-Bi-Sr oxygen layers. Since Cu-O_4 planes are in turn sandwiched between SrCa and Sr layers, all of the neighboring cations along the c axis have the same valence. As a consequence, the Cu^{2+}-Cu^{3+} ordering would have to be influenced by the elastic effects of differences in the Ca^{2+} (~ 1.0 A) and Sr^{2+} (~ 1.15 A) ionic radii, rather than charge variations among the A cations. If the source of the Cu^{3+} polarons is the O^{2-} concentration (the y value) in this case, there remain important questions related to the O^{2-} ion distribution and stability. Although there is an improvement in the critical temperature, it should also be pointed out that the maximum current density may be smaller than in the YBa system because of the lower fraction of B cations, i.e., maximum carrier density N (see Table IV).

REFERENCES

1. J.G. Bednorz and K.A. Muller, Z. Phys. B **64**, 189 (1986).
2. J.G. Bednorz, K.A. Muller, and M. Takashige, Science **236**, 73 (1987).
3. M.K. Wu, J.R. Ashburn, C.J. Torng, P.H. Hor, R.L. Meng, L. Gao, Z.J. Huang, Y.Q. Wang, and C.W. Chu, Phys. Rev. Lett. **58**, 908 (1987).
4. J.M. Tarascon, L.H. Greene, W.R. McKinnon, G.W. Hull, and T.H. Geballe, Science **235**, 1373 (1987).
5. R.J. Cava, B. Batlogg, R.B. van Dover, D.W. Murphy, S. Sunshine, T. Siegrist, J.P. Remeika, E.A. Reitman, S. Zahurak, and G.P. Espinosa, Phys. Rev. Lett. **58**, 1676 (1987).
6. E.J.W. Verwey, *Semi-Conducting Materials*, (Academic Press, New York, 1951) p. 151.
7. J.H. van Santen and G.H. Jonker, Physica **XVI**, 599 (1950).
8. C. Zener, Phys. Rev. **82**, 403 (1951).
9. J.B. Goodenough, Mater. Res. Bull. **8**, 423 (1973). DTIC-AD 763576
10. P.W. Anderson, Phys. Rev. **115**, 2 (1959).
11. J. Bardeen, L.N. Cooper, and J.R.Schrieffer, Phys. Rev. **106**, 162 (1957); **108**, 1195 (1957).
12. J.B. Goodenough, Prog. in Solid State Chem. **5**, 145 (1972).
13. J. Bardeen, *Handbook of Physics*, Chap. 6 (McGraw-Hill, New York, 1958).
14. J.B. Goodenough, *Magnetism and the Chemical Bond*, (Interscience Publishers, John Wiley, New York, 1963) p. 66.
15. Reference 14, Chapter III.
16. P.W. Anderson, Phys. Rev. **79**, 350 (1950).
17. J.B. Goodenough, J. Phys. Chem. Solids **6**, 287 (1958).
18. J. Kanamori, J. Phys. Chem. Solids **10**, 87 (1959).
19. J.B. Goodenough and A.L. Loeb, Phys. Rev. **98**, 391 (1955).
20. J.B. Goodenough and J.M. Longo, *Landolt-Bornstein*, (Springer-Verlag, Berlin, 1970) Group III, **Vol. 4**, p. 126.
21. G.F. Dionne and B.J. Palm, J. Magn. Reson. **68**, 355 (1986). DTIC-ADA 170498

22. Reference 14, p. 182.
23. G. Shirane, Y. Endoh, R.J. Birgenau, M.A. Kastner, Y. Hidaka, M. Oda, M. Suzuki, and T. Murakami, Phys. Rev. Lett. **59**, 1613 (1987).
24. J. Smit and H.P.J. Wijn, *Ferrites*, (John Wiley & Sons, New York, 1959) p. 153.
25. J.B. Goodenough, G. Demazeau, M. Pouchard, and P. Hagenmuller, J. Solid State Chem. **8**, 325 (1973).
26. G.F. Dionne, J. Appl. Phys. **57**, 3727 (1985). DTIC-ADA 156350
27. D.S. McClure, Solid State Physics **9**, 399 (1959).
28. Reference 14, p. 164.
29. Reference 14, p. 213.
30. G.F. Dionne and J.A. MacKinnon, Phys. Rev. **172**, 325 (1968). DTIC-AD 678985
31. L. Pauling, *The Nature of the Chemical Bond*, (Cornell University Press, Ithaca, New York, 1960) p. 507.
32. C. Kittel, *Introduction to Solid State Physics*, (John Wiley, New York, 1966) p. 329.
33. Reference 14, p. 185.
34. G.H. Jonker and S. van Houten, *Halbeiterprobleme* **6**, 118-151 (1961).
35. R.R. Heikes and W.D. Johnston, J. Chem. Phys. **26**, 582 (1957).
36. R.J.D. Tilley, *Defect Crystal Chemistry and Its Applications*, Chapter 6 (Blackie, Glasgow and London, 1987).
37. C. Gorter and H.B.G. Casimir, Physica **1**, 306 (1934).
38. D.W. Murphy, S. Sunshine, R.B. van Dover, R.J. Cava, B. Batlogg, S.M. Zahurak, and L.F. Schneemeyer, Phys. Rev. Lett. **58**, 1888 (1987).
39. B. Batlogg, quoted in Science **237**, 249 (1987).
40. T.K. Worthington, W.J. Gallagher, and T.R. Dinger, Phys. Rev. Lett. **59**, 1160 (1987).
41. T. Wada, S. Adachi, T. Mihara, and R. Inaba, Japan J. Appl. Phys. **26**, L706 (1987).
42. J.R. Schrieffer, *Theory of Superconductivity*, (W.A. Benjamin, New York, 1964) p. 10.
43. Reference 32, p. 339.
44. D.C. Johnston, J. Low Temp. Phys. **25**, 145 (1976).
45. G. F. Dionne, Mater. Res. Bull. **7**, 1393 (1972). DTIC-AD 758945
46. K. Kishio, K. Kitazawa, S. Kanabe, I. Yasuda, N. Sugii, H. Takagi, S. Uchida, K. Fueki, and S. Tanaka, Chem. Lett. **25**, 429 (1987).
47. Y. Khan, J. Mater. Sci. Lett. **6**, 1221 (1987).

48. R.N. Bhargava, S.P. Herko, and W.N. Osborne, Phys. Rev. Lett. **59**, 1468 (1987).
49. Reference 20, p. 194.
50. P.N. Iyer and A.J. Smith, Acta. Cryst. **23**, 740 (1967).
51. T. Ogushi and Y. Osono, Appl. Phys. Lett. **48**, 1167 (1986).
52. M.A. Subramanian, C.C. Torardi, J.C. Calabrese, J. Gopalakrishnan, K.J. Morrissey, T.R. Askew, R.B. Flippen, U. Chowdhry, and A.W. Sleight, Science **239**, 1015 (1988).
53. J.M. Longo and P.M. Raccah, J. Solid State Chem. **6**, 526 (1973). DTIC-AD 763151
54. K.K. Singh, P. Ganguly, and J.B. Goodenough, J. Solid State Chem. **52**, 254 (1984).
55. P.M. Grant, S.S.P. Parkin, V.Y. Lee, E.M. Engler, M.L. Ramirez, J.E. Vasquez, G. Lim, R.D. Jacowitz, and R.L. Greene, Phys. Rev. Lett. **58**, 2482 (1987).
56. A.M. George, I.K. Gopalakrishnan, and M.D. Karkhanavla, Mater. Res. Bull. **9**, 721 (1974).
57. E.W. Gorter, Adv. Phys. (Philos. Mag. Suppl.) **6**, 336 (1957).
58. G.F. Dionne, to be published.
59. Reference 12, p. 199.
60. M.E. Hawley, K.E. Gray, D.W. Capone II, and D.G. Hinks, Phys. Rev. B **35**, 7224 (1987).
61. J. Moreland, A.F. Clark, H.C. Ku, R.N. Shelton, Cryogenics **27**, 227 (1987).
62. Z. Schlesinger, R.L. Greene, J.G. Bednorz, and K.A. Muller, Phys. Rev. B **35**, 5334 (1987).
63. N.F. Mott and R.W. Gurney, *Electronic Processes in Ionic Crystals,* (Oxford University Press, 1948) p. 86.
64. Reference 12, Table 4.
65. M. Pardavi-Horvath, P.E. Wigen, A. Thavendrarajah, and P. DeGasperis, paper BB-05, Conf. Magn. & Magn. Mater. 1987; J. Appl. Phys. (in press).
66. P.H. Hor, R.L. Meng, Y.Q .Wang, L. Gao, Z.J. Huang, J. Bechtold, K. Forster, and C.W. Chu, Phys. Rev. Lett. 58, 1891 (1987).
67. P. Bordet, C. Chaillout, J.J. Capponi, J. Chenavas, and M. Marezio, Nature **327**, 687 (1987).
68. J.B. Goodenough, private communication.

REPORT DOCUMENTATION PAGE

1a. REPORT SECURITY CLASSIFICATION Unclassified	1b. RESTRICTIVE MARKINGS
2a. SECURITY CLASSIFICATION AUTHORITY	3. DISTRIBUTION/AVAILABILITY OF REPORT Approved for public release; distribution unlimited.
2b. DECLASSIFICATION/DOWNGRADING SCHEDULE	
4. PERFORMING ORGANIZATION REPORT NUMBER(S) Technical Report 802	5. MONITORING ORGANIZATION REPORT NUMBER(S) ESD-TR-87-277
6a. NAME OF PERFORMING ORGANIZATION Lincoln Laboratory, MIT 6b. OFFICE SYMBOL *(If applicable)*	7a. NAME OF MONITORING ORGANIZATION Electronic Systems Division
6c. ADDRESS *(City, State, and Zip Code)* P.O. Box 73 Lexington, MA 02173-0073	7b. ADDRESS *(City, State, and Zip Code)* Hanscom AFB, MA 01731
8a. NAME OF FUNDING/SPONSORING ORGANIZATION Air Force Systems Command, USAF 8b. OFFICE SYMBOL *(If applicable)* XTK	9. PROCUREMENT INSTRUMENT IDENTIFICATION NUMBER F19628-85-C-0002
8c. ADDRESS *(City, State, and Zip Code)* Andrews AFB Washington, DC 20334	10. SOURCE OF FUNDING NUMBERS PROGRAM ELEMENT NO. 63250F; PROJECT NO. 227; TASK NO.; WORK UNIT ACCESSION NO.
11. TITLE *(Include Security Classification)* Transition-Metal Oxide Superconductivity	
12. PERSONAL AUTHOR(S) Gerald F. Dionne	
13a. TYPE OF REPORT Technical Report 13b. TIME COVERED FROM _____ TO _____	14. DATE OF REPORT *(Year, Month, Day)* 20 April 1988 15. PAGE COUNT 100
16. SUPPLEMENTARY NOTATION None	

17. COSATI CODES		
FIELD	GROUP	SUB-GROUP

18. SUBJECT TERMS *(Continue on reverse if necessary and identify by block number)*

cation ordering; copper perovskites; covalent bonding; critical temperature; itinerant polarons; magnetic exchange; polaron activation energy; superconductivity in oxides

19. ABSTRACT *(Continue on reverse if necessary and identify by block number)*

Superconductivity in transition-metal oxides is discussed from the standpoints of electron transfer mechanisms and the transition from superconduction to normal conduction. As explanations for the reported superconducting effects, it is suggested that polarons associated with ion pairs of the $d^9 \rightarrow d^8$ ion combination in 180-degree bond geometries (e.g., $Cu^{2+} \rightarrow Cu^{3+} + e^-$ in perovskites) and $d^1 \rightarrow d^0$ combination in 90-degree geometries (e.g., $Ti^{3+} \rightarrow Ti^{4+} + e^-$ in spinels) become itinerant within cell boundaries through energy-free electron transfers made possible by strong orbital exchange coupling. The proposed superconduction model is based on continuous linkages between cells that result in moving chains of uniformly spaced charge carriers. Calculated estimates indicate that radii of polaron cell boundaries on the order of 30 to 40 A may be anticipated in the perovskite system, in general agreement with estimates based on experiment. The superconducting state can exist below a critical temperature, where the fraction of electrons with thermal energies below the activation energy for electron hopping ($E_{hop} \leq 10$ meV for Cu oxides) is sufficient to sustain continuous supercurrent paths. A phenomenological theory of normal resistivity and superconduction transition temperature as functions of composition for the $La_{2-x}Sr_xCuO_4$ and $YBa_2Cu_3O_y$ perovskite families provides excellent agreement with experiment. Reported superconduction and structural data for the related $Bi_2(Sr,Ca)_3Cu_2O_{8+y}$ system are also included in the discussion. An important conclusion from these analyses is that optimized lattice ordering of the sources that produce the mixed-valence $Cu^{2+(3+)}$ ions could result in critical temperatures above 300 K.

20. DISTRIBUTION/AVAILABILITY OF ABSTRACT ☐ UNCLASSIFIED/UNLIMITED ☒ SAME AS RPT. ☐ DTIC USERS	21. ABSTRACT SECURITY CLASSIFICATION Unclassified
22a. NAME OF RESPONSIBLE INDIVIDUAL Lt. Col. Hugh L. Southall, USAF	22b. TELEPHONE *(Include Area Code)* (617) 981-2330 22c. OFFICE SYMBOL ESD/TML

DD FORM 1473, 84 MAR

83 APR edition may be used until exhausted.
All other editions are obsolete.